

POLITECNICO DI TORINO

Department of Electronics and Telecommunication

Master's Degree Thesis in Biomedical Engineering

Development of a saliva test method for monitoring chronic diseases via detection of salivary markers



Supervisors:

Prof. Danilo Demarchi
Prof. Tao Dong

Candidate:

Francesca De Meis

April 2019

Alla mia famiglia, la bussola della mia vita ...

Abstract

La broncopneumopatia cronica ostruttiva (BPCO) è una malattia comune e trattabile, che comporta una limitazione del flusso aereo e un'inflammatione polmonare. Oggigiorno la sua diffusione cresce rapidamente tanto che l'Organizzazione Mondiale della Sanità ha stimato diventerà, entro il 2030, la terza causa di mortalità nel mondo. Esacerbazioni e comorbidità contribuiscono alla gravità complessiva dei singoli pazienti. Al giorno d'oggi, il Gold Standard utilizzato per la diagnosi della BPCO è la spirometria, considerato come un test non invasivo ma fortemente dipendente dallo stato fisico del paziente. Gli studi più recenti si concentrano, invece, a valutare il ruolo di alcuni Biomarcatori coinvolti nei processi di inflammatione della BPCO come le proteine Interleuchina -6 (IL-6), Interleuchina -8 (IL-8), Metalloproteina-8 (MMP-8), Metalloproteina-9 (MMP-9), Fattore di Necrosi Tumorale α (TNF- α), Elastasi Neutrofila (NE) e la Proteina C-Reattiva (CRP). Il fine è quello di valutarne il loro ruolo diagnostico. I campioni di fluidi corporei più studiati sono il sangue e la saliva. E' stata osservata la possibilità di differenziare una persona sana da una malata basandosi sulla concentrazione, nel campione fluido, dei Biomarcatori citati; la loro concentrazione media tende inoltre ad aumentare nei giorni precedenti ad un'Esacerbazione. Da queste nuove scoperte nasce l'esigenza di creare un metodo di analisi, che si avvalga dell'utilizzo delle nuove tecnologie 'Point-of-Care' (PoC) e di campioni non invasivi come la saliva, al fine di garantire la prevenzione e il follow-up del paziente. In questa tesi viene proposto il modello di un dispositivo ottico microfluidico in polimetilmetacrilato (PMMA), che analizzi la concentrazione di un cluster di tre Biomarcatori in un piccolo volume di saliva. Il dispositivo di analisi appartiene alla classe PoC, e si propone di utilizzare materiali innovativi come i Quantum Dots e fototransistori ibridi di grafene. Il dispositivo proposto è stato testato numericamente nel software di simulazione *COMSOL Multiphysics 5.3.a*. Un suo possibile processo di fabbricazione, la soft-litografia, è stato testato in laboratorio. Inoltre, è stata valutata e studiata la concentrazione di IL-8 nella saliva di 5 persone sane, utilizzando il convenzionale ELISA Kit per le analisi di laboratorio. I risultati ottenuti nell'analisi numerica microfluidica mostrano il possibile funzionamento del dispositivo per effetto capillarità. Il processo di fabbricazione studiato si è dimostrato facile da eseguire ed a basso costo, caratteristiche fondamentali per una produzione di massa del dispositivo.

proposto. I test di saliva hanno invece dimostrato e confermato che la proteina IL-8 può essere rilevata nel campione non invasivo; essa tende ad avere una concentrazione media comparabile nei diversi soggetti ed inoltre stabile nei diversi giorni di analisi. Queste caratteristiche rafforzano il suo possibile ruolo diagnostico.

Abstract

Chronic obstructive pulmonary disease (COPD) is a common and treatable disease that results in airflow limitation and pulmonary inflammation. Nowadays its spreading grows too rapidly that the World Health Organization has estimated it will become, by 2030, the third cause of mortality in the world. Exacerbations and comorbidities contribute to the overall severity of individual patients. Nowadays, the Gold Standard used for the diagnosis of COPD is spirometry, considered as a non-invasive test but strongly dependent on the patient's physical state. The most recent studies, on the other hand, focus on the role of some biomarkers involved in the inflammation processes of COPD such as proteins Interleukin -6 (IL-6), Interleukin -8 (IL-8), Metalloproteinase- 8 (MMP- 8), Metalloproteinase-9 (MMP-9), Tumor Necrosis Factor- α (TNF- α), Neutrophil Elastase (NE) and C-Reactive Protein (CRP). The aim is to evaluate their diagnostic role. The most studied body fluid samples are blood and saliva. The possibility of differentiating a healthy person from a patient has been observed based on the concentration, in the fluid sample, of the mentioned Biomarkers. Their mean concentration also tends to increase in the days preceding an Exacerbation. From these discoveries, the need arises to create a method of analysis, which makes use of the new 'Point-of-Care' (PoC) technologies and non-invasive samples such as saliva, in order to ensure prevention and patient follow-up. In this thesis, the model of a polymethyl methacrylate (PMMA) microfluidic optical device is proposed, which analyzes the concentration of a cluster of three Biomarkers in a small volume of saliva. The analysis device belongs to the PoC class, and it is proposed to use innovative materials such as the Quantum Dots and graphene hybrid phototransistors. The proposed device was tested numerically in the simulation software COMSOL Multiphysics 5.3.a. A possible manufacturing process, the Soft-lithography, has been studied in the laboratory. Furthermore, the IL-8 concentration in the saliva of 5 healthy people was evaluated and studied using the conventional ELISA Kit for laboratory analyzes. The results obtained in the microfluidic numerical analysis show the possible operation of the device by capillary effect. The studied manufacturing process has proved easy to perform and low cost, fundamental characteristics for mass production of the proposed device. Saliva tests have instead demonstrated and confirmed that the IL-8 protein can be detected in the non-invasive sample. It tends to have a comparable mean

concentration in the different subjects and is also stable over the various days of analysis. These characteristics reinforce its possible diagnostic role.

Table of contents

List of figures	xiii
List of tables	xvii
Nomenclature	xix
1 Motivation	1
2 General knowledge about COPD	3
2.1 What is Chronic Obstructive Pulmonary Disease?	3
2.2 Pathology	3
2.3 COPD in the World: statistics	4
2.4 COPD symptoms	5
2.5 COPD risk factors	6
2.5.1 Acquired risk factors for COPD	6
2.5.2 Genetic risk factors for COPD	7
2.6 Pathophysiology	8
2.7 COPD evaluation of GOLD tests	12
2.7.1 Spirometry, CAT questionnaire and mMRC questionnaire	12
2.7.2 CT technique	17
3 COPD Biomarkers	19
3.1 Blood biomarkers for COPD	21
3.2 Sputum biomarkers for COPD	24
3.3 Salivary biomarkers for COPD	28
4 Experimental study case: Human IL-8 ELISA Test	31
4.1 Saliva collection and processing	31
4.2 Set-up and Methods	32

4.3	Materials and experimental procedure	35
4.4	Data analysis	37
4.5	Results	38
5	Point-of-Care devices: State of Art and Proposal for COPD	43
5.1	POC devices	44
5.1.1	Capillary flow paper based POC devices	44
5.1.2	Microfluidic POC devices	48
5.1.3	Electrochemical POC devices	52
5.1.4	Electrochemiluminescence POC devices	54
5.1.5	Optical POC devices	56
5.2	Used nanoparticles in POC devices	58
5.2.1	Quantum dots (QDs)	58
5.2.2	Gold nanoparticles (AuNPs)	59
5.2.3	Magnetic Nanoparticles (MNPs)	60
5.3	Proposal of an innovative microfluidic device for COPD	62
6	Microfluidic device numerical simulation	71
6.1	Microfluidic theory	71
6.1.1	Non-Newtonian Fluid	71
6.1.2	Pressure Drop	75
6.1.3	Laminar two-phase flow fluid model	75
6.2	Design proposal	79
6.3	2D Cross-section FEM simulation	82
6.3.1	Geometry	82
6.3.2	Boundary conditions	82
6.3.3	Mesh	83
6.3.4	Results	83
6.4	2D Top-section FEM simulation	97
6.4.1	Geometry	97
6.4.2	Boundary conditions	97
6.4.3	Mesh	98
6.4.4	Results	98
7	Building process experience: the Soft-lithography	113
7.1	Soft-lithography process	113
7.2	Work Methodology	116

7.3 Results and final considerations	124
8 Conclusions and future work	127
References	129
Appendix A Costs analysis	147

List of figures

1.1	Project vision	2
2.1	COPD statistics	5
2.2	Emphysema	8
2.3	Chronic bronchitis	9
2.4	Exacerbation inflammatory process	11
2.6	COPD questionnaires	14
2.7	COPD Gold tests combination	15
4.1	ELISA test illustration	33
4.2	Saliva collection	34
4.3	ELISA plate	34
4.4	Standard curve for IL-8 concentration	38
4.5	Results from ELISA test (comparison 1)	39
4.6	Results from ELISA test (comparison 2)	40
4.7	Results from ELISA test (comparison 3)	41
4.8	Results from ELISA test (comparison 4)	42
5.1	3D microfluidic device proposal	62
5.2	PMMA skeletal formula	63
5.3	Chemical reactions illustration	65
5.4	PMMA surface treatment	66
5.5	Graphene- methylammonium lead iodide (MAPbI ₃) perovskite hybrid photo-transistor	69
6.1	Viscosity-Shear rate relation for general fluids	72
6.2	Viscosity-Shear rate relation for saliva	73
6.3	Viscosity-Shear rate relation in Carreau and Newtonian fluids	73
6.4	Stress-Shear rate relation for Non-Newtonian fluids	74

6.5	Microfluidic device geometry	79
6.6	Cross-section geometry	82
6.7	Cross-section mesh	83
6.8	Meniscus shape in the cross-section simulation	84
6.9	Meniscus development along the microfluidic device: cross-section simulation	85
6.10	Velocity drop in the cross-section simulation	87
6.11	Velocity profile in the cross-section simulation	87
6.12	Velocity profile in the reaction chamber: cross section simulation	88
6.13	Velocity values development along the microfluidic device: cross section simulation	89
6.14	Reynolds values development along the microfluidic device: cross-section simulation	90
6.15	Pressure gradient development along the microfluidic device: cross-section simulation	92
6.16	Pressure values development along the microfluidic device:cross-section simulation	93
6.17	Dynamic viscosity values along the microfluidic device: cross-section simu- lation	95
6.18	Shear rate values along the microfluidic device: cross-section simulation . .	96
6.19	Top-section geometry	97
6.20	Top-section mesh	98
6.21	Meniscus shape in the top-section simulation	99
6.22	Meniscus development along the microfluidic device:top-section simulation	100
6.23	Velocity profile in the reaction chamber: top section simulation	101
6.24	Velocity values along the microfluidic device: top-section simulation	102
6.25	Velocity drops in the top-section simulation	103
6.26	Reynolds values along the microfluidic device: top-section simulation . . .	104
6.27	Pressure values along the microfluidic device: top-section simulation	106
6.28	Pressure gradient comparison in the microchannel	107
6.29	Pressure gradient comparison in the reaction chamber	108
6.30	Pressure gradient comparison in the outlet microchannel	109
6.31	Dynamic viscosity values along the microfluidic device: top-section simulation	111
6.32	Shear rate values along the microfluidic device: top-section simulation . . .	112
7.1	Key materials for the Soft-lithography	114
7.2	Resist layer	114
7.3	Soft-lithography process	115

7.4	Thickness-spin speed relation for the negative photoresist SU8-100	116
7.5	Spin speed time evolution	118
7.6	Hot plate and Spinning machine	118
7.7	Master building process	119
7.8	Micro-replica molding	120
7.9	Microfluidic PDMS final structure	122
7.10	Soft-lithography parameters	123
7.11	Veeco machine (Dektat 150)	124
7.12	Veeco machine (Dektat 150). Channel thickness	125
7.13	Veeco machine (Dektat 150). Chamber thickness	125

List of tables

2.1	Spirometry COPD classification [135].	12
3.1	Blood biomarkers for COPD.	23
3.2	Sputum biomarkers for COPD.	27
3.3	Salivary biomarkers for COPD.	30
5.1	Capillary flow paper based POC devices relative to COPD biomarkers. . . .	47
5.2	Microfluidic POC devices relative to COPD biomarkers.	51
5.3	Electrochemical (EC) and electrochemiluminescence (ECL) POC devices relative to COPD biomarkers.	55
5.4	Optical POC devices relative to COPD biomarkers.	57
6.1	List of constants and values used in the simulation.	81

Nomenclature

Acronyms / Abbreviations

ACOS Asthma COPD overlap syndrome

ATS American Thoracich Society

AuNPs Gold nanoparticles

CAT COPD assessment test

CE Counter electrode

COPD Chronic Obstructive Pulmonary Disease

CRP C Reactive Protein

EC Electrochemical

ECL Electrochemiluminescence

EHIS European Health Health Interview

FCV Force vital capacity

FEM Finite element method

FEV Forced expiatory volume

FLFIA Fluorescence lateral flow immunoassay

GP General practitioners

ICTS Immunochromatography test strip

IL-6 Interleukin 6

IL-8 Interleukin 8

LFIA Lateral flow immunoassay

LoC Lab on Chip

MMP-8 Metalloproteinase 8

MMP-9 Metalloproteinase 9

MNPs Magnetic nanoparticles

MRC Medical research council

NE Neutrophil Elastase

NICE National Institute for Care Excellence

PDMS Polydimethylsiloxane

PEG Polyethylene glycol

PMMA Polymethyl methacrylate

POC Point of Care

QDs Quantum dots

RE Reference electrode

SAM Self assembled monolayer

SPR Surface Plasmon Resonance

TNF- α Tumor necrosis factor alpha

TRFIA Time resolved immunofluorescence assay

WE Working electrode

WHO World Health Organization

Chapter 1

Motivation

The vision of this thesis is to develop a comprehensive strategy for efficient follow-up of the chronic obstructive pulmonary disease (COPD) patients in Norwegian municipalities by introducing a new saliva assay device. It can predict their worsening than the conventional tests, subsequently triggering early treatments and significantly reducing the total cost over the national insurance system. The proposed idea is an innovative solution based on a few drops of saliva, providing a portable device accompanied by a smartphone APP, which would be possible to perform for all COPD patients. It is based on detecting the critical biomarkers in the sample to predict exacerbation or worsening, newly found in recent medical studies. As it will be explained, it has been proven that some salivary biomarkers have increased levels in saliva of COPD patients 2 or 3 days before an exacerbation comes. The currently available procedure to analyse these biomarkers is to send samples to central labs, similar to blood tests. Thus, a problem arises: the analysis done in central labs takes at least 48 to 72 hours, during which worsening of patient's health condition can occur before knowing the analysis results. To remove the foregoing obstacles has motivated the development of a revolutionary strategy comprising a portable biomarker-detection device together with a smartphone APP.

The user friendly device is to be used for point of care (POC); all the elements necessary for the analysis must be included in it. In one step the patient should insert the saliva sample in the device, or with the assistance of a nurse at home care services. The analysis for the biomarkers can significantly be shortened, without sending to a central lab. Ideally, the device measures the analytes through photoelectrical signals on the spot corresponding to the levels of the biomarkers in saliva. The signals are transferred wirelessly to a smartphone, in which an APP would display and record the results of biomarker detection (figure 1.1). When the APP displays the "red level" for the measured salivary biomarkers, the General practitioners (GPs) in the municipality are immediately notified. The early notification of

biomarker-level increasing will allow the GP to step in at the early stage. The GPs will then proceed with immediate alternation of medication to the patient or promote the initiation of preventive treatment.

This thesis is structured as follow: in the second chapter there is an introduction to the discussed disease, where its spreading and importance is put in relevance; the third chapter is about the literature research of the most important COPD biomarkers in the body samples. On the basis of this, experimental research was done for taking data about the biomarker Interleukin-8 protein in the saliva of healthy people, as explained in the fourth chapter. In the fifth chapter, new literature research was done for describing the state of the art of the point-of-care devices linked to COPD biomarkers; this was useful for developing the idea of the innovative prototype proposed in this work. In the sixth chapter, a microfluidic simulation with FEM analysis of the new device is done by using the software COMSOL Multiphysics 5.3.a. In the seventh chapter a possible fabrication method for the proposed device is practically studied. In the last chapter, the conclusions of this work are described, also with the future work that will be developed thanks to the contributions of this thesis.

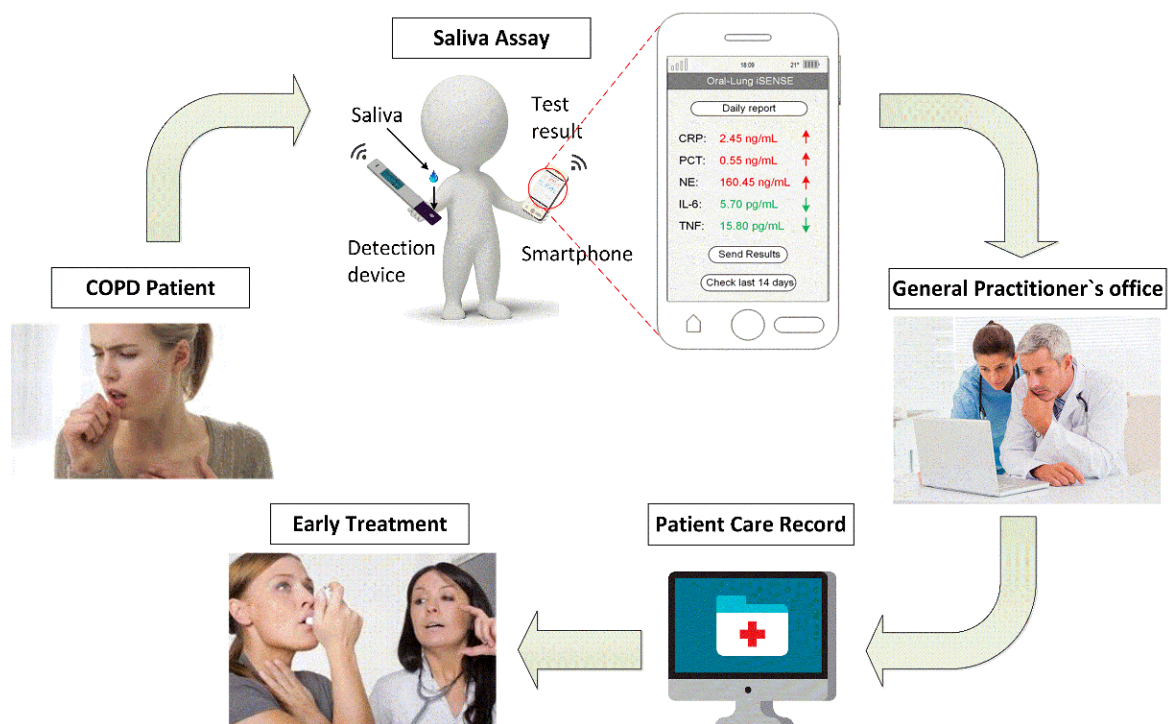


Fig. 1.1 Innovation strategy for convenient and efficient follow-up of COPD.

Chapter 2

General knowledge about COPD

2.1 What is Chronic Obstructive Pulmonary Disease?

" Chronic Obstructive Pulmonary Disease, a common preventable and treatable disease, is characterized by persistent airflow limitation that is usually progressive and associated with an enhanced chronic inflammatory response in the airways and the lung to noxious particles or gases. Exacerbations and co-morbidities contribute to the overall severity in individual patients [172]."

Chronic obstructive pulmonary disease (COPD) is a great problem for the social healthy nowadays; it is the fourth cause of chronic morbidity and mortality throughout the world, but World Health Organization (WHO) in 2015 predicted it would be the third cause of mortality until 2030, affecting more than 80 million people worldwide.

According to the GOLD COPD 2017 guide, more than 3 million of people died because of COPD in the last 2012, representing the 6% of all deaths. The prevalence it is expected to rise over the next 30 years because of the increasing prevalence of smoking in developing countries, the prevalence of air pollution and aging populations [97].

2.2 Pathology

In the COPD the small airways inflammation (Obstructive bronchiolitis) and parenchymal destruction (emphysema) contribute to the development of the disease.

Usually, the small airways change in their structure because of chronic inflammations. They lose the alveolar attachments leading to the decreases of lung elastic recoil. Consequently, the airways diminish the ability to remain opened during expiration.

Furthermore, a deregulated production of extracellular matrix proteins is observed, so it is more difficult for the organism to sustain connective and epithelial tissue repair [146].

2.3 COPD in the World: statistics

COPD is a significant, growing public health problem nowadays.

According to the World Health Organization (WHO), the continued exposure to risk factors together with the population aging and growth will contribute to its increasingly becoming the third leading cause of death by 2030 [160].

The European Community Respiratory Health indicated that the 10% of adults was affected by non-reversible airway obstruction in the last decade.

In detail, according to the WHO, in 2002 more than 50 million people could be included in the group of moderate to severe COPD patients.

In the 2005, the costs of total health care reached 38.6 billion Euros only for COPD. As reported from the European Union (EU), they represented almost the 3% of the total costs [27].

The prevalence of COPD increased from 1.2% to 6.2% in 2008, considering the European population as reported from the European Health Interview Survey (EHIS).

The 2010 Global Burden of Disease (GBD) study reported that COPD was responsible for about 5% of global disability and 5% of total deaths (2.9 million) [108, 93].

In 2011, the total annual cost per case in Europe was €6147 (ERS White Book). According with Global Health Observatory (GHO), in 2012 COPD became the third leading cause of deaths.

In 2014, the American Thoracic Society (ATS Society) reported that about 6% of the total European Union health care budget expenditure was on respiratory problems with 56% of it is constituted by COPD.

On the base of these data, it is evident the importance of the growing of COPD disease and the great weight it has on the healthy social economy.

In recent research of 2018 [15], a big cohort from European countries was studied for examining the spreading of COPD in the whole territory. By using a geographic interpolation technique they represented the spatial distribution of COPD in a red-blue scale (Figure 2.1). Black spots indicate the places of origin of the samples. The maximum values are represented from dark-red colors (28%), while light colours between brown and orange represent the moderate COPD prevalence (15%-20%). Finally tones from light yellow to blue represent minimal values (0%-5%). Italy results to have a moderate prevalence of COPD throughout the country (from 11.7% to 23.4%), so for this reason it is important developing a prevention

program for this disease and an accurate system of follow up for the current patients; the main goal of this thesis is to reduce hospitalization risk for COPD patients, by adopting a control method based on saliva biomarkers that can predict an adverse event (Figure 2.1) .

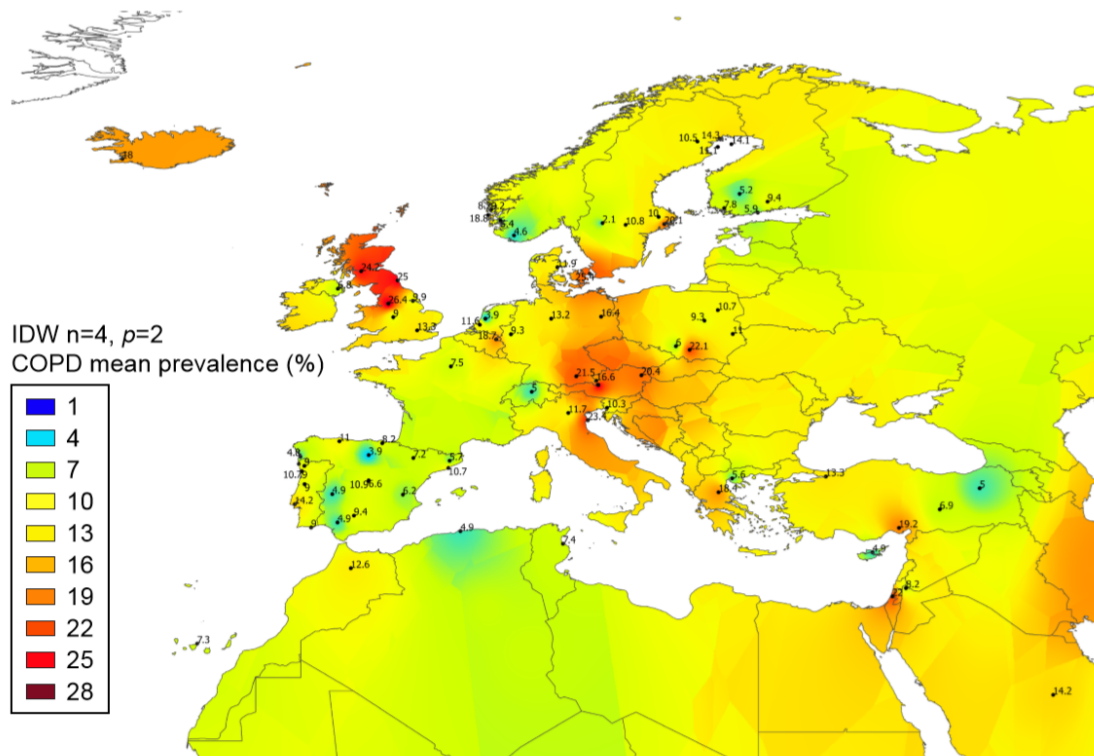


Fig. 2.1 Results from geographic information system inverse distance weighted (IDW) interpolation for COPD spreading [15].

2.4 COPD symptoms

When a person is affected by COPD, firstly shows difficult to breath coupled with production of mucus. This involves the cough manifestation that can become chronic and also, during the time, the mucus increases in purulence and volume. Finally wheeze and noisy breathing are characteristic of this disease, as reported from NICE in 2010. As a consequence, the patient becomes not more able to perform breathing as a passive action but he starts to involve the use of accessory muscles and also to take air from lip breathing. The breathing pattern becomes altered and this comports the presence of less oxygen in the peripheral vessels; from this the most evident consequence is the inability from the patient to complete a sentence without interruptions. Apnoea periods are the cause of this condition.

Finally some patients manifested tremor, heart arrhythmia and changes in skin's colour [104].

2.5 COPD risk factors

2.5.1 Acquired risk factors for COPD

Active and passive smoke have a relevant role in the development of the disease. The use of cigarette and similar tobacco substances like the pipe, cigar, water pipe [10] and marijuana [54] is a risk factor for developing COPD.

People who live in high-income countries are more exposed to this disease (73 % of COPD mortality) than who live in low-and-middle- income countries (only 40% of COPD mortality), because of the different lifestyle and quality of life [144].

The passive smoke is dangerous too, especially for people frequently exposed to it or , in a different case, for the fetus during pregnancy period; the baby can develop airways diseases, abnormalities on lung growth that leads to lung disease premature birth with incomplete development of the lungs [172]. In this conditions the child has a major risk to suffer from airways inflammation during his life and so to develop COPD disease.

Furthermore, *indoor pollution* has to be considered as a risk factor. The exposure to biomass fuels used for cooking or heating in poorly ventilated dwellings or poorly functioning stoves, is a big risk factor for COPD especially for developing countries; the elements that contribute to this pollution are for example wood, animal dung, crop residues and coal, typically burned in open fires. The COPD can also be linked to *occupational exposures*. The prolonged exposure to organic and inorganic dusts and chemical agents and fumes in the workplace plays a big role as a risk factor for COPD.

A recent industry-based study on the European Community Respiratory Health Survey has examined the relationship between occupation and COPD-related outcomes. It has been estimated that about 15% of COPD cases are attributable to exposures at the workplace, with a higher population attributable fraction among non-smokers.

The main dangerous exposure substances are biological dust, mineral dust, gases and fumes, vapors, herbicides, insecticides, fungicides, pesticides, an aromatic solvent, chlorinated solvents and metals [94].

Nowadays, *outdoor pollution* plays a role in respiratory diseases. For example the ozone can affect lung inflammation and the alveolar epithelial damage [1].

WHO estimates that ambient air pollution was responsible for 3.7 million premature death worldwide in 2012. Furthermore, some indicators are related to the *socioeconomic status and*

lifestyle such as income, education, type of work, house conditions, poor nutritional status, exposure to pollutants and poor access to health care [96].

2.5.2 Genetic risk factors for COPD

Alpha-1 Antitrypsin (AAT) deficiency is a genetic disorder that can cause the onset of emphysema at younger ages coupled to liver disease [57].

A recent large screening study followed people who were identified at birth as having alpha-1 antitrypsin deficiency to examine the natural course of the disease. It demonstrated that severe AAT deficiency (typically PiZZ homozygosity) is associated with the increase of airflows obstructions, specially gene-by-smoking interaction contributes to the pathogenesis of the disease [75]. Regarding *gender and age*, COPD in women is distinct from in men concerning phenotype, symptom burden and comorbidities, for example because of female sex hormones that influence airways to function in several ways [136].

Data demonstrate that women have different susceptibility to cigarette smoke and development of airways disease; for example women are more predisposed to the 'chronic bronchitis' phenotype than to the 'emphysema' that is more frequent in men and also they suffer from more dyspnoea than men [136].

Overall, women suffer a higher risk of developing COPD and develop a disease that is phenotypically distinct from that of their male counterparts; they appear to have a mortality advantage.

Nowadays the world's population lives longer thanks to the excellent nutrition, the reduction of infectious diseases. On the other hand, it is a risk for chronic medical disorders such as COPD [96]. *Pre-existing asthma* can be relevant to the development of COPD. Sometimes asthma and COPD may develop physiologic features that are quite similar. Usually asthma, that is caused from eosinophilic inflammation, is present from younger ages while COPD shows itself only in the adult age, and it is associated with neutrophilic inflammation [102]. Data from a 20-years follow-up study showed that 'active' asthma was significantly associated with subsequent development of emphysema and COPD [85]; 'Active' asthma is associated with the showing of asthma symptoms or disease attack in a period of the last 12 months. The increased risk is associated with active asthma but not inactive asthma [157]. It is linked with an increased rate of decline FEV_1 . When asthma and COPD coexist the term asthma-COPD overlap syndrome is used for representing this condition. It includes patients who have airflow obstruction because of smoking and also have features of asthma or who have pre-existing asthma [152].

Finally, according to GOLD POKET GUIDE 2018 COPD [103], *infections* have an important role in both the development and progression of COPD. If a person is exposed to infections in young age, it risks developing changes in the airway working.

2.6 Pathophysiology

The airways walls in our system are made of cartilage for preventing collapse, smooth involuntary muscle and inner lining of the mucose membrane. These elements are damaged in the presence of the chronic inflammation of central airways, lung parenchyma and alveoli that leads to increasing the resistance and the compliance respectively of the small airways and the lung. The lung tissue results dilated beyond terminal bronchiole (Emphysematous lung destruction), comporting a prolonged time constant for lung emptying [62] (Figure 2.2). Furthermore, there is an increase of the goblet cells and mucus production from the glands of the central airways leading to *pulmonary hypertension* [77] and *chronic bronchitis* (Figure 2.3).



Fig. 2.2 Emphysema [60].

Besides, the alveoli attachments to the small airways are partially destroyed, contributing to obstruction [62].

These events all together diminished the ability of the airways to remain open during the expiration. This event is called *air trapping*.

Expiration is typically a passive process, but in case of airflow limitation, it becomes an active process involving accessory muscles (i.e the abdominal muscles, sternocleidomastoid, trapezius and scalene) and requires more energy.

Gaseous exchanges take place at the alveolar capillary membrane, and this phenomenon is known as external respiration, that involves a process of diffusion. As well known, the blood

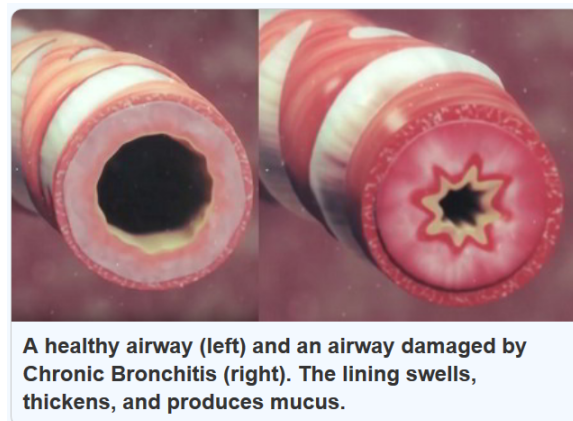


Fig. 2.3 Chronic bronchitis [60].

poor of oxygen comes from the right side of the heart and goes to pulmonary capillaries; here, in the healthy cases, it is reached of oxygen thanks to the alveoli action. After this blood can travel to the left side of the heart saturated with oxygen. In some patients gas exchange at the alveoli becomes altered [105] over time because of the trapped air in the conducting airways. The air cannot reach the alveoli and take part in the diffusion process, so the body activates a protective mechanism to equalize ventilation and perfusion. This mechanism, in the presence of low oxygen levels, diverts blood away from poorly ventilated alveoli thanks a pulmonary arteries constriction.

In our system, cilia are important components of airways , they are designed for filtering debris from the air on inhalation. Inhaled fumes and gases and active or passive cigarette smoke, damage the airways epithelium and cilia function [186]. Therefore, inflammatory cells expanded in number and size and can infiltrate in the mucosa, sub-mucosa and glandular tissue, allowing an increase of the production and viscosity of mucus and a disturbance in tissue repair and thickening of the small airways, causing luminal occlusion of the airways [104]. This phenomenon is known as *mucus hypersecretion*.

Chronic airways inflammation could cause *pulmonary hypertension* , as explained before. In this case, the vascular bed is modified as a consequence of the destruction of lung parenchyma or of alveoli hypoxia. This last one comports and increase of muscularization of no muscularized arteries, resulting in pulmonary hypertension [147].

In COPD, the worsening consequence is the *exacerbation*. According to GOLD COPD 2018 [103] , an exacerbation is defined as follow:

"An exacerbation of COPD is dened as an event in the natural course of the disease characterized by a change in the patient's baseline dyspnoea, cough, and/or sputum that is beyond normal day-to-day variations, is acute in onset, and may warrant a change in regular medica-

tion in a patient with underlying COPD."

COPD exacerbations are associated with reductions in quality of life and lung function. They increase the risk of death. They are caused by many factors that interact with others, like the relation between the host, respiratory viruses and airway bacteria in the airways (Figure 2.4). Other risk factors that contribute to increasing the airways inflammation are smoking and air pollution, severe airflow limitation, bronchiectasis, prior exacerbations and comorbidities [173].

Exacerbations can be classified on the base of three cardinal symptoms presence and gravity, these are increased breathlessness, increased sputum purulence and volume. The exacerbation is type 1 if all the symptoms are present, type 2 if two of them are present and also type 1 if only one symptom is presently coupled with one of the supporting symptoms (cough, wheezing, fever with an obvious source) [114, 112]. Furthermore the gravity of the exacerbation can be:

- mild, in which the patient needs more medications but they can be managed at home;
- moderate, in which the person has a sustained worsening of respiratory status that requires medical treatment.
- severe, in which the person experiences a rapid deterioration in respiratory status that requires hospitalization.

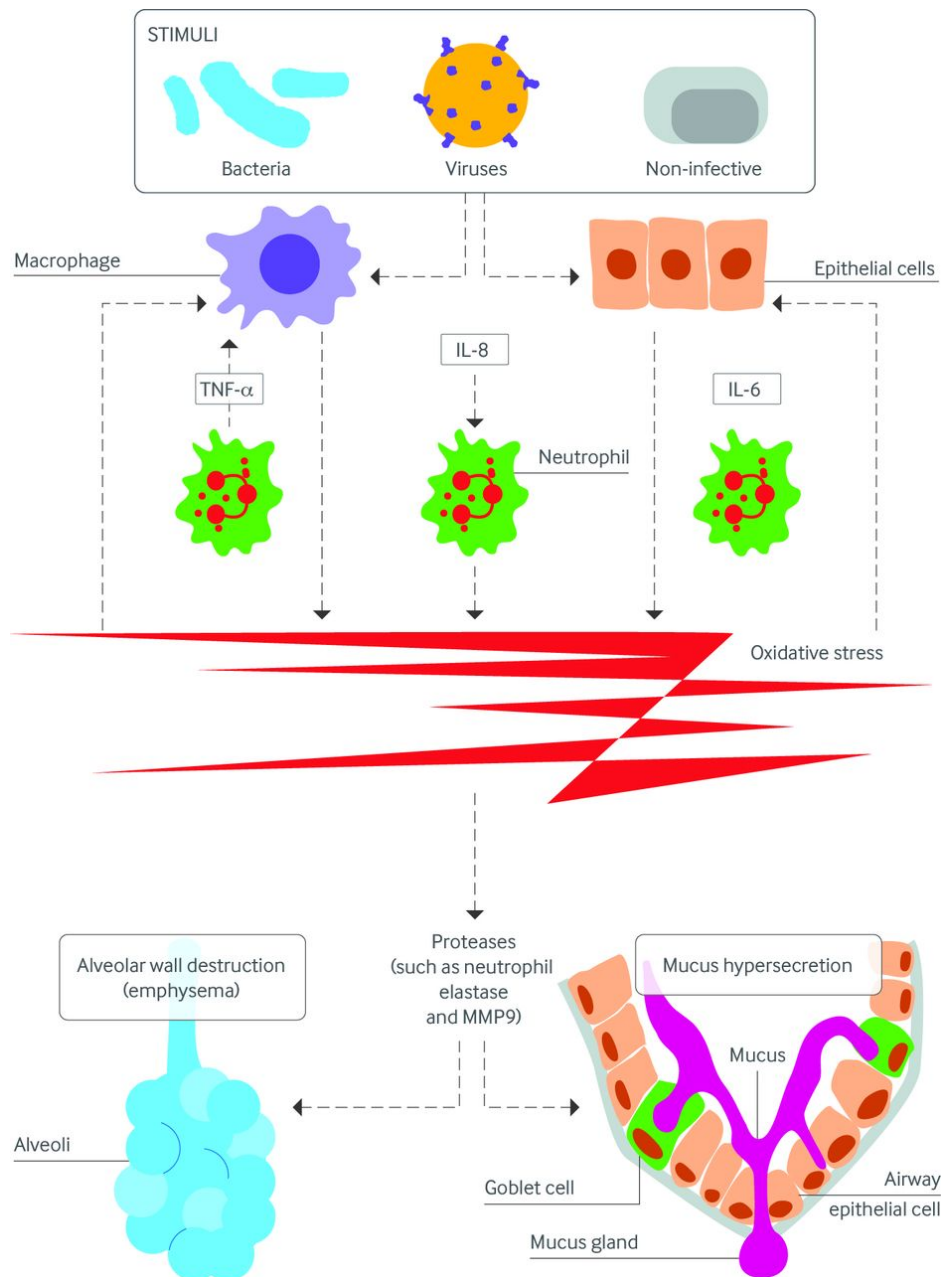


Fig. 2.4 During an acute exacerbation event, airway neutrophils like interleukin 6 and interleukin 8 increase compared to the stable state. They are mediators of the inflammation, such as tumor necrosis factor α ($\text{TNF-}\alpha$), and they promote the activity of other proteins such as neutrophil elastase (NE) and MMP-9. Furthermore, the reactive oxygen species start to work because of the cited mediators and damage the airway epithelium. This condition leads to worsening of airflow limitation [4].

Finally, *comorbidities* have a great impact on quality life and exercise capacity [133]; they also are greatly linked to exacerbation risk. It is possible to split the ones that affect the organism directly because of COPD, in terms of metabolism and body conditions such as malnutrition and pulmonary artery disease. While some comorbidities are not directly linked to COPD, such as osteoporosis, obesity, diabetes, thromboembolism and anemia. Some patients showed also sleep disturbance, anxiety and depression. These aspects can increase the COPD morbidity, leading to increased hospitalizations and healthcare costs [21].

2.7 COPD evaluation of GOLD tests

2.7.1 Spirometry, CAT questionnaire and mMRC questionnaire

The new guideline GOLD 2018 [103] for COPD patients describes the gravity classification of the disease considering the respiratory symptoms such as dyspnea, chronic cough and sputum production, the exacerbation history, the presence of comorbidities, the history of exposure to risk factors for the disease, family history of COPD and childhood factors. Finally, post-bronchodilator has to be evaluated.

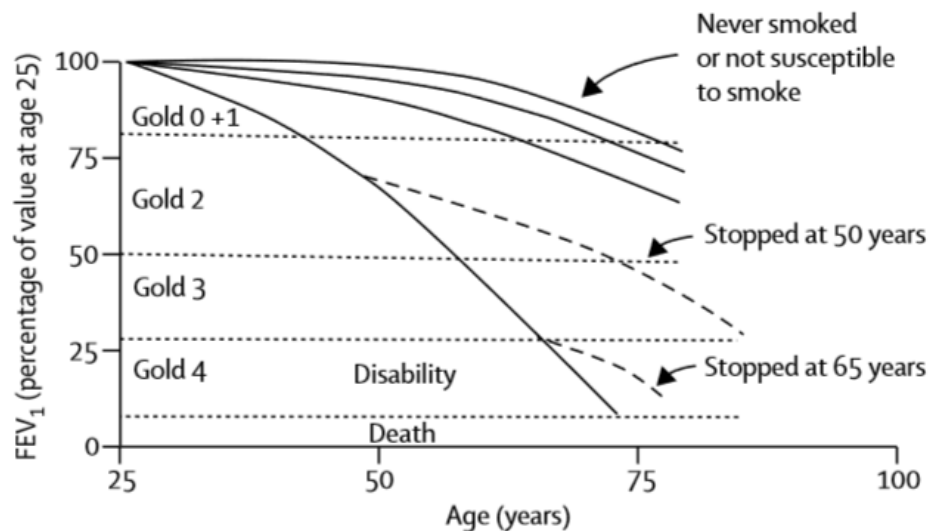
Expiratory airflow is usually measured as the forced expiratory volume in 1 s (FEV_1) and lung volume as the force vital capacity (FCV) by using a simple non-invasive test, that is spirometry. In the analysis, if the post-bronchodilator FEV_1/FVC is less of 0.8 it means that is present an important limitation of the airflow. This confirms the diagnosis of COPD [100]. Referring to the GOLD, the spirometry classification of airflow limitation severity in COPD identifies four classes by using specific spirometry cut-points for purposes of simplicity [172] (Table 2.1). GOLD 1-2 indicate Low Risk, while GOLD 3-4 indicate High Risk.

The severity of airflow limitation in COPD by considering FEV_1		
Patients with $FEV_1/FVC < 0.8$		
GOLD 1	Mild	$FEV_1 > 80\%$ predicted
GOLD 2	Moderate	$50\% < FEV_1 < 80\%$ predicted
GOLD 3	Severe	$30\% < FEV_1 < 50\%$ predicted
GOLD 4	Very severe	$FEV_1 < 30\%$ predicted

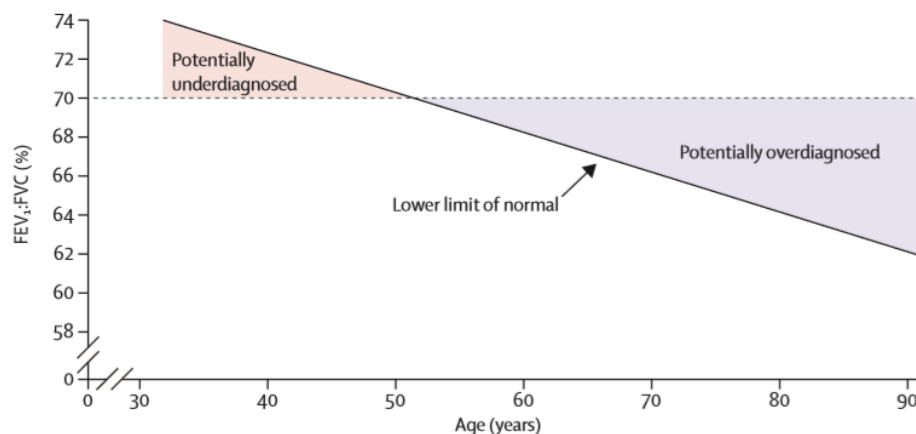
Table 2.1 Spirometry COPD classification [135].

The increased risk of exacerbations and death are directly related to the worsening of airflow limitation.

For defining COPD, conventional thresholds are set on the base of different FEV_1/FVC values. However, this variable can change during the time, becoming lower, so they cannot be used alone for a predictive role. As a consequence the ratio diminishes with age.




(a) The figure explains the rate of decline in FEV_1 with age [182, 62].



(b) The diagram shows how the FEV_1/FVC ratio declines with aging. The overdiagnosed elderly patients are represented from the blue part, while the orange part represents the underdiagnosed younger adults [141].

These data come from Fletcher and colleagues studies [182] in which they show how FEV_1 changes with age are declining during the time. Furthermore it results that stopping smoking has a beneficial effect at any age. Because of the age-related changes, the elderly patients could be overdiagnosed while the younger adults underdiagnosed [141]. Nowadays in addition to the spirometry test, the patients use questionnaires for checking the development of dyspnoea (mMRC questionnaire 2.6b) and symptoms (CAT questionnaire 2.6a). A mMRC grade ≥ 2 or a CAT score ≥ 10 indicates a high level of symptoms.

Your name: Today's date:

 **CAT**
COPD Assessment Test

How is your COPD? Take the COPD Assessment Test™ (CAT)

This questionnaire will help you and your healthcare professional measure the impact COPD (Chronic Obstructive Pulmonary Disease) is having on your wellbeing and daily life. Your answers, and test score, can be used by you and your healthcare professional to help improve the management of your COPD and get the greatest benefit from treatment.


For each item below, place a mark (X) in the box that best describes you currently. Be sure to only select one response for each question.

Example: I am very happy (0) ☒ (1) ☐ (2) ☐ (3) ☐ (4) ☐ (5) I am very sad

		SCORE
I never cough	(0) <input type="radio"/> (1) <input type="radio"/> (2) <input type="radio"/> (3) <input type="radio"/> (4) <input type="radio"/> (5) I cough all the time	<input type="text"/>
I have no phlegm (mucus) in my chest at all	(0) <input type="radio"/> (1) <input type="radio"/> (2) <input type="radio"/> (3) <input type="radio"/> (4) <input type="radio"/> (5) My chest is completely full of phlegm (mucus)	<input type="text"/>
My chest does not feel tight at all	(0) <input type="radio"/> (1) <input type="radio"/> (2) <input type="radio"/> (3) <input type="radio"/> (4) <input type="radio"/> (5) My chest feels very tight	<input type="text"/>
When I walk up a hill or one flight of stairs I am not breathless	(0) <input type="radio"/> (1) <input type="radio"/> (2) <input type="radio"/> (3) <input type="radio"/> (4) <input type="radio"/> (5) When I walk up a hill or one flight of stairs I am very breathless	<input type="text"/>
I am not limited doing any activities at home	(0) <input type="radio"/> (1) <input type="radio"/> (2) <input type="radio"/> (3) <input type="radio"/> (4) <input type="radio"/> (5) I am very limited doing activities at home	<input type="text"/>
I am confident leaving my home despite my lung condition	(0) <input type="radio"/> (1) <input type="radio"/> (2) <input type="radio"/> (3) <input type="radio"/> (4) <input type="radio"/> (5) I am not at all confident leaving my home because of my lung condition	<input type="text"/>
I sleep soundly	(0) <input type="radio"/> (1) <input type="radio"/> (2) <input type="radio"/> (3) <input type="radio"/> (4) <input type="radio"/> (5) I don't sleep soundly because of my lung condition	<input type="text"/>
I have lots of energy	(0) <input type="radio"/> (1) <input type="radio"/> (2) <input type="radio"/> (3) <input type="radio"/> (4) <input type="radio"/> (5) I have no energy at all	<input type="text"/>
		TOTAL SCORE <input type="text"/>

COPD Assessment Test and the CAT logo is a trade mark of the GlaxoSmithKline group of companies.
© 2000 GlaxoSmithKline group of companies. All rights reserved.
Last Updated: February 24, 2012

(a) CAT questionnaire [166].

 **MODIFIED MEDICAL RESEARCH COUNCIL DYSPNEA SCALE**

ID NUMBER:

FORM CODE: MRC VERSION: 1.0 10/26/10 Visit Number SEQ #

0a) Form Date 0b) Initials

Instructions: This form should be completed during the participant's visit. Choose the one best response.

Please choose the one best response to describe your shortness of breath.

Grade

0 "I only get breathless with strenuous exercise"

1 "I get short of breath when hurrying on the level or walking up a slight hill"

2 "I walk slower than people of the same age on the level because of breathlessness or have to stop for breath when walking at my own pace on the level"

3 "I stop for breath after walking about 100 yards or after a few minutes on the level"

4 "I am too breathless to leave the house" or "I am breathless when dressing"

1. Grade

(b) mMRC questionnaire [151].

Fig. 2.6 COPD questionnaires.

The aim of these tests together with the spirometry exam is to separate patients with a significant symptom burden from those with fewer symptoms. The groups of patients can be summarized as follow (Figure 2.7):

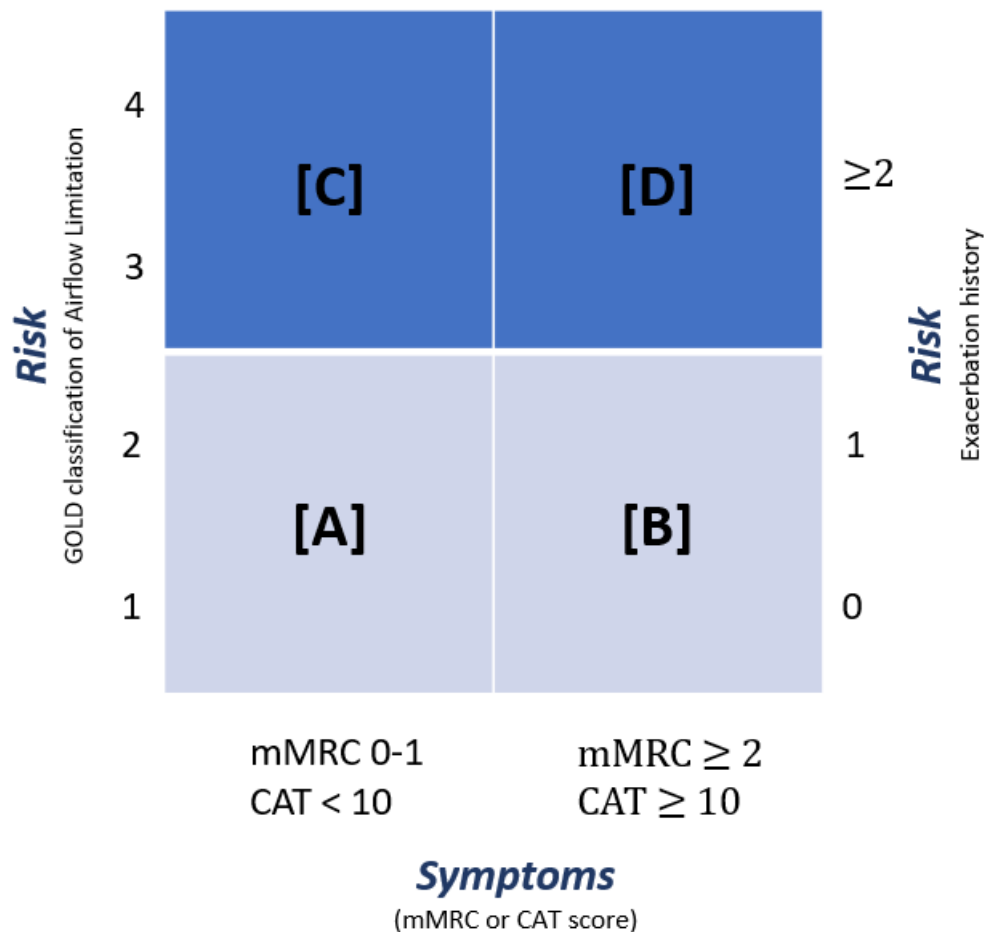


Fig. 2.7 The number represents the severity of airflow limitation (spirometry grades 1 to 4) while the letter (groups A to D) the symptom burden and risk of exacerbation [135]. The Low Risk for the patients is associated with the bottom part of the box, while the High Risk with the top part of the box.

- "Patient Group A: Low Risk, Less Symptoms
 GOLD 1-2 → Mild or Moderate airflow limitation
 0-1 exacerbation per year
 mMRC grade 0-1 or CAT score < 10

- Patient Group B: Low Risk, More Symptoms
GOLD 1-2 → Mild or Moderate airflow limitation
0-1 exacerbation per year
mMRC grade > 2 or CAT score > 10
- Patient Group C: High Risk, Less Symptoms
GOLD 3-4 → Severe or Very Severe airflow limitation
≥ 2 exacerbations per year or ≥ 1 hospitalized exacerbation per year
mMRC grade < 2 or CAT score < 10
- Patient Group D: High Risk , More Symptoms
GOLD 3-4 → Severe or Very Severe airflow limitation
≥ 2 exacerbations per year or ≥ 1 hospitalized exacerbation per year
mMRC grade > 2 or CAT score > 10"

2.7.2 CT technique

Nowadays computed tomography technique (CT) is a complementary diagnosis method for better evaluate the COPD gravity disease. Some airway abnormalities such as emphysema and airway-wall thickening can contribute to the progression of COPD.

Different studies extract quantitative measurements of emphysema and airways disease from thoracic computed tomography [52]. The used methods consider CT scans from a single inspiratory act, or also include the expiratory act. Furthermore, extra-pulmonary manifestations can be evaluated. Overall, CT can detect changes in vessels, which usually are strongly linked with COPD but this analysis technique requires specialized personnel and expensive machines for being performed [32].

Chapter 3

COPD Biomarkers

The worst state of COPD is the manifestation of an Acute Exacerbation; for a patient, the happening of this condition means that the inflammation of bronchial wall increases with an influx of eosinophils, neutrophils and lymphocytes. These products can be detectable in the body fluids such as sputum, saliva or urine also that in the blood; it is proved that their concentration in the body samples is linked with the inflammation gravity, so new tools for COPD monitoring consider to study their levels in non invasive samples as a new ideal technique for assessing the development of COPD. Nowadays the used technique for the COPD diagnosis and follow up is blood analysis, but it has disadvantages such as the requirement of specialized medical personnel and sterile materials and analysis machines added to the fact that it is considered an invasive method, time-consuming and expensive [91]. New studies proved the presence of some blood biomarkers involved in the inflammation processes and representative of COPD gravity in a stable state and not, also in non invasive samples such as sputum and saliva [12]; the future goal is to find a cluster of the most relevant of them for predicting the onset of the worsening of COPD, the acute exacerbation. It is demonstrated that people suffering from numerous exacerbation attacks risk more in term of life condition respect to patients in the stable state, especially the hospitalized patients risk higher mortality and morbidity than patients can be managed at home [5, 124]. In this context, it is important to define that patients in the stable state are those do not have changes in the gravity of their inflammatory symptoms and life condition from the time of the diagnosis and their status continues to be the same associated with the initial gravity classification. The day-to-day increasing (two or more consecutive days) variations in two or more symptoms determines the end of the stable state and the necessity for the patients of changing in the regular medication, while in the worst case the needing of hospitalization and medical intervention [11]. Frequent acute exacerbations of COPD are associated with accelerated decline in lung function, in severity increasing of the disease resulting in the

decline of the quality of life and higher difficulties to accomplish daily activities [5]. In the worst case it causes hospitalization [11]. COPD exacerbations are often triggered by airway infections such as Bacterial Infections, Viral Infections, Co-existing viral and bacterial infections, and other [11, 5, 177] ; as introduced before, during an acute exacerbation, airway neutrophils such as Interleukin-6 (IL-6) and Interleukin-8 (IL-8) increase compared to the stable state; they together with Tumor Necrosis Factor (TNF- α) are mediators of the inflammation and stimulate the release of proteases such as Neutrophil Elastase (NE) and metalloproteinase 8 and 9 (MMP-8, MMP-9) and also of reactive oxygen species which damage the airway epithelium and lead to worsening of airflow limitation [5]. Furthermore, C-reactive protein (CRP) concentrations are elevated in inflammatory cases, so it is true for conditions such as COPD [66]. On the base of these data, in this chapter a review of the concentration of these biomarkers and their evolution and correlation in the time is reported for blood , sputum and saliva samples of different cohorts including healthy and COPD patients. There is, therefore, the need of creating a ‘ cluster of biomarkers’ that can improve sensibility, consistency and accuracy and provide objective prediction of exacerbation. The goal also would be monitoring the stable state of COPD and be able to differentiate different stages [189]. A symptom-based definition method for exacerbation should be developed, which considers the daily evolution of the airway inflammatory markers, quality of life, and rate of decline in FEV₁. A daily recording of the symptoms variation on a diary by patients such as increasing in sputum purulence, can be coupled with the interpretation of the quantitative biological data registered by a point-of-care device and sent from home to the specialized personal thanks to the advantages in recent Tele-healthcare.

3.1 Blood biomarkers for COPD

In literature, great importance is given to the correlation between biomarkers concentration in body samples and the COPD severity state [155, 22, 46]. For example IL-6 is a pro-inflammatory cytokine that increases locally in the airways and systemically in COPD, especially in association with acute exacerbations [71]. It has a role in the enhancement of organ inflammation and also creates a stimulus to the CRP formation; however, biological elements such as lymphocytes, macrophages, epithelial cells and neutrophils produce IL-8, which is a chemotactic cytokine with the role of recruiting neutrophils. *Bradford et al.* [19] in their study analyzed the concentration of 9 cytokines and chemokines in a significant cohort, evaluating the criteria for studying COPD. From the results, IL-6 and IL-8 were independently associated with the decline of ($FEV_1\%$) and FEV_1/FVC . IL-6 could differentiate the COPD stages and it was associated with more rapid progression of airflow obstruction, emphysema progression and more rapid rate of decline in lung function. Furthermore IL-8 was directly associated with progression of emphysema. They concluded that these biomarkers might add additional predictive value on data clinically collected with spirometry. Furthermore, in [22] IL-6 was also directly associated with the wall area as a percentage of total airway area (WA%). The biomarker CRP is a protein usually present in acute-phase inflammation conditions; its production is stimulated from the IL-6 activity and raises in conditions such as infections or sistemical morbidity. Together with IL-6, CRP could, therefore, provide a link between airway inflammation and systemic inflammation [66]. *Hurst et al.* [66] studied plasma samples at exacerbation of COPD for confirming the diagnosis; the most selective biomarker resulted being CRP which concentration increased at the Acute exacerbation. At the same time, the patients recorded the increase of some important symptoms such as sputum volume and purulence, and changes in the brief rhythm. CRP concentration alone cannot be sensitive for an accurate exacerbation prediction. Furthermore, *Zemans et al.* [189] proved that multiple biomarkers can predict disease severity, progression and mortality in COPD; in the combination of biomarkers chosen, CRP was also included. They demonstrated that CRP tends to be elevated in patients with frequent exacerbations, it can be individually associated with airflow limitation (FEV_1/FVC and FEV_1). Similar result are reported in [37, 34]. In [22] CRP was directly associated with wall area as a percentage of total airway area (WA%). In *Karadeniz et al.* study [72], CRP values were found in high levels in patient with low FEV_1 in COPD. Its values were higher in ex-smoker and current smoker than in non-smoker patients, it reached the highest value for smoker patients with COPD. In their study, they did blood analysis for a cohort of 64 patients at the hospital acceptance. From the CRP level results obtained, they demonstrated the potential role of this biomarker in predicting outcome in acute exacerbations; they specified a threshold of 10 mg/dl for delimiting the risk

area. Furthermore, they concluded that CRP can be associated with the gravity of airflow inflammation and risk of death. They also reported increased CRP values in the presence of Bacteria Virus and infections. Furthermore, during inflammation processes the Matrix MMP-9 degrades components of the extracellular matrix; it is considered to be a gelatinase B while MMP-8 a neutrophil collagenase. *Ji et al.* [71] found a relationship between MMP-9 and disease severity in COPD, by observing elevated levels in patients serum. *Brajer et al.* [59] also studied the concentration of MMP-9 in COPD patients and healthy controls, and they found that COPD patients had increased serum MMP-9 concentration compared with the control group, it was also negatively correlated with FEV₁ and FEV₁/FVC; they proved that higher MMP-9 serum concentration is connected with higher airway obstruction and disease progression. Furthermore, *Linder et al.* [90] reported same considerations regarding MMP-9 concentration in COPD patients serum, and found a link also with productive cough and decreasing of FEV₁; the increasing levels of serum MMP-9 indicated an enhanced proteolytic activity that is related to disease severity. The inflammatory response is also dominated by pleiotropic, proinflammatory mediator such as TNF- α that is capable of macrophage activation and stimulation of metalloproteinase production. *Ji et al.* [71] found lower levels of TNF- α in saliva and serum in smokers with COPD than in non-smokers; according to this, it seems that in the stable state it is a quiescent biomarker, that has higher values during exacerbations becoming biologically active. In a study of *Pinto-Plata et al.* [127] there was a positive relationship between the blood levels of TNF- α and the severity of the disease in patients with COPD. Furthermore, *Franciosi et al.* [49] demonstrated that serum IL-8, TNF- α and CRP showed a trend toward separation between COPD stages. In [11] serum TNF- α and CRP resulted in increasing in hospitalized patients at exacerbation. Neutrophil Elastase is a mediator in the pathogenesis of COPD [121]; at neutrophil degranulation, NE concentration increases. It can represent an ideal biomarker of COPD and disease activity. *Carter et al.* [20] studied different COPD biomarkers including NE and IL-8 and NE -specific fibrinogen degradation product, demonstrating its higher values in COPD patients respect to the controls, and also in the exacerbation onset. Furthermore, *Pawar et al.* [122] reported significantly increased levels of serum neutrophil elastase in COPD patient as compared to healthy controls.

Below there is a table where all the cited biomarkers are summarized (Table 3.1).

Table 3.1 Blood biomarkers for COPD.

Reference	Samples	Stable state COPD	Acute exacerbation
[19]	3240 COPD		
	551 controls	↑IL-8 ↑IL-6	-
[66]	90 COPD	↑IL-6 ↑CRP	↑CRP
[22]	146,255 COPD	↑IL-6 ↑CRP	-
[72]	64 COPD	↑CRP	↑CRP
[71]	23 Controls, 28 Smokers 29 Smokers with COPD	↑MMP-9 ↑TNF- α	↑TNF- α
[59]	23 COPD 23 Controls	↑MMP-9	-
[189]	>3000 COPD	↑CRP	↑CRP
[127]	48 COPD 48 Controls	↑TNF- α	-
[49]	COPD	↑IL-8 ↑TNF- α ↑CRP	-
[11]	145 COPD	↑TNF- α ↑CRP	↑TNF- α ↑CRP
[20]	COPD	↑IL-8 ↑NE	↑IL-8 ↑NE

3.2 Sputum biomarkers for COPD

Collection and analysis of sputum are a commonly used non-invasive means of assessing airway inflammation in COPD. Sputum is a product of the lungs; as explained before, it is a fluid which production increases in COPD patients as a consequence of the inflammatory process where inflammatory cells increase in number and size penetrating in the mucosa and conducting to its hypertension. Induced sputum can provide important information about the inflammatory process, it is easy to collect as a non-invasive sample. Biomarkers in sputum soluble phase can be measured using immunoassay such as ELISA test, and the repeatability of inflammatory mediators results consistent [169]. However, some disadvantages could present, such as neutrophilic inflammation caused by the inhalation of hypertonic saline solution, required from the standard procedure for sputum induction and collection; for this reason collection of non-induced sputum is preferred when it is possible. Inflammatory mediators in sputum during stability may predict future risk of exacerbations [155]. In *Paone et al.* [119] study, IL-8 sputum levels resulted increasing in individuals with COPD and also had a negative correlation with FEV₁ and FEV₁/FVC. *Franciosi et al.* [49] observed a trend toward separation of IL-8 between COPD stages and also registered increasing values of IL-6 in COPD patients compared with controls. *Fujimoto et al.* [51] studied the changing of IL-8 concentration between the stable state and during an acute exacerbation; they observed a significantly increase in its levels during the adverse attack from values in a stable phase. *Ji et al.* [20] found higher levels of IL-6 in sputum of smokers than non-smokers, and also IL-8 [31] levels higher in COPD patients compared with non-smokers. In [168] IL-8 resulted increasing at the visit prior to the exacerbation and also during the adverse event together with CRP; from these results IL-8 should be used as a predictor for a forthcoming exacerbation. *Eickmeier et al.* [43] compared COPD patients and cystic fibrosis (CF) ones with controls, and they observed more elevated levels of IL-6 and IL-8 in CF and COPD than controls; IL-8 was also correlated with lung functions. In [50] an increase is reported in COPD sputum of CRP levels during an acute exacerbation together with IL-6 and IL-8; however CRP biomarker requires further investigations in literature. Regarding the other biomarkers, *Paone et al.* [119] reported an increase of MMP-9 levels in sputum samples of COPD patients compared with the controls. The increased expression of MMPs is considered to be a key factor in the development of COPD, for this reason it was well inspected by *Vernooy et al.* [171] by using immunocapture assays. In their study they included MMP-8 and -9, which resulted higher in COPD patients than in controls. They were also strongly correlated to each other and positive related to the degree of airflow limitation. These results in subjects with mild-to-moderate COPD, support the concept of an impaired proteinase-antiproteinase balance in COPD. *Kleniewska et al.* [81] in their study included

COPD, asthmatic patients and healthy controls; they reported higher concentrations of MMP-9, IL-6 and TNF- α in induced sputum of COPD patients compared with healthy subjects and asthmatic patients; their data also confirmed that CRP is an important systemic biomarker while IL-6, TNF- α and MMP-9 are local biomarkers of an inflammatory process in the airways of COPD patients. *Illumets et al.* [68] found that MMP-8 may differentiate Stage 0 in COPD patients from healthy smokers; also MMP-9 levels were elevated in the induced sputum of non-symptomatic smokers and Stage 0 COPD. In [71] sputum TNF- α levels were under detection limit in almost cases, but its receptors TNFR1 and TNFR2 resulted positively related to IL-6 and IL-8 concentrations and higher in levels in COPD patients. In [74] TNF- α and IL-8 resulted to be involved in the inflammation process of COPD, and their levels in COPD sputum samples were higher than controls; similar results were reported in [11], where the TNF- α and IL-6 concentrations also increased at exacerbation, especially for hospitalized patients. In contrast, *Vernoy et al.* [171] did not find differences in TNF- α values in COPD patients and controls, but its receptors could differentiate the groups together with IL-8 in induced sputum, by presenting higher levels. TNF receptors were related with the degree of airflow limitation in patients with COPD. In [43] TNF- α differentiated between COPD and CF patients, resulting in higher values in these last ones. *Aaron et al.* [3] compared TNF- α and IL-8 values in sputum samples collected from COPD patients when they were clinically stable, during the time of an acute exacerbation, and one month later. Results show an important increment of their concentrations at exacerbation compared with when they were clinically stable, and also a consequent decline 1 mo later. In another study [6] they demonstrated that IL-8 too is higher in COPD patients than in controls. *Paone et al.* [119] reported increased NE sputum concentrations in individuals with severe airway obstruction as compared to subjects with mild and moderate COPD; so, NE could be capable of differentiating the COPD stages. Furthermore, from the obtained results it was correlated with the degree of airway obstruction linked to the Gold parameters. Data also demonstrated a correlation between NE and IL-8 sputum samples and pulmonary functions. In [24] elevated NE activity in sputum was associated with a higher frequency of exacerbations and independently associated with FEV₁ decline; it showed good discrimination for severe exacerbations and its levels increased during the happening of them. *Papi et al.* [120] demonstrated that sputum neutrophils increase in exacerbations of COPD patients and they were related to their severity independently of the association with viral or bacterial infections present in the samples. Similar results were reported from *Sethi et al.* [153] that in their study obtained sputum and serum samples before, at, and following exacerbations; the biomarkers included were sputum IL-8, TNF- α , NE and serum CRP. Exacerbations onset was associated with significantly greater increases from the baseline in sputum TNF- α and NE and serum

CRP. Clinical exacerbation severity was significantly correlated with levels of all markers. In another study [154] they evaluated the role of the same biomarkers as predictors for acute exacerbation; obtained results were valued and developed an area under the ROC of 0.79 for TNF- α , 0.68 for IL-8 and 0.76 for NE. They demonstrated that when they are combined with each other and considered all together, the area under the curve is 0.71, showing consistency and sensitivity for the prediction role.

Below there is a table where all the cited biomarkers are summarized (Table 3.2).

Table 3.2 Sputum biomarkers for COPD.

Reference	Sample	Stable state COPD	Acute exacerbation
[119]	42 Smokers, 42 COPD	↑NE ↑IL-8 ↑MMP-9	-
[49]	67 CG 37 I COPD, 23 II COPD, 19 III COPD	↑IL-6 ↑IL-8	-
[51]	68 COPD	↑IL-8 ↑NE	↑IL-8 ↑NE
[71]	29 COPD 28 Smokers 23 Non Smokers	↑IL-6 ↑IL-8 ↑MMP-9 ↑TNF- α	-
[168]	1 I COPD 14 II COPD 16 III COPD 9 IV COPD	↑IL-8 ↑CRP	↑IL-8 ↑CRP
[43]	19 Cystic fibrosis (CF) 26 COPD 21 Non Smokers	↑IL-6 ↑IL-8	-
[171]	17 COPD, 10 Smokers 7 Non Smokers	↑MMP-8 ↑MMP-9	-
[81]	20 COPD 24 Asthmatics 22 Controls	↑IL-6 ↑TNF- α ↑MMP-9	-
[68]	20 Non Smokers 12 Ex Smokers 28 Smokers 18 I-III COPD	↑NE ↑MMP-8 ↑MMP-9	↑NE ↑MMP-8 ↑MMP-9
[11]	145 COPD	↑IL-6 ↑TNF- α	↑IL-6 ↑TNF- α
[74]	14 COPD 12 Smokers 18 Non smokers, 23 Asthmatics	↑IL-8 ↑TNF- α	-
[171]	18 COPD, 17 Smokers	↑TNF- α receptors ↑IL-8	-
[43]	19 CF 26 COPD, 21 Controls	↑IL-6 ↑IL-8 ↑TNF- α	-
[6]	21 COPD, 8 Smokers 13 Ex Smokers	↑IL-6 ↑IL-8	-
[4]	50 COPD	↑IL-8 ↑TNF- α	-
[120]	64 COPD	↑NE ↑CRP	↑NE ↑CRP
[50]	33 COPD	↑IL-8 ↑IL-6	↑IL-8 ↑IL-6

3.3 Salivary biomarkers for COPD

Saliva is the last non-invasive sample described in this chapter; as explained before, the goal of this work will be to find a practical method for early diagnosis of diseases, that is crucial to prevent complication that could have a negative impact on patient's quality life. Saliva sample is easier and safer to use and work than serum. Its collection does not require medical invasive instruments but just a sterile container, and it can be done at home. Risk of contamination results minimum and its processing time requiring [70]. The hypotonic nature of saliva comes from the homogeneous composition of a mix of water, electrolytes and organic molecules [101]. These elements come from the serum and thanks to the intracellular passive diffusion that acts in the capillaries bed, enter into saliva. For this reason, a great number of molecules in saliva are representative of systemic diseases. The osmotic gradient takes place for driving electrolytes to enter in the saliva; the mechanism is also regulated by the rate of secretion and nature of stimulus [101]. Protein synthesis is the responsible of the organic components of glandular saliva. The data utility given from the samples depends on the kind of saliva analysed. The main salivary glands are the parotid, submandibular and sublingual. The whole saliva derives for 65% from submandibular, 23% parotid and 4% sublingual glands while the remaining part derives from minor salivary glands and contains constituents of non-salivary origin such as serum derived from mucosa and sites of inflammation, food debris and many microbes. Saliva can be collected in two ways, these are stimulated and non-stimulated; for diagnosis applications this last one is not preferred because it could contain foreign substances used to stimulate saliva and finally influence the final analysis results [101]. In literature there are many studies which prove the presence of the same blood and sputum biomarkers seen before, also in saliva samples [188]. The presence of salivary IL-6 and IL-8 was proved in patients with oral cancer or cardiovascular diseases; regarding COPD, further studies are necessary for exploring the correlation of its role with lung function. An interesting research was conducted by Blicharz *et al.* [16] that tested their electrochemiluminescence lab-on-chip device by analyzing saliva samples from COPD and asthmatic patients; in their results, values of IL-8 and IL-6 were definitely higher in COPD patients than in controls. Furthermore, in the European Respiratory Society annual congress 2013, it was reported a negative correlation between lung function and IL-8 and MMP-9 in smokers with COPD; they were also correlated with COPD severity. In this thesis, the goal will be to explore the IL-8 role in saliva samples of healthy people. This biomarker keeps attention because of its good characteristics reported for blood and sputum samples. Consistent results relative to its salivary concentrations may be an innovative method for disease assessment. Furthermore, elevated values of serum CRP are linked with inflammation and cardiovascular disease; the chance to measure it in non-invasive samples could be a great

opportunity for the development of non-invasive assessment of disease risk. *Dillon et al.* [41] investigated the relationship between blood and saliva CRP levels in healthy subjects, they did not find correlation but they were well measurable in both kind of samples. In contrast, *Patel et al.* [121] proved a strong correlation between salivary CRP and its serum counterparts. It also was able together with NE, to distinguish COPD patients in different stages, resulting higher than in controls. CRP concentrations were related to breathing scores and sputum features, but not for NE; patients with acute exacerbation had a median increase in both biomarkers. Furthermore, *Bhavasara et al.* [13] reported a positive correlation between serum and saliva CRP in COPD patients, that presented higher values than those in the controls. *Ji et al.* [71] reported a negative correlation between lung function and salivary MMP-9 and IL-8 in COPD patients in the stable state, confirming that their role may be related with the disease severity. MMP-9 presents an increase activity in COPD patients, corresponded with the airway obstruction and the destruction of the extracellular matrix [149]. It was confirmed also by *Mulyadi et al.* [107]; in their study unfortunately resulted that salivary MMP-9 was poorly correlated with FEV_1 , FVC, and FEV_1/FVC ratio. Furthermore, *Ji et al.* [71] reported lower concentration of TNF- α in COPD smokers in the stable state than in non-smokers, showing an attenuated response in moderate disease; it seems to be quiescent in the stable state while it becomes biologically active in more severely ill patients. *Patel et al.* in a first study proved that salivary NE and CRP increase during acute exacerbation; in a second moment [121], they showed how NE was able to distinguish between different stages of COPD disease, resulting higher than in controls and also increasing in its median value during an acute exacerbation. Together with CRP, they are reliable and reproducible in saliva, providing clinical-relevant information on health status in COPD.

Below there is a table where all the cited biomarkers are summarized (Table 3.3).

Table 3.3 Salivary biomarkers for COPD.

Reference	Sample	Stable state COPD	Acute exacerbation
[16]	Asthmatic COPD	↑IL-6 ↑IL-8	-
[60]	23 Smokers 28 Smokers COPD 29 COPD	↑IL-8 ↑MMP-9	-
[121]	20 Smokers 25 Non Smokers 16 I COPD 32 II COPD 39 III COPD 11 IV COPD	↑CRP ↑NE	↑CRP ↑NE
[13]	100 COPD 100 CG	↑IL-8 ↑MMP-9	-
[71]	23 Non Smokers 19 Smokers 28 Smokers COPD	↑IL-8 ↑MMP-9 ↑TNF- α	↑IL-8 ↑MMP-9 ↑TNF- α
[107]	30 Smokers COPD	↑MMP-9	↑MMP-9

Chapter 4

Experimental study case: Human IL-8 ELISA Test

4.1 Saliva collection and processing

The goal of this work is to explore the role of the biomarker IL-8 in human saliva of healthy people; the work is planned for evaluating differences between the subjects in different days, differences relative to the same subjects within the same day and also in different days; possible correlation with the smoke activity of the subjects is considered. The samples collection took place in the biology laboratory of the University of South-Eastern Norway (USN); a small cohort of five healthy people under 30 years old was analyzed. The saliva samples were obtained from Caucasian and Asian, males and females. Following the protocol for the saliva collection [190, 61], the volunteers were required not to drink, eat, smoke, have hygienic personal procedures one hour before the collection procedure. Saliva samples were collected two times a day at 10 am and 3 pm, immediately after lunch. The subjects rinsed their mouth with water for 1 minute. Five minutes later this oral rinse, the subjects started to spit into a 15 mL sterile tube, putting it on ice while they were producing more saliva. To the subjects was required not to cough up mucus as the goal to passively collect saliva, not phlegm. A minimum of 5 mL volume of saliva was collected from each person, as shown in figure 4.2. In the laboratory, the centrifuge was set to 4°C before the collection procedure, to make sure that it had reached the proper temperature for processing. The samples were centrifuged at 2,600g for 15 min at 4°C; the spin was repeated in the cases of incomplete separation of pellet and supernatants has occurred. The supernatants were collected into 15 mL Falcon tube and mixed briefly; 1 mL of supernatants was pipetted into 2 mL cryotubes (able to accommodate -150°C temperature) and treated for protein analysis as well described

below. The 2 mL cryotubes were put on the ice, later the following protease inhibitors per 1 mL of saliva supernatant were added, according to the protocol:

- 1 μ L Aprotinin stock 10 mg/mL
- 3 μ L Na_3VO_4 stock 400 mM
- 10 μ L PMSF stock 10 mg/mL

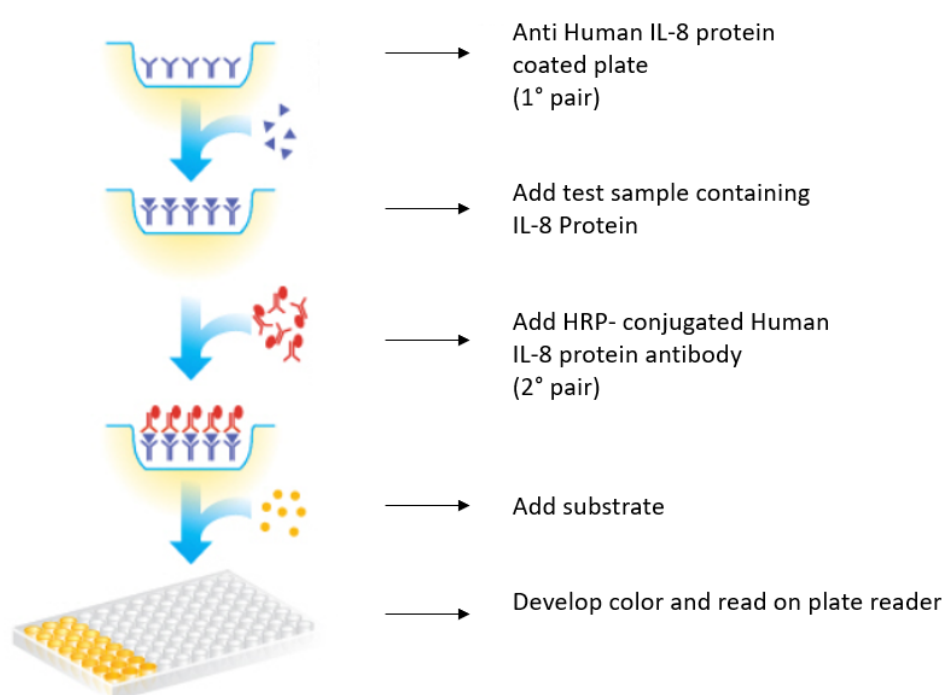
The tubes were inverted gently to mix, and later stored at -150°C in a cryofreezer. All the stock solutions were made with the help of the Doctor. Birgitte Kasin Hønsvall of USN.

4.2 Set-up and Methods

The ELISA Set used in this experiment comes from the OriGene company. It allows qualitative and quantitative determination of IL-8 in saliva supernatants, and it is able to recognize both natural and recombinant Human IL-8. The solid phase sandwich immunoassay is thought for a 'do it yourself' use. IL-8 is common in the form of 8.4 [Da], with a chain of 72 amino acids residues, which includes five additional N-Terminal amino-acids. As for all the CXC chemokines, it has four conserved cysteine residues. Data indicate that IL-8 may participate in the pathogenesis of COPD.

The ELISA method includes a capture Antibody highly specific for IL-8 coated to the wells in a microliter strip plate. During the incubation period, IL-8 samples bind to the capture antibodies in a first step. Subsequently in the same period, the complexes bind to the secondary capture antibodies. The unbound analyte and secondary antibody are removed by using a washing buffer. Following the protocol [40], the HRP conjugate solution is added to every well and finally the plate is washed for removing the excess conjugate. The progressive blue colored development is visible when the chromogen substrate is added to every well and reacts with the conjugate.

The colour development is then stopped by the addition of acid, turning the resultant final product yellow, as shown in the figure 4.3. The IL-8 concentration in the sample is directly proportional to the color intensity of the complex in the wells. The absorbance of the colour complex is then measured and the generated OD values for each standard are plotted against expected concentration forming a standard curve. The standard curve can then be used to accurately determine the concentration of IL-8 in the samples tested. The ELISA test procedure is schematically illustrated in figure 4.1.



The concentration of IL-8 protein is directly proportional to the color intensity.

Fig. 4.1 ELISA method illustration.



Fig. 4.2 a) Saliva collection b) Ice container c) Minimum of 5 mL of collected saliva d) Work table.

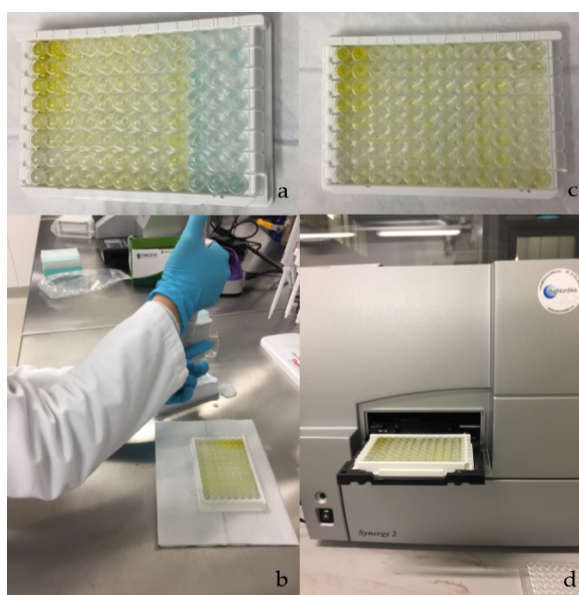


Fig. 4.3 a) ELISA plate not completely filled with the stop solution; b), c) The colour change is visible from light blue to yellow after the addition of the stop solution. d) ELISA plate positioned in the Synergy2 (BioTek) machine for the reading.

4.3 Materials and experimental procedure

The used reagent and materials were:

- IL-8 Standard: 2000 pg/ml
- Capture Antibody
- Biotinylated anti IL-8
- Streptavidin-HRP-Horseradish peroxidase
- TMB substrate
- 96 well microtitre plate
- Reconstitution Buffer (1xPBS, 0.09% Azide)
- Coating Buffer (1xPBS, pH 7.2-7.4)
- Wash Buffer (1xPBS, 0.05% Tween 20)
- Blocking Buffer (1xPBS, 5% BSA)
- Standard and Secondary Antibody Dilution Buffer (1xPBS, 1% BSA)
- HRP Diluent Buffer (1xPBS, 1% BSA, 0.1% Tween 20)
- Stop reagent (1M Sulfuric Acid)
- Microtitre plate reader with appropriate filters (Synergy2)
- 10,50,100,200 and 1000 μ L adjustable single channel micropipettes with disposable tips
- 50/300 μ L multi-channel micropipette with disposable tips
- Multichannel micropipette reagent reservoirs
- Distilled water
- Vortex mixer
- Miscellaneous laboratory plastic and/or glass sterile

For the plate preparation, the diluted Capture Antibody for one plate of 96 wells was prepared by adding 50 μL of Capture Antibody into 10 mL of Coating Buffer in a 50 mL sterile tube; consequently, 100 μL of diluted Capture Antibody was added to every well. The plastic plate was covered and incubated at 4° C overnight. In the successive morning, the plate was washed on the plate washer ELx50 with the standard program of three wash cycles, using wash buffer contained in a plate-washer bottle. Furthermore, 250 μL of Blocking buffer was added to every well after the washing step; the plastic plate was covered and incubated at room temperature (18 to 25°C) for 2 hours. Before starting the use of the plate, it was washed again in the ELx50 with the standard program.

The samples were fixed in the wells with a logical order for a successive easier study. Each sample, standard and zero was tested in duplicate. The run samples in total were 80, considering a total of four people and samples twice for day from each one, for a total of four days. As indicated in the protocol [40], for the standard preparation, "standard vials were reconstituted with the volume of the standard dilution buffer shown on the vial immediately prior to use; this reconstitution gave a stock solution of 2000 pg/mL of IL-8. The reconstituted standard was mixed gently by inversion only. The serial dilutions of the standard were made directly in the assay plate to provide the concentration range from 2000 to 62.5 pg/mL. Immediately after reconstruction 200 μL of the reconstituted standard were added to wells A1 and A2, which provided the highest concentration standard at 2000 pg/mL. 100 μL of appropriate standard diluent was added to the remaining standard wells B1 and B2 to F1 and F2. 100 μL was transferred from wells A1 and A2 to B1 and B2. The well contents were mixed by repeated aspirations and ejections taking care not to scratch the inner surface of the wells. The 1:1 dilution was continued using 100 μL from wells B1 and B2 through the wells F1 and F2 providing a serial diluted standard curve range from 2000 pg/mL to 62.5 pg/mL. 100 μL was discarded from the final wells of the standard curve (F1 and F2). After this, 100 μL of each sample were put into the respective well. 100 μL of standard dilution buffer was added into zero wells too.

Immediately prior to use, Biotinylated anti IL-8 Detection Antibody solution was prepared, by diluting the reconstituted biotinylated anti IL-8 with the biotinylated antibody diluent in an appropriate clean glass vial. For one plate, 100 μL of the reconstituted Detection Antibody was added into 5 mL of Biotinylated Antibody dilution buffer". Biotinylated Detection Antibody was provided in liquid form. After this, 50 μL of diluted Detection Antibody was added into all wells and the plastic plate was covered and incubated at room temperature (18-25 °C) for 1 hour. The next step was the washing one, with the same standard program used before on the ELx50. Immediately before use, Streptavidin-HRP solution was prepared; the vial was centrifugated for a few seconds in a microcentrifuge to collect all the volume at

the bottom. HRP solution was prepared by adding 5 μL of Streptavidin-HRP into 0.5 mL of HRP diluent buffer. After this, 150 μL of the diluted HRP solution was taken into 10 mL of HRP diluent buffer. Finally, 100 μL of Streptavidin-HRP solution were added into all wells. The plate was covered with a plastic cover and incubated at room temperature (18-25 $^{\circ}\text{C}$) for 30 minutes; after this, the plate was washed again with the standard program in the ELx50. Subsequently, 100 μL of ready-to-use TMB Substrate Solution was added into all wells. The plate was incubated in the dark for 5-15 minutes at room temperature; direct exposure to light was avoided by wrapping the plate in aluminum foil. Finally, 100 μL of H_2SO_4 was added into all wells as Stop Reagent. The absorbance value of each well was read in the Synergy2 using 450 nm as the primary wavelength and using 610 nm for the reference wave length.

4.4 Data analysis

The average absorbance values were calculated for each set of duplicate standards and samples. A standard logarithmic curve was generated by plotting the average absorbance of each standard on the vertical axis versus the corresponding IL-8 standard concentration on the horizontal axis (figure 4.4); the standard logarithmic curve was preferred respect the linear standard curve because of the value of R^2 that results to be 0.985 in confront of 0.8619 of the linear relation. This value represents the square of the correlation coefficient, and if it is near 1, it means that the predicted value of the dependent variable is reliable. The amount of IL-8 in each sample was determined by extrapolating OD values against IL-8 standard concentrations using the following equation (4.1) derived from the standard curve:

$$x = e^{\frac{y+1.3454}{0.353}} \quad (4.1)$$

where x is the dependent variable and represents the concentration [pg/ml] while y is the independent variable and represent the OD value.

From the results, these following comparisons were studied:

- IL-8 concentration differences between the different people in the different days referred to the two hours date for the collection;
- IL-8 concentration differences referred to one person on the same day, for a total of four days;
- IL-8 concentration differences referred to one person at the same hour within the four days.

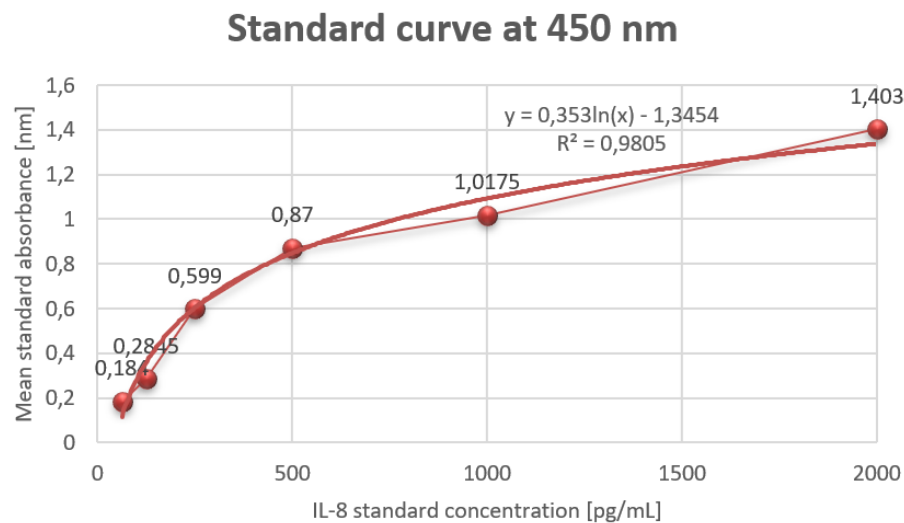


Fig. 4.4 Standard logarithmic curve for IL-8 ELISA Test.

4.5 Results

From the results the mean values and the respective standard deviations of the IL-8 protein concentration in saliva samples were 70.56 ± 4.28 [pg/ml] for the person 1, 77.36 ± 3.58 [pg/ml] for the person 2, 69.78 ± 4.95 [pg/ml] for the person 3, 95.40 ± 13.03 [pg/ml] for the person 4 and 66.98 ± 6.95 [pg/ml] for the person 5. The protein concentration in all the cases was not under the lower detection limit of 62.5 [pg/ml], as shown in the figures 4.5 and 4.6. In general, the absolute concentrations obtained depend on the used kit; results differ within kits of different manufacturers. Every kit provides its own cytokine standards and antibody, so it is not possible to compare the absolute concentration values in literature because they come from different kits and companies. In this study, the female subjects (person 2 and person 4) showed higher values of concentration compared with male ones, as shown in the figures 4.5 and 4.6. This observation was reported in another study of a bigger cohort [38]. It is known that immune defence capacity differs between men and women. For both genders, the IL-8 values resulted in being higher in the afternoon compared to the ones in the morning, for each day, as shown in the figure 4.7. One explanation could be that in the morning the human metabolism is in a sleep mode, however the mechanism under this results is unclear. It is known that cytokines levels during the day can change as a consequence of daily immunological reactions in the human organism. This is in agreement with the literature results, where IL-8 protein concentrations tend to be of low levels compared with other proteins during the days, showing a slight rise in the afternoon of each day compared with the morning [170]. Furthermore, it was studied that diurnal activities like sportive

exercises influence IL-8 levels making them higher [163, 123] . Moreover, every person seems to have a constant concentration trend during the different days, referred to the same collection hour, as shown in figure 4.8. However, from the results, IL-8 appears to be a stable biomarker in healthy people, in terms of concentration and daily trend. From the literature, it is known that its concentration tends to show high differences in inflammatory cases and starts to rise before an acute inflammation or, in the worst case, before an acute exacerbation. From these considerations, it is a good candidate as a sensor biomarker for the prevention goal, because there is the needing of a predictable biomarker.

Furthermore, doing a differentiation between smokers and non-smokers, in this little cohort only the people number 2 and 5 were healthy-smokers, but their IL-8 concentrations were not able to differentiate them from the other healthy non-smokers, as visible in the figures 4.5 and 4.6 .

The future work will be to measure IL-8 protein concentration in saliva samples of COPD patients; the results will be compared with ones obtained in this part. The goal will be to find the perfect cluster of biomarkers for the COPD exacerbation prediction. On the base of the literature research done, also the most relevant COPD biomarkers such as IL-6 and MMP-9 will be analyzed.

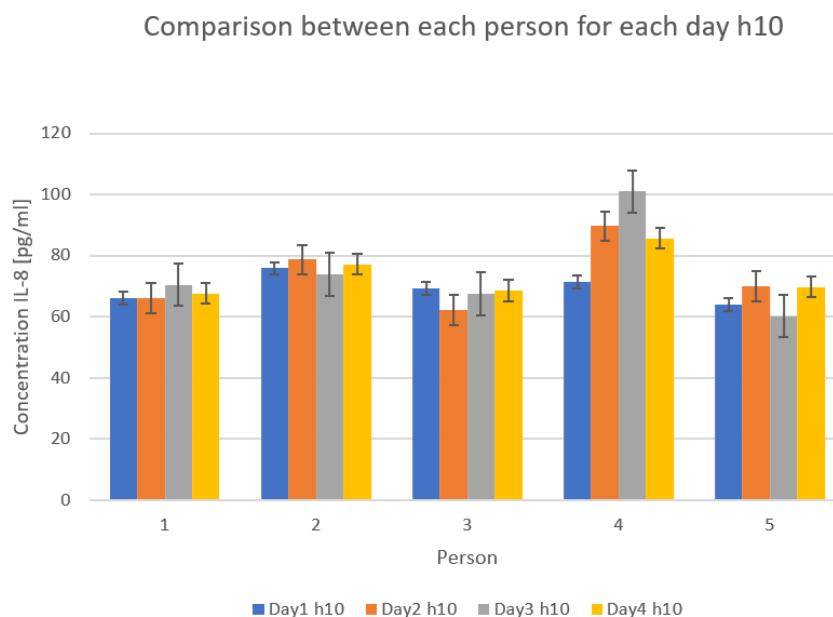


Fig. 4.5 From this graph it is possible to observe that IL-8 values are medially present in the range of 60-100 [pg/ml]; the subjects 2 and 4 shown higher values, maybe because of they are female. The subject 5 is a smoker, but the IL-8 concentration does not mark relevant differences compared with the other components of the cohort.

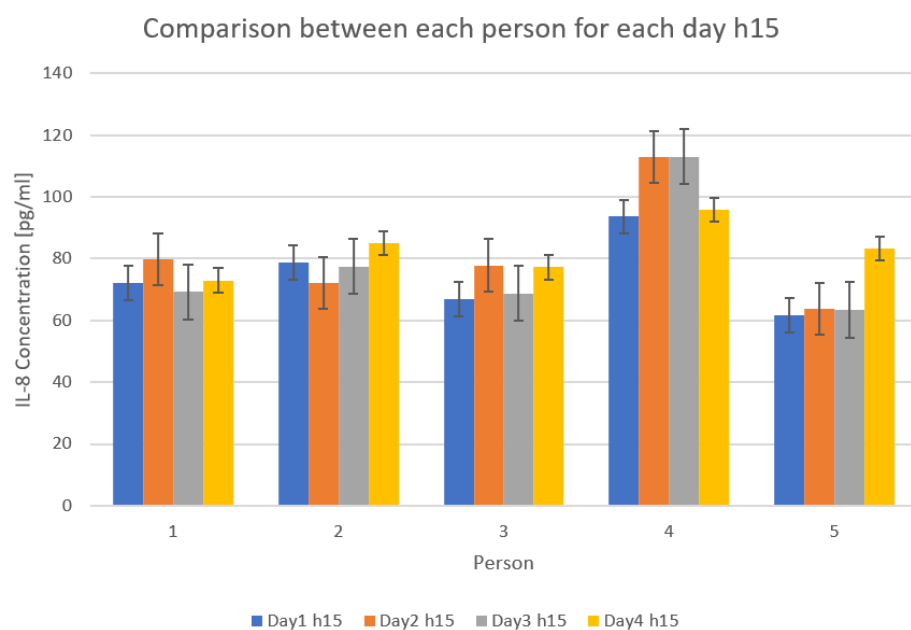


Fig. 4.6 From this graph the same considerations of the first one can be done, with the difference that IL-8 values tend to be higher and different if compared with ones in the morning.

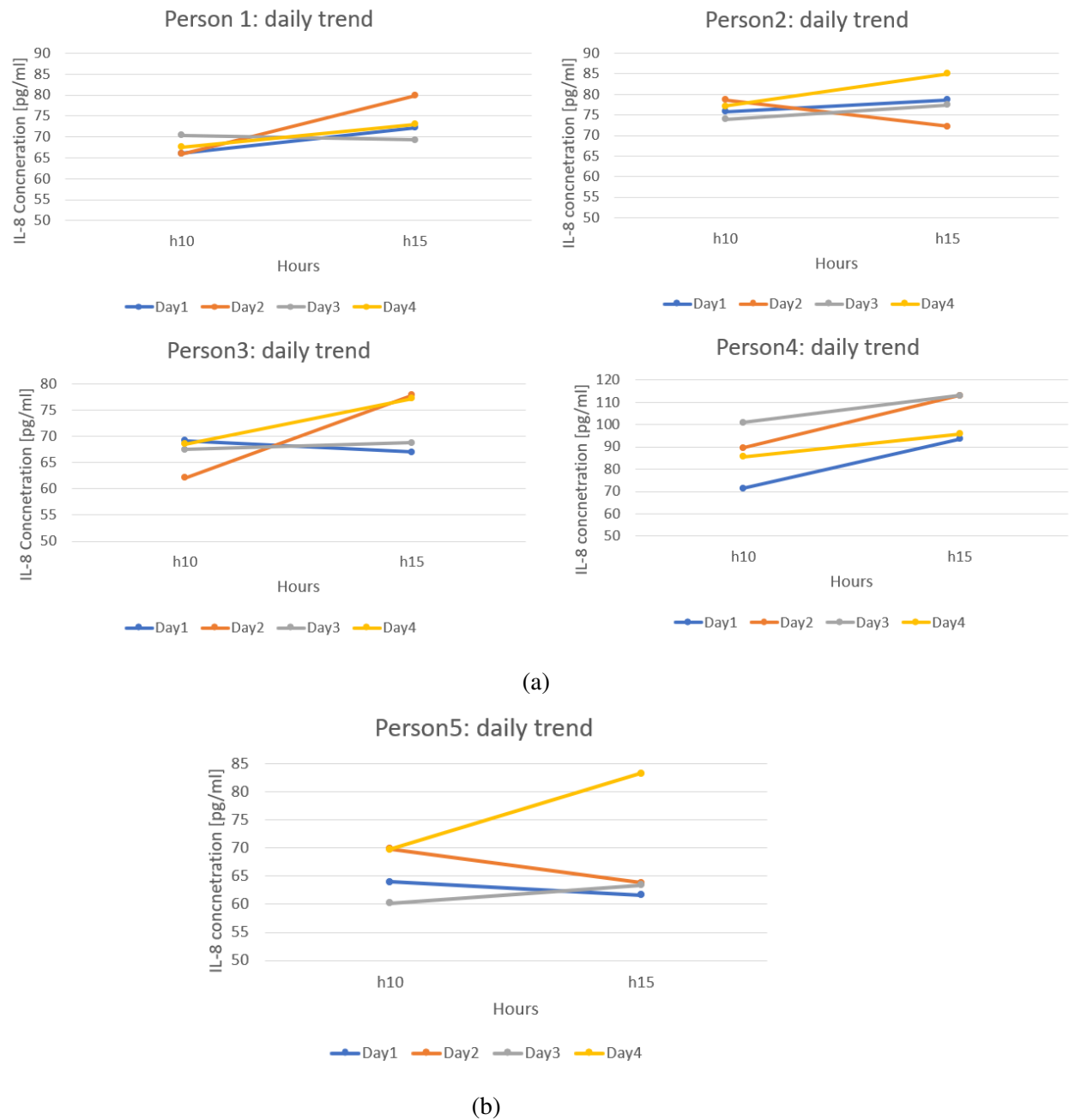
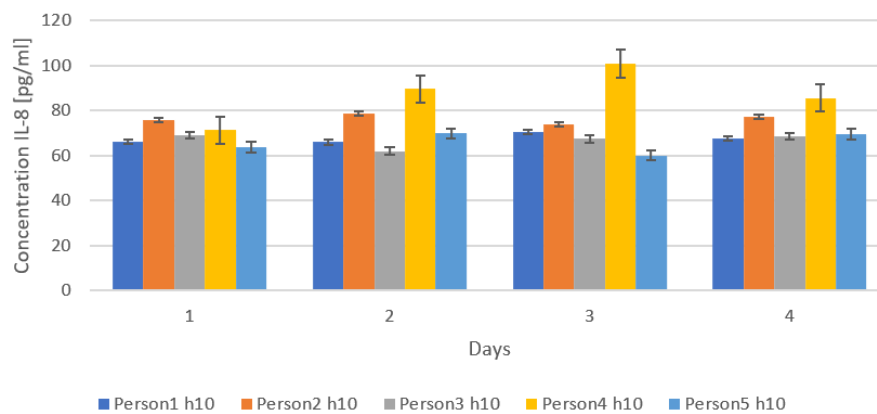


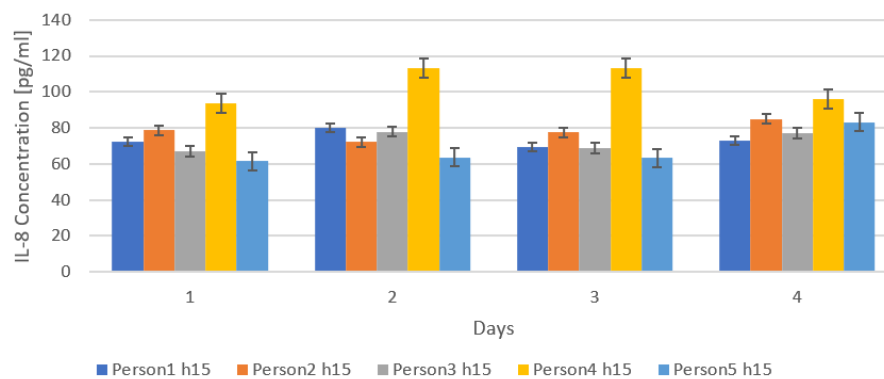
Fig. 4.7 In these graphs the differences are evident between the concentration values in the morning and in the afternoon; they tend to be higher in the afternoon.

IL-8 concentration trend for each person in 4 days: h10



(a)

IL-8 concentration trend for each person in 4 days: h15



(b)

Fig. 4.8 In the afternoon IL-8 values medially change in the range of 65-100 [pg/ml], reaching values higher than 100 [pg/ml] in the case of subject 4. Furthermore, referring to the same hour and to the same person, IL-8 values tend to be similar each day.

Chapter 5

Point-of-Care devices: State of Art and Proposal for COPD

Nowadays new technologies are adopted to monitor diseases such as cardiovascular or lung cancer, based on the concentration evaluation of biomarkers that are products of the inflammation processes, in invasive or non-invasive body samples, like blood, serum, supernatants, saliva, urine, sweat and other biologic fluids. A great number of studies concerns on the multi-detection of relevant biomarkers, for a better evaluation of the disease and for increasing the sensitivity and sensibility of the results. Studies demonstrate that the measurement of a single biomarker is not enough to diagnose a disease. Therefore simultaneous detection of multiple biomarkers at low concentrations simplifies treatment monitoring and diagnosis. The most conventional methods for biomarkers detection are microwell-plate based immunoassays such as ELISA kit, or polymerase chain reaction based, however, those require long analysis time (8 hours) [28] because of the low test speeds, complicated procedures that need specialized personal and finally high costs due to the products and the analysis machines and readers [183]. For these reasons this instrumental analysis method is unable to be used in on-site rapid detection. From these considerations, there is an urgent need for a more efficient detection method capable of measuring a defined number of correlated COPD biomarkers, that could allow an accurate, rapid, quantitative and easy operating kit for the analysis. Nowadays compact platforms called Lab-on-chip (LoC) have been spread thanks their capability to allow biomarker sensing and analysis through simple preparation method. These devices usually are portable, fast in the detection time and allow to manipulate chemical reactions in one step with high sensitivity. They also integrate new detection methods based on fluorescence, luminescence [183] electrochemiluminescence and electrochemical [185], biosensors and smartphone technologies. Furthermore, these devices are based on point-of-care (PoC) nanotechnologies, that have the goal to realize an accurate analysis

from a small body sample. Especially a non-invasive sample-based device is the key for a new self-portable approach for early- detection, diseases monitoring and follow-up, and in COPD case it is a promise for preventing exacerbations. LoC- PoC devices are known as BioMEMS; they are portable and contain all the necessary miniaturized elements for the analysis performance, such as electronic chip, detectors led and marker elements. The advantages are the ability to provide rapid and accurate results, easy to use, low cost and the little need for specialized equipment [164]. The goal of this work is to study the possibility of a new diagnostic and monitor device specific for COPD.

5.1 POC devices

5.1.1 Capillary flow paper based POC devices

Paper-based analytical devices are developed for rapid detection of one or more different analytes and are applied in a wide range of fields such as food-control, drug-control, pollution control and diagnosis of oral and systemic diseases at the PoC. The first design of these platforms is the ‘immunochromatography test strip’ (ICTS) [164] and it allows a qualitative or semi-quantitative (yes/no) analysis of the analyte presence just by looking the colour changing in the sensible test zones. When antibodies are deposited on the paper as bioreceptors, the device is also called ‘lateral flow immunoassay’ (LFIA). *Ran et al.* [139] in order to perform both qualitative and quantitative detection of disease biomarker such as Interleukin-6, made a highly sensitive peroxide test strip (PTS) based enzyme-linked immunosorbent assay (ELISA) in which a biorthogonal reaction was used as signal amplification; the change of color was visible from naked eyes for a qualitative test while a portable detector provided the quantitative analysis. This strip can be used as an effective signal readout strategy for detecting different analytes and can be applied in POC diagnosis. Nowadays LFIA is studied for quantitative analysis, that is necessary for diagnosis or prevention in the medical field, by improving the design and the signal intensity with materials that have luminescent, fluorescence or electric properties and allow the reading of the output signal through optical or electrical systems. These strips are known as ‘time-resolved immunofluorescent assay’ (TR-FIA) or ‘fluorescence lateral flow immunoassay’ (FLFIA). The reaction membrane is usually made of a nitrocellulose (NC) because of its excellent properties. However, polystyrene [31] or cross-linked silica [164] can be used; aspects such as assay sensitivity, accuracy, reagent deposition and test consistency are influenced by factors like the material, its shape and pore size that also influence the chemical, physical and flow proprieties in capillary action and incubation time. Thanks to the capillary property, the membrane does not need of external

forces or pumps for moving the sample. For selecting the best cellulose membrane sample properties, speed and device costs must be considered [185]; advantages are factors such as biocompatibility, biodegradability, flexibility and easiness of production worldwide, functionalization and disposal [9]. The LFIA consists of different main components that include the sample pad, conjugate pad, reaction membrane and the absorbent pad. These elements are assembled together and supported by a backing card. Typically conjugate pads are made of glass fiber. A small size of sample is loading on the sample pad that provides the pre-storage function and filters the analyte from particles and cells unwanted. The conjugation pad provides the dry-reagent storage for the antibodies specific to the bioamarkers linked to the particles that will generate the signal. After this pad, on the membrane there are the test line (it could be more than one for a multiple detection) and the control line, where specific antigens for the analyte are predisposed; here the reaction happens, and the results could be visible from a color change [7], from the emission of a luminescence or fluorescence signal [88, 159, 187] or from the registration of an electrical signal from the test zone if the paper is integrated with technologies such as electrodes [126, 125]. The absorbent pad collects the remaining sample part. An example of a single detection of one of the inflammatory biomarkers cited for COPD is from *Song et al* [159], that in their work developed a time-resolved luminescent lateral flow assay for the detection of CRP in serum. They provided a home-made fluorescence strip-reader capable of detecting the output signal in ambient condition, from the home made phosphorescent nanoparticles. Generally, the reaction on the test line can be based on a competitive or a sandwich immunoassay; a multiple detection is possible developing the LFIA with multiple test lines functionalized with different antibodies specific for the analytes, or by using new paper designs inspired to LTS [98, 99, 47]. The nanoparticles that provide the signal for the analysis, can be employed directly on the test lines or with the analytes in the sample before the deposition on the sample pad or also on the conjugation pad [73]. Nowadays simultaneous detection of different biomarkers is required essentially for time-saving and high accuracy and sensitivity; new designs are studied for reducing the cross-talking of the results between the different analytes. *Li et al.* [86] focused on two new paper configurations called 'Fork' and 'Peace-sign', for the detection of two whole cell bacteria on a nitrocellulose membrane; in both they rearranged the classical rectangular design of the LFTS. In their configuration the sample needed to be dropped onto the centre of the paper-design and it was capable of flowing through the test strip due to capillary action. *Martinez et al.* [98] proposed a method for lithographically patterning a paper to create well-defined microchannels, comprising hydrophilic paper bounded by hydrophobic polymer that allowed a multiple detection. In the 'tree' pattern, the central channel absorbed the sample by capillary and the pattern directed the sample from the wet zone into three

separate dry test areas, where the central one was used as test control; the presence of the analyte was detectable by paper color change due to colorimetric reagents. *Fenton et al.* [47] inspired by these works, proposed an alternative method of fabricating multiplexed lateral flow assays. They created a two-dimensional shape by using a plotter that could control the cutting in the x-y plane. *Wang et al.* [176] introduced a more elaborate design for a self-powered, one-step analysis chip. It allowed rapid, quantitative and multiplexed detection of proteins. The studied protein included CRP and IL-8; the lateral flow paper chip was pre-filter for removing the blood cells. The multiplexed ELISA assay was completed in the four reservoirs on the chip while a serpentine microchannel provided for reagent mixing upstream of the assay region. Furthermore there are studies about salivary applications of this kind of devices, such as *PerioSafe* [140], the lateral flow chromatography device, a MMP-8 oral fluid PoC-immunotest. This device was largely used in Africa, USA and Europe and had a great success as primary diagnosis test for oral diseases. Another application was the *ImplantSafe*, a MMP-8 rapid lateral flow chromatography immunotest for in-vitro diagnostic. It is a dip-stick test for the use in dental implantology. Both these tests were based on a Sandwich ELISA immunoassay and revealed a positive result by showing the two colored test and control lines. *Wignarajah et al.* [180] proposed a multiplex hand-held colorimetric diagnostic biosensor for the detection of Human Neutrophil Elastase (HNE) in saliva. The platform consisted of a protease substrates covalently bound to a round permanent paper magnet from one end while on the other hand to the two gold sensor surfaces. The analyte was dispensed on the gold surfaces and left at room temperature until dryness; during the proteolytic cleavage, the magnet attracted the cleaved magnetic beads and caused a visual observation of the bright gold surfaces by inducing the detachment of the monolayer on the two sensitive zones; the colorimetric results were available until 30 seconds and visible by naked eyes.

In this context, the specific devices relative to COPD biomarkers are summarized in the table 5.1.

All the discussed devices can be easily produced, stored and transported; these are advantages for clinicians and patients, especially those who live in developing countries.

Table 5.1 Capillary flow paper based POC devices relative to COPD biomarkers.

Device	Analytes detected	Sample	Detection	LOD	Time assay	Ref.
Chipbased on lateral flow immunoassay	CRP IL-8	Whole blood	Colorimetric	IL-8 (15 pg/ml)	<40min	[176]
PerioSafe	MMP-8	Saliva	Colorimetric	-	-	[140]
ImplantSafe	MMP-8	Saliva	Colorimetric	-	-	[140]
Luminescent lateral flow assay	CRP	Serum	Luminescence	< 0.2 ng/mL	-	[159]
Peroxide test strip ELISA	IL-6	Serum	Colorimetric	3.98 pg/mL	5s	[139]

5.1.2 Microfluidic POC devices

In the last years, the PoC applications of 3D microfluidic have grown considerably because of their ability to easy-drive fluids in combination with low costs and rapid fabrication. Firstly materials such as silicon, inorganic glass and ceramic were used for the fabrication process but nowadays the most common materials used are the ones with soft and rigid thermostatic and thermoplastic attributes, biodegradable paper [7, 8] and hydrogels [78]. Furthermore different fluidic operations like mixing, splitting, separation and filtration can be easy-adapted to POC devices by controlling many various design elements. An interesting application of this kind of devices was from *Chen et al.* [28], that developed a nanoplasmonic biosensor microarray label free device based on multiarray localized-surface plasmonic resonance for monitoring the concentration of serum biomarkers including IL-6 and TNF- α . They used a polydimethylsiloxane(PDMS)-glass substrate for parallel microfluidic channels functionalized with nanorods (AuNRs) necessary for the reaction with the analytes. Generally, PDMS has good proprieties such as optically transparency, elastic and cures at low temperature; it also can interact with a great range of materials after being exposed to air plasma [148] and it has other advantages such as the lowest autofluorescence across the visible spectrum of many plastic and glass materials also used in these kind of applications, and at the end hydrophobic properties that allow easy coating of protein with simple adsorption from solution [53]. The microfabrication is easy and low cost, including methods such as soft-lithography [113], photolithography [45, 30], casting injection molding [128], imprinting, hot embossing, laser cutting [148] and others; for all these reasons, it is one of the most common elastomers used for these applications. *Gervais et al.* [53] used PDMS substrate for making a one-step immunoassay for PoC diagnostic; in this case they wanted to detect CRP in human serum or plasma, so developed a device capable to solve this goal itself by just adding a drop of sample. Capillary forces dominated the device's work, but the flow rate was improved by including microfluidic functional elements on the platform. Another good substrate material is polymethylmetacrilate (PMMA), that compared to PDMS has the advantage of absorbing proteins directly onto its surface without the requirement for additional surface modification. *Mohammed et al.* [106] used this material for the realization of their platform in which through a sandwich immunoassay detected the biomarkers of interests. The sample moved thanks capillary force, in the microchannels made by CO_2 laser etching system. The chip was easy in the fabrication requiring just 5-6 minutes for the complete building. The fluorescence excitation was provided from a portable light source. The signal reader was in-house built. For focusing the excitation light on the sensing area, a biconvex planar lens was built on the substrate; in this case too, microfluidic elements such as capillary action stop, triggered and delay valves and also

meandering/turbulence structures were used to provide smart functionality of the autonomous system; the shape of the chambers minimized the formation of air bubbles. However, paper-based microfluidic have the ability of integrating the capabilities of microfluidic systems with the flexibility of the lateral fluorescence test strip technology; microchannels allow to restrict fluids and to direct them in a controlled manner to the sensing areas for single or multiple biomarkers detection. Methods for paper-based fabrication are photolithography, construction of hydrophobic barriers in the hydrophilic paper matrix by channel patterning, 2D-cutting that acts through computer-controlled X-Y knife plotters or CO₂ laser cutters [148], and others. This last technique is preferred when contaminations or interferences with chemical reactions are undesirable on the device; with these methods, the reagents and analytes interact in a defined area without cross-contamination or mixing and spreading in the surrounded area in simultaneous detection cases. *Abe et al.* [8] proposed inkjet printing as alternative construction technique, that is a promise in terms of time-saving and low-cost alternative especially for income countries, because it does not require the use of a specific mask and cleanroom. They developed a microfluidic multianalyte chemical sensing device paper based for the simultaneous detection, where the 3D hydrophilic microfluidic patterns were connected on a central sample inlet area; three sensing areas and a reference area were firstly made on filter hydrophobic paper by inkjet etching, and thereby by locally dissolving a hydrophobic poly(styrene) layer. Secondly with the same inkjet printing device, chemical sensing inks were printed and also the gold-labeled antibodies were spotted for the analyte-specific colorimetric reaction, resulting in an ‘all-inkjet-printed’ microfluidic system. This structure prevented the uncontrolled spreading and dilution of the samples and also no external pumping systems were necessary because of the capillary action. The same group of researchers also made a new prototype of ICTS [7], deleting the needing to assemble different pad components that is always present in the classical LFS design and concerning on a new one for a ‘single-pad’ ICTS; the proposed immunochromatographic device was made from a single piece of filter paper, where the microfluidic channels pattern and the dispensing of immunosensing inks for a sandwich immunoreaction were realized by a single apparatus; the inkjet-printed antibodies on the test line and control line were immobilized by physical absorption, they reacted with the analytes of the sample that moves from the inlet area to the sense lines thanks capillary action. *Han et al.* [58] proposed a 3D slip-PAD where the 3D microfluidic network was developed by layered construction of wax-patterned papers and provided different fluidic paths for the sequential delivery of multiple fluids in a single step, without the needing for peripheral equipment. The manually movable slip design made it user-friendly; the fluids delivery to the detection zone of MMP-9 was allowed by the overlap of the multiple paper layers that composed the device, providing a 3D fluidic channel and

also by the wax hydrophilic/hydrophobic barriers patterned. The colorimetric output signal was visible after 10 min, gave by the reactions of the analytes with the AuNPs. A quantitative detection was done by software analysis. *Nie et al.* [110] developed a microfluidic device for multiplex biomarkers detection in saliva samples. The studied proteins included IL-8 and MMP-9 that interacted with a PDMS substrate, worked with surface passivation for improving the compatibility with the biological analytes. The platform included an array of cylindric microwells designed for hosting the sandwich immunoassay between the protein and the antibody-functionalized microsphere. This architecture differentiates from other applications where the deposition of the antibodies onto the surface happens trough spotting. Its advantages are the reproducibility in the attachment of antibodies on the surface and also allows shorter analysis time. Integrated actuator valves on the SDR were used to control the delivery of the analytes and the mixing of the saliva sample, biotinylated detection antibodies, fluorescent probe and washing buffer automatically. Thanks the good performance demonstrated by the LOD values of this platform, this rapid and sensitive microfluidic chip could be utilized in POC applications. Furthermore, *Wu et al.* [184] proposed a PDMS microfluidic platform for evaluating IL-8 concentration to sputum samples from COPD patients. They used a SU-8 photoresist, creating microfluidic channels with a zig-zag shape: this technique improved the pressure gradient between inlet and outlet, developing a laminar flow without the help of external elements. In this study, a negative correlation was demonstrated between the IL-8 concentration and FEV₁/FVC value in COPD patients and also the chance to detect different stages of COPD severity; this microfluidic system could assist COPD diagnosis and be useful to monitoring at POC. The concentration of IL-8 in saliva samples was also studied by *Qiu et al.* [134], that presented the building blocks for a disposable, luminescence-based microfluidic immunoassay cassette and they demonstrated their integration in a POC diagnostic system. All the reagents needed for the analysis were prestored on the platform by liquid form and the fluid motion was driven from the top storage to the bottom chambers by depressing finger-actuated pouches. In this context the devices relative to COPD biomarkers are summarized in the table 5.2.

Table 5.2 Microfluidic POC devices relative to COPD biomarkers.

Device	Analytes detected	Sample	Detection method	LOD	Time Assay	Ref.
Localized surface plasmon resonance (LSPR)-based microfluidic optical biosensing device	IL-6 TNF- α	Human serum	Localized surface plasmon resonance	TNF- α (11.43 pg/mL) IL-6 (11.29 pg/mL)	40 min	[28]
Capillary-driven microfluidics device	CRP	Human serum	Fluorescence	1 ng/mL	< 14 min	[53]
Microfluidic device	MMP-9	Saliva	Fluorescence	10 pM	30 min	[58]
Microfluidic	IL-8 MMP-9	Saliva	Fluorescence	IL-8 (4 pg/mL) MMP-9 (3 pg/mL)	>2h	[110]
Microfluidic platform	IL-8	Sputum	Fluorescence	-	2 h	[183]
Microfluidic platform	IL-8	Saliva	Luminescence	-	<20 min	[134]

5.1.3 Electrochemical POC devices

Electrochemical biosensors are a powerful alternative to luminescence or fluorescence based devices, thanks some advantages like the ability to allow the detection in different strategies such as amperometric [134], potentiometric [131, 191] or by impedance [132] and capacitance detection [23, 2, 48], the easy nanofabrication and integration on chip. Comparing the electrochemical devices with the luminescence based sensors, they are insensitive to ambient illumination conditions and impurities in the samples, granting good sensitivity and stability [191]. These new technologies can be integrated with paper-based devices and also with PADs; furthermore, they are low cost and allow simultaneous detection. One disadvantage could be that not all the biomarkers are electrochemically active and this is one of the necessary conditions for being detected, so other strategies must be adopted [117]. The available designs for synchronous detection are multi-label [23] and multi-electrode platforms [191, 167, 181] but especially these last ones are preferred in PoC applications, due to their capability to accurately separate the detection areas reducing cross-talk and improving SNR, robustness sensitivity and accuracy. Basically, three electrodes of metal conductive material are printing on the sensible area [132] where the reaction happens when they are immersed in the sample solution, those are the working (WE), reference (RE) and counter (CE): the WE is sensible to the current developed by the boundary reaction for example between an antigen and an antibody element, so its detection allows the definition of the analyte concentration; the RE is used to maintain the solution at a given potential and the CE provides a current that allows the redox reaction in the solution. *Rodriguez et al.* [167] developed an electrochemical bio-platform for the simultaneous determination of interleukin (IL)-8 mRNA and IL-8 protein in saliva; the amperometric detection was based on the signal sent by the functionalized magnetic beads (MBs) linked on the dual screen-printed carbon working electrodes (SPCEs). For simultaneous detection of multiple biomarkers, each sensible area must have the printed CE and RE, a WE for each biomarker and the board circuit for the signal transmission and also each WE must be functionalized with the respective antibody specific for the analyte bounding. The WEs position on the device was structured and optimised for reducing the signal cross-talking between the adjacent sensible zones, that could give erroneous results. *Wan et al.* [174] proposed a multiplexing electrochemical immunosensor based on disposable screen-printed carbon electrode array of 16 channels for the detection platform; the multi-labeled assay was realised by functionalizing the WE with capture antibodies following a three step protocol, and also multiwalled carbon nanotubes were used. The screen-printed CE (SPCE) array could accurately detect biomarker sample with very high sensitivity and broad dynamic range, as demonstrated from the LOD for IL-8 that was 8 pg/mL, so that could be a promise for the POC applications.

Furthermore, *Malhotra et al.* [95] used single wall carbon nanotubes in the configuration of forest electrodes, functionalized with capture antibodies for detecting the protein IL-6 through an electrochemical sandwich immunoassay, and dispensed on a basal plane pyrolytic graphite disks; the multilabel amplification improved the high sensitivity. The electrochemical detection of the label gave signals proportional to the amount of the antigen. *Ojeda et al.* [115] studied the concentration of protein IL-6 in human saliva by using an innovative electrochemical magnetoimmunosensor device. They used carboxyl magnetic nanoparticles, covalently bound to the antibodies thanks a surface functionalization. Furthermore the use of poly-HRP-streptavidin allowed the signal amplification. The obtained results were statistically in agreement with those provided by commercial ELISA kit. Moreover, *Wei et al.* [109] studied an electrochemical device for the detection of IL-8 protein and IL-8 RNA by introducing a conducting polymer based interface put on the top of the metal electrode for reducing the protein denaturation that occurs when it is immobilized on the surface. The results demonstrated that the bio-abiotic interface greatly improved the signal transduction process; the pattern of chip consisted of 16 sets of 3-electrode system fabricated via photolithography, each one had a cyclic square-wave form electrical field and was used for electro-polymerisation. In this part, the electrochemical and electrochemiluminescence devices related to COPD are summarized in table 5.3.

5.1.4 Electrochemiluminescence POC devices

Electrochemiluminescence (ECL) devices combine the advantages of chemiluminescence and electrochemistry, those also include microfluidics platforms advantages for simultaneous detection. For example *Dong et al.* [129] realised a PMMA chip integrated with an array of eight ring-shaped organic photodiodes. They used gold nanoparticles attached to the microfluidics chambers. The chemiluminescence was directly correlated with the concentration of the molecules. In this device only one inlet point was present and from that eight microchannels drove the sample into the chambers. For each one there was an outlet port for discarding the content after each incubation step was performed. The photocurrent signals were detected by the OPDs aligned with the corresponding chambers. The excellent optical detection properties coupled with the advantages given by the GNPs that improve the performance of the biosensor, grantee the device as a future PoC application. In a second work they tested the same device with saliva samples for detecting IL-8 concentrations, showing good consistency [42]. Another example of COPD biomarker detection is from *Sardesai et al.* [150] that reported the fabrication of a novel electrochemiluminescence immunosensor array. The materials used were carbon nanotube forests disposed onto the bottom of wells with hydrophobic polymer walls. These last ones were made on a conductive pyrolytic graphite chip connected to a potentiostat. The barrier separation allowed the multiple detections of biomarkers including IL-6. Light was measured with a charge-coupled device camera and results were well-correlated with single-protein ELISA; the array is easily adaptable to microfluidics POC devices.

In this part, the electrochemical and electrochemiluminescence devices related to COPD are summarized in table 5.3.

Table 5.3 Electrochemical (EC) and electrochemiluminescence (ECL) POC devices relative to COPD biomarkers.

Device	Analytes detected	Sample	Detection method	LOD	Time assay	Ref.
EC device	IL-8 protein IL-8 mRNA	Raw saliva	Amperometric	IL-8 protein (72.4 pg/mL) IL-8 mRNA (0.21 nM)	5h	[167]
EC device	IL-8	PBS buffer	Electro-reduction current	8 pg/mL	Real time after 50 s	[174]
EC device	IL-6	Squamous cell carcinomas of head and neck	Amperometric	0.5 pg/mL	Real time	[95]
EC magneto immunosensor	IL-6	Human saliva	Amperometric	0.39 pg/mL	245 min	[115]
EC device	IL-8 protein IL-8 mRNA	PBS buffer	Amperometric	IL-8 protein (100-200 fg/mL) IL-8 mRNA (10 aM)	Real time after 60 s	[109]
ECL device	IL-6	Calf serum	Electrochemiluminescence	10 fg/mL	1.1 h	[150]

5.1.5 Optical POC devices

Optical biosensors are recently increasingly developed because of their portability, simplicity, quick response and availability for various quantitative measurement techniques such as fluorescence, surface plasmon resonance (SPR), local SPR, absorption, refraction, Raman, luminescence and interferometric [79]. These devices can be classified into label-free and label-based modes; in the first category the analyte directly interact on-site with the transducer and generates the signal. In the second category, the labeling with a specific material generates the optical signal such as colourimetric, luminescence or fluorescence response [79]. A significant number of optical devices is based on nanomechanics and cantilever technologies, where the analyte binding is linked to the deflection of the mechanic part due to the changing of surface stress. SPR and waveguide interferometry utilise the evanescent field in close proximity to the biosensor surface to detect the interaction of the analytes with the specific nanomaterial. SPR phenomenon occurs when an interface is present between two materials of opposite conductivity. When it is excited with light at the specific angle, the conduction electrons enter in a resonant oscillation [79]. Another class of new biosensors is fiber-optic based; they use an optical fiber as biosensing platform that is in contact with the analyte of interest, and light is propagated through it to the sample. The same fiber or an additional one measures the light absorbed by the analyte, that is proportional to target concentration [36]. Furthermore, transmittance-based detection is commonly used for real-time quantitative analysis by measuring the absorbance of the light transmitted through a substrate such as paper positioned between a LED and a photodiode; *Rajeev et al.* [138] integrated this method with label-free TNF- α detection. The anodic transducer consisted of a thin film of nanoporous aluminium, functionalized for hosting the biomolecules. The bounding of TNF- α to the conjugates within the pores caused a change in effective optical thickness (EOT) of the NAA thin film. The quantitative analytes detection was done by monitoring the time evolution of EOT in software analysis. The optical detection method commonly uses fluorescence principle coupled with CMOS technologies for light detection and colour discrimination, allowing the creation of new POC solutions [126, 125, 156]. In this context it is important to specify the difference between fluorescence and chemiluminescence, where this last one is the luminescence generated by the development of chemical reactions while the fluorescence is a consequence of the excitation wave on the nanomaterial used in the different applications. An interesting application for COPD biomarkers is from *Kemmler et al.* [76] that reported about a POC device for multiple detection of CRP and IL-6 on-chip, by detecting the fluorescence comes from an immunoassay reaction. The measurement system was based on Total Internal Reflection Fluorescence (TIFR). The planar waveguide introduced into the chip drove the light excitation. The fluidic system was fully automated

and was capable of performing fluid handling steps such as dilution, mixing, metering, separating, pre-incubating, incubating and washing controlled by the system software in a scripting process.

In this part all the optical POC devices related to COPD are summarised in table 5.4.

Table 5.4 Optical POC devices relative to COPD biomarkers.

Device	Analytes detected	Sample	Detection method	LOD	Time assay	Ref.
Optical device	TNF- α	Human serum or plasma	Interferometric Reflectance Spectroscopy (IRS)	0.13 g/ mL	Real time	[138]
Optical device	CRP IL-6	Human serum or plasma	TotalInternal Reflection Fluorescence (TIFR)	CRP (0.35 ng/mL) IL-6 (0.27 ng/mL)	25 min	[76]

5.2 Used nanoparticles in POC devices

5.2.1 Quantum dots (QDs)

Quantum dots are semiconducting crystals with a core and shell structure of a distinct semiconducting material, and with a diameter in the range of few nanometers. Typical configurations are CdS/ZnS, CdSe/ZnS, CdSe/CdS and InAs/CdSe. Core quantum dots have low fluorescence quantum yield due to surface related trap states; the adding of shell layer solves this problem because it increases quantum yield by passivating the surface trap states. The quantum yield can be defined as the ability to emit photons from the number of absorbed photons. QDs are capable of emitting in a wide range of wavelengths thanks their building in controlled temperature and pressure conditions. It is possible to obtain QDs of specific size and shape respectively of core and shell [130]. Physical characteristics of semiconducting materials are the conduction and the valence band, divided by a band gap. These components give optical properties to the material. The fluorescence phenomenon happens when enough energy is added in the system for allowing to QD to absorb a photon; in consequence, an electron jumps from the valence band to conduction band, leaving a hole in the valence band. The photon or light is emitted when electron and hole recombine. In QDs the energy can be directly quantised because of it is directly related to the dots size. They can be engineered to emit light from ultraviolet to infrared, and they do not suffer of photobleaching. The emission wavelength can be chosen by changing the particle size so that a single light source can be used for simultaneous excitation of all different-size dots [25]. These QDs are typically synthesised in organic solvents using organometallic precursors [145]. For many biological applications it is necessary to cover the QDs surface with a hydrophilic coating which enables conjugation to biologically active compounds such as antibodies, peptides or small ligands. Another main method used for allowing biological applications is based on exchange of the original hydrophobic surfactant layer with a hydrophilic one [69]. Conventional fluorescent dyes and water-soluble QDs can suffer from photobleaching and poor stability [31]. These can results difficult to use in the multiplexed detection requiring high performances. For these reasons *Chen et al.* studied new hydrophobic quantum dots, core/shell made with CdSe/ZnS materials [31], resulting in the solving of these problems. It is proved that their quantum yield is higher; they are also more stable and emit with a symmetrical peak in specific wavelength [185]. QD-FRET detection has also found a place in LoC applications. The acronym FRET means Fluorescence resonance energy transfer. This is a physical phenomenon between two particles, in which one gives the photon and the second one accept its transfer if it is inside the distance limit known as Förster radius [145, 69]. In this condition, the donor's emission declines while the acceptor's emission intensity increases. This phenomenon was applied

by *Li et al.* [88] by using a quencher system composed of carbon dots (CQDs) and silver nanoparticles; CQDs resulted in having advantages compared with the common QDs, such as low toxicity and excellent biocompatibility; they also perform of good light stability, easy functionalization, low cost and large quantities synthesis. In particular, graphene QDs are requiring great interest. They are two dimensional materials, with a maximum lateral size of 100 (nm). From many reviews [29, 193], they are classified as compatible for biological applications and possess low biological toxicity. They can be easily fabricated in large number through top-down or bottom-up low cost techniques; a top-down example is cutting different carbon sources (graphene sheet, carbon fibers, carbon nanotubes). A bottom-up method is starting from a solution of organic molecules or polymers which show reactive groups ($-\text{COOH}$, $-\text{NH}_2$) that can react through approaches such as hydrothermal, microwave, combustion methods. The high stability of GQDs comes from the presence of the crystalline chemical structure of the carbon core. The presence of a certain number of reactive groups on the surface, the size and the shape of GQDs influence the optical properties. They have the ability to absorb in a large wavelengths range and consequently to emit with a specific wavelength in a specific region that can be ultraviolet, visible or infrared. Different sources show their higher performances if compared with the conventional fluorescent QDs.

5.2.2 Gold nanoparticles (AuNPs)

AuNPs are new interesting particles used in different fields for their excellent characteristics such as the plasmonic resonance properties [28], easy synthesis and functionalization and unique tunable and distinct electronic properties. In the sensing applications, they can give colorimetric [86, 142], fluorescence-based [65, 28], electrochemical [129] and electrochemiluminescence [126, 125] output signals integrated with sensor technologies [44]. They exist in 1D, 2D and 3D configuration and their signal can be captured with different techniques such as optical absorbance, optical density measurement [142], fluorescence, Raman scattering [39], electric conductivity and magnetic or atomic force microscopy. They have good qualities, some in parallel with QDs, such as strong output signal, photobleaching absence, low toxicity, large surface-to-volume ratio and also, they are biocompatible [118]. They offer the chance to use the localized surface plasmon resonance (LSPR) phenomenon in array binding, where surface binding of analyte molecules is detected in real time from a shift in photon absorbing and scattering behaviours [28]. The band range for this phenomenon depends on AuNPs morphology and physiology [44]. They can be used for multiple detection thanks to their capability to give a colored output signal that differs for the size and shape of the fabricated nanoparticles [39, 86]. Nanorods (AuNRs) result to be superior to the common spherical gold nanoparticles thanks to their structural, optical,

electronic and magnetic properties and also their anisotropy structure allows simultaneous plasmon absorption in the visible region and the near infrared. The transversal band is linked with the visible region while the longitudinal band with the near infrared one [44]. Many different bottom-up and top-down anisotropy AuNPs construction techniques exist, including main synthesis methods for biological applications such as seed-mediated method that consists on making the structures in a ‘growth’ solution including the mix of metal precursors, reductant agents and surfactants, or the Lithography method based on the gold bulk sputtering from ion injection [87]. In the sensing field, AuNPs are commonly used especially in the biomedical domain thanks their easy surface functionalization with various biomolecules such as DNA, peptides and antibodies [83]. Furthermore they have a good biological stability in aqueous solution if functionalized with an external hydrophilic layer such as polyethylene glycol (PEG) based that is the most commonly used polymer [118]. FRET applications with AuNPs as fluorophores are also reported [65].

5.2.3 Magnetic Nanoparticles (MNPs)

Nowadays MNPs are commonly used in different biomedical fields such as magnetic resonance imaging (MRI) as contrast elements for imaging and targeting, cancer therapy due to their ability to induce local hyperthermia if stimulated by a magnetic force, drugs delivery, hard tissue repair, tissue engineering and also in biosensors [89]. They are usually made of pure metal materials such as Fe, Co, Ti, Ni, metal oxides materials such as iron oxides and ferrite [89], these are also magnetic elements. The magnetic properties depend from the nanoparticle size: nanoparticles with a diameter less of 20 nm show superparamagnetic properties [143], they have a permanent magnetic moment and the ability of agglomeration. If the diameter is from 20 nm and 200 nm they are called multi-domain nanoparticles and they do not have a magnetic moment if the magnetic field is not present and also they cannot agglomerate; the magnetic fields change along with the change of the size but also it is possible to specifically control the magnetic properties by making core/shell nanocomposite particles such as FePt/CoFe₂O₄ with different dimensions of the respectively diameters [117] and different concentrations of soft and hard magnetic phases [89]. MNPs are easy to synthesize by chemical methods such as coprecipitation, sol-gel reactions, aerosol/vapor methods and more [164]. The functionalization is required for numerous aspects such as prevention of MNPs aggregation for improving colloidal stability, increase of water compatibility, protection of the surface and also linkage to specific antibody, that can give a magnetic signal if excited by adequate magnetic forces [18]. Typical functionalization methods are ‘in situ surface functionalization’ where precursors for MNPs and coating material are simultaneously used in one step reaction mixture, and ‘post synthesis surface functionalization’ where the final

functional group is added after the synthesis with one of the three mechanisms that are ligand addition, ligand exchange and encapsulation [18]. Finally, for biological applications they can be easily modified with conjunction strategies for targeting the biomolecules of interest; with mechanism such as physical interactions or using covalent chemistry it can be easily added an external layer of small bioactive molecules, peptides, proteins or nucleic acid [18]. Furthermore for improving NPs biocompatibility and for preventing irreversible agglomerations the most popular co-ligand used is poly- (ethylene)-glycol (PEG) [143, 17]. In chemical biosensing applications, when the reaction with the analyte happens MNPs appear with a strong brown color if observed by naked eyes, and the chromatography intensity is proportional to the concentration of the analyte of interest. For these reasons they are commonly used in POC applications [167, 192, 111, 165], especially Fe₃O₄ MNPs have shown to have good properties for the amplification or generation of the signal and also low toxicity profile [89] and biocompatibility with antibodies and enzymes [143]; other advantages of these nanoparticles are high coercivity, good monodispersity [117], large surface area and high mass transference [143].

5.3 Proposal of an innovative microfluidic device for COPD

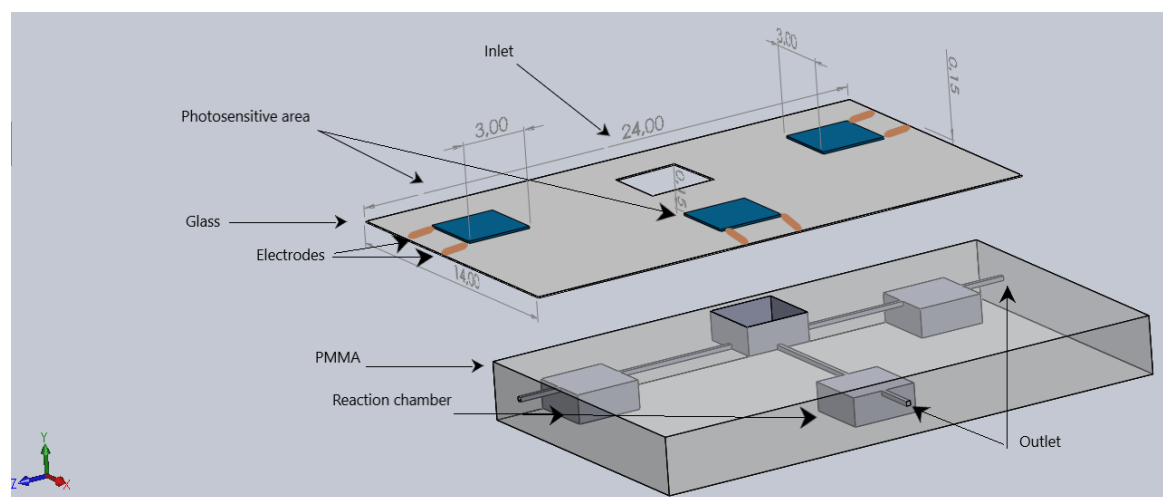


Fig. 5.1 3D microfluidic device model.

In this section the idea is explained of an innovative microfluidic device proposed for the COPD case. The material chosen for its building is Poly(methyl methacrylate) (figure 5.2), better known as PMMA, that has excellent properties. It is a cheap thermoplastic polymer that has good mechanical stability, a low water-absorption percentage, and organic solvent, and acid/base resistivity. It is the least hydrophobic one in the common plastic material (contact angle with water $>70^\circ$). Furthermore, at high temperature, the PMMA is capable of decomposing into methyl methacrylate (MMA) and it can be reused. It is possible to define this material as a 'green material' that is another advantage to add to its low price, rigid mechanic property, excellent optical transparency, its ease of fabrication and modification. The microfluidics structures can be easily controlled in the building phase by CO₂-laser micromachining. However, for mass production, other techniques are available such as soft-lithography, hot-embossing, solvent imprinting, thermal bonding, injection moulding and laser ablation, defined as highly reliable. PMMA is largely used for microfluidic analysis chips. These devices can be easily coupled with cover plates or cover films made of glass or paper, bonded to each other thanks bonding techniques for the fabrication of PMMA-based microfluidic chips. These include microwave bonding, thermal fusion bonding and adhesive bonding.

The goal of this proposal is to realise a capillary based optical device, by using graphene quantum dots as detection nanoparticles, because of all the excellent properties regarding costs, fabrication and efficiency compared with another kind of detectors described before. The saliva will be used as the non-invasive sample. Photodetectors for the QDs fluorescence

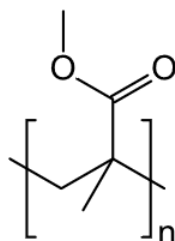
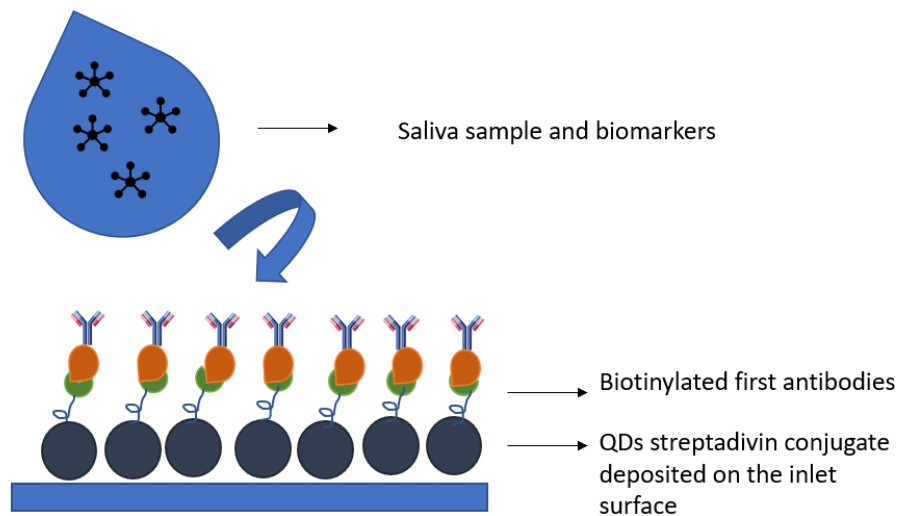


Fig. 5.2 Skeletal formula of the polymethyl methacrylate repeating unit (Perspex, $(C_5O_2H_8)_n$).

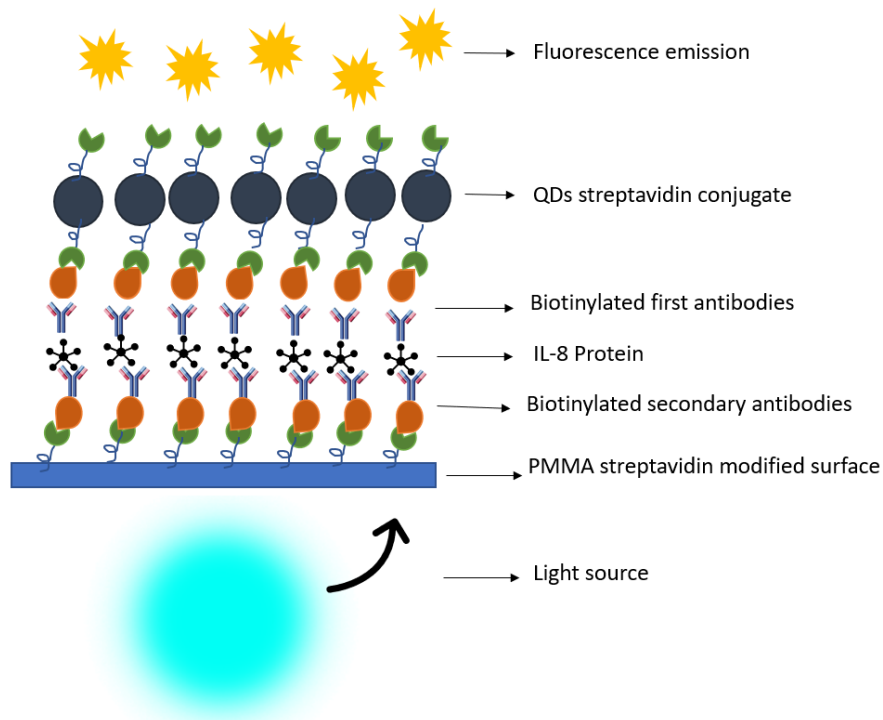
measuring will be placed on the top of the detection chambers of the device, supported by a glass substrate. All the necessary elements must be included into the portable device (figure 5.1).

The geometry design of the microfluidic device will be explained in detail in the next chapter, while in this part the goal is to describe the mechanism with which the detection nanoparticles can interact at the same time with the PMMA surface and with the biomarkers of interest present in the sample. Furthermore, the photodetectors will be described. The idea is to have a cluster of three biomarkers, which concentration will be independently measured in three different detection chambers; for this purpose, there is the need of three different groups of QDs, specifically labelled with the three respective antibodies to be used. These QDs can be placed on the surface of the inlet chamber, that is the first one the saliva sample meets on its way. In this point ideally QDs functionalized with the first antibodies, covalently link with the specific biomarkers in the sample and start to migrate through capillary action in the reaction chambers. Here they must be immobilised through a strong linkage with the secondary antibodies disposed of onto the bottom surface, allowing the creation of a sandwich immunoassay. A led placed outside the microfluidic chip, will give the excitation wavelength for the QDs. The emitted QDs fluorescence will be absorbed from the photodetector attached to the glass substrate aligned with the respective chamber, allowing a quantitative measurement by converting light in amperometric values. It will be directly proportional to the concentration of the biomarkers in the saliva sample. Here two solutions are proposed for the deposition of the QDs in the inlet chamber. The first one consists of directly deposit the QDs on the PMMA substrate. The spin coating technique easily allows this deposition. It was used in other works for creating a homogeneous QDs layer on the top of a PMMA thin layer [161, 80, 56]. There are different methods for making thin-resist layers or film on a substrate, but the simplest method is spin-coating. It consists of a first step in which the dilution of the material to be deposited in a solvent is done. In the second step, this solution is dispensed on the substrate interface. Finally,

the wafer support is spin at high speed. The spinning speed, together with the surface tension and the viscosity of the solution, determine the thickness of the film. The final planar surface results from the evaporation of the solvent during the deposition and the backing step. The second proposed solution consists of putting a layer of hydrophobic paper on the bottom of the inlet chamber. In this case, the device will be a hybrid PMMA/paper model. Here the QDs can be disposed of by spray coating technique [185, 64]. In this case, too, QDs are diluted into a solution, that will evaporate during the deposition and the backing step. The hydrophobic paper properties should improve the non-absorption of the fluid for allowing the capillary mechanism. It can be linked to the PMMA surface by treating this last one with oxygen plasma technique [175, 194] or corona discharge [137] for maximizing the adhesion properties. Focusing on QDs, they should be linked with the first antibody of the biomarker of interest. There are different ways for functionalizing QDs, like non-covalent attachment, covalent attachment and electrostatic conjugation. A classical non-covalent method consists of using the streptavidin-biotin linkage, defined as one of the strongest non-covalent one in chemistry [33]. QDs streptavidin conjugate are commercially available such as biotin human antibodies conjugate. In this case, these elements have to react into a solution before the deposition of the labelled complexes onto the inlet surface. Bioconjugates can be linked to QDs by using standard protein conjugation technique such as covalent linkage, that involves the binding of primary antibodies of the biomarkers onto the QDs surface, after the activation of its carboxylic groups through plasma treatment [14]. Finally, focusing on the reaction chamber, its surface must also be functionalized with biotinylated antibodies for allowing the sandwich immunoassay, so the covalent labelling with the protein of interest in the saliva sample. It means that the PMMA surface must be patterned with streptavidin. A simple solution for this purpose could be a method of different steps; firstly, the PMMA surface must be chemically activated by plasma treatment. After this, the microstamping technique can be used to print μ CPEZ-Link-biotin-PEO-LC-amine ((+)-biotinyl-3,6,9-trioxaundecanediamine) (biotin-amine) onto PMMA. Finally, the surfaces of the polymers must be incubated with recombinant streptavidin in HEPES buffered saline (HBS, pH 7.4) [67]. After this process, the treated surface must be incubated with the solution of biotinylated antibodies. Below there are simple illustrations of the discussed concepts (figures 5.3, 5.4).



(a) From the picture, it is possible to see the deposition of the streptavidin conjugate QDs linked with the biotinylated antibodies in the inlet chamber. These complexes will interact with the respective biomarkers contained in the saliva sample.



(b) In this picture, it is possible to see the complexes streptavidin conjugate QDs-biotinylated antibodies, linked with the respective antibodies by covalent attachment in the reaction chamber. These are transported into the saliva through the microchannels by capillary action. In the reaction chambers they react with the secondary antibodies disposed on the treated surface, developing a sandwich immunoassay complex. The QDs emit fluorescence light when excited from the light source. It is directly proportional to the concentration of the biomarkers in the saliva sample.

Fig. 5.3 Explanation of the interactions between detection elements into the chambers.

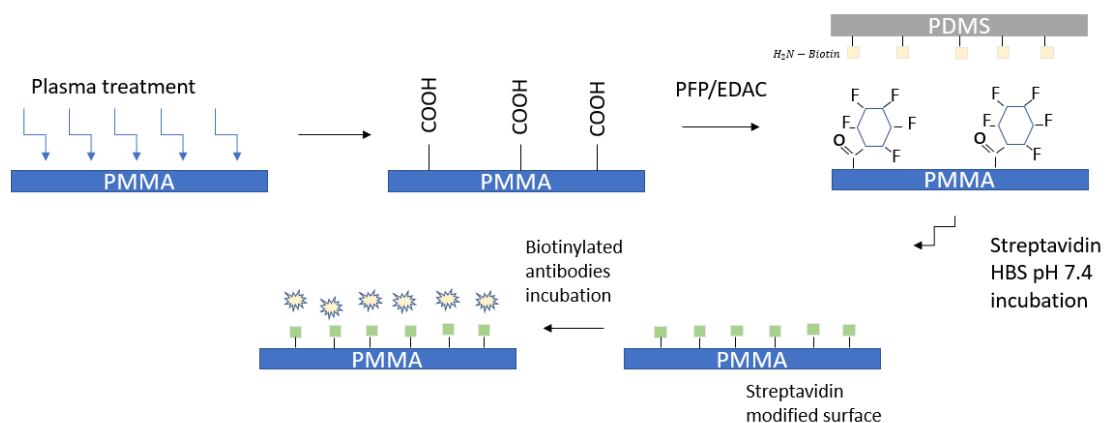


Fig. 5.4 Schematic explanation of the PMMA surface modification by microstamping technique.

In the proposed optical device, the protein concentration is directly proportional to the intensity of the emitted fluorescence from the QDs. The photodetectors allow its quantitative measurement by converting the light in photocurrent values. The goal of this work is to use graphene not only for the QDs but also as characteristic material of the photodetectors. The electronic device chosen for this purpose would be a phototransistor; it consists of a transistor channel activated by a gate optically sensible that converts incident light into current. It is available in both the P-N-P and N-P-N configurations, and it has three contact terminals which are a drain, source and gate. In the configuration, the letter 'P' indicates a 'P-type material', which is a semiconducting material positively doped while the letter 'N' stays for 'N-type material', so negatively doped. The 'doping' procedure consists of injecting into the semiconducting material impurity atoms. Moreover, impurity atoms can be with 5 or 3 valence electrons, producing respectively p-type and n-type semiconductors because of the presence of extra electron in the first case and a 'hole' or electron deficiency in the second case. When the two different semiconducting materials are put together, they make a junction where electrons and holes diffuse to the zone with less presence of them: free electrons in the N-type material go from the present conductive band to the one in the N-type material. On the other hand, free holes present in the P-type material go from the present valence band to the one in the N-type material. They make an equilibrium state, because of the recombination between electrons and holes in both sides. In this region around the junction interface the free carriers are depleted, so, for this reason, this zone is called depletion zone. Due to the majority charge carrier diffusion, this area is charged. The resulting electric field consists of the N-side positively charged and the P-side negatively charged, it provides a force opposing to the charge diffusion. The depletion zone reaches the equilibrium when the force of the electric field stop the diffusion of the free carriers. This condition represents for the phototransistor the OFF state. When the device is not under illumination, there will be a small current (dark current) flow due to thermally generated hole-electron pairs. With light falling (ON state) the current flow increases; when a specific energy photon strikes the device, it generates an electron-hole pair. The total photocurrent is defined as the difference between the device current under illumination and dark current. Furthermore, there are two contributes for photocurrent in photodetectors; the first one is given from the photoconductivity effect, due to the increase in free charge carriers from photon absorption and the creation of electron and hole. The second one is given by the photogating effect, due to the charge trapping from disorders and defects; it comports the change in transistor threshold voltage (V_T) in dark conditions, to $V_T - \Delta V_T$ under optical illumination. The change of the effective gate potential under illumination causes a threshold shift and a change in source-drain current. The key properties which must be considered in a phototransistor are the high carrier

mobility, the high photoresponsivity, the detectivity, the sensitivity, the high effective quantum efficiencies, the reliability and the absorption cross-section in the active regions [116]. The carrier mobility indicates how quickly a charged carrier can move through a semiconductor when pulled by an electrical field. The photoresponsivity represents the amount of signal current generated per unit power of a specific wavelength radiation. The detectivity represents the capability of detecting low-level light signals; it is influenced by the noise. There are three main kinds of noise, of which one comes from the presence of the dark current in the device when electrons are thermally generated in the absence of light (dark noise). The other two groups represent the noise under light conditions, linked to the statistical production (shot noise) and thermal fluctuations nature (Johnson noise) of the generated electrons. The sensitivity of the device depends on the spectral response bandwidth; usually this includes a wide range of frequencies, starting from very low frequencies. The device mechanical properties determine the maximum limit frequency. Thus, higher the photocurrent to dark current ratio, higher will be the sensitivity of the device. The quantum efficiency concerns photon detection and is usually expressed in percentage; it determines how efficiently the photodetectors convert the incoming photons into conduction electrons. Finally, the absorption cross-section in the active area is a measure from the probability of a light absorption process.

In the optoelectronic field, Graphene is taking great interest in its application in light detection. It allows broadband light absorption, fast response time and ultrahigh carrier mobility ($\sim 200000 \text{ [cm}^2/(\text{V s})]$). On the other hand, it can not be used for pure graphene-based phototransistor because of its single monolayer relatively low absorption cross-section (2.3%), low responsivity ($\sim 0.01 \text{ [A/W]}$), fast recombination rate and absence of a gain mechanism that can generate multiple charge carriers from one incident photon [179]. Nevertheless, recent studies showed that the hybrid use of graphene with 2D materials such as QDs or the combination with a layer of materials such as organometal halide perovskite [179, 26] which is a semiconducting light absorber, have shown improvements in photoconductive gain. Thus, the idea is to create vertical or horizontal heterostructures. Organometal halide perovskites are easy to process into solution as organic semiconductors and also the charge carrier mobility is high, as results for inorganic semiconductors. Furthermore, it has an effective light absorption showing tremendous potential for the development of high-performance photodetectors [178].

In this work, the goal is to reproduce the model proposed by *Chang et al.* [26] and adapt it to the proposed device (figure 5.5). They realized a hybrid phototransistor in a vertical structure, by using sequential vapour deposition. In this technique, the deposited material goes from a condensate phase to a vapour one, and finally after the coating it comes back

to the condensate phase, developing a thin layer. The photodetector is organized as follow: in the bottom there is the p-doped silicon substrate. Onto this layer, a Si-O₂ substrate is deposited by Self-assembled monolayer (SAM) technique into thermal oxidation process conditions. The vapor deposition is also used for making the graphene transistor that will give the field effect. At this point, the (MAPbI₃) perovskite film is deposited as the active layer of the hybrid phototransistor. Finally, PMMA is spin-coated on the entire surface of the device for passivation, to prevent contamination from ambient moisture and oxygen. This kind of phototransistor bases the gain mechanism on the photogating effect and works in the hole conduction region (the gate voltage is lower than the charge neutrality point). Under illumination, additional photo-induced holes are injected into graphene, causing the shift of charge neutral point to the higher gate voltage. On the other hand, electrons are trapped by perovskite islands. This process produces a photo-induced p-doping effect to graphene. The positive shift of the charge neutrality point varies with light intensity due to the number of photo excited holes generated; as a consequence, the drain current raises. Finally, the holes in the graphene sheet are more recruited resulting in a large increment of conductivity and ultrahigh photoconductive gain. The proposed hybrid photodetector results in ultrahigh responsivity ($> 4 \cdot 10^5$ [A/W]), effective quantum efficiencies (10^8 %) under an illumination intensity of $\sim 2.6 \mu$ [W / cm²] in the visible region (450-700 nm). The detectivity achieved is of $2 \cdot 10^{15}$ Jones under low-intensity white light illumination. Furthermore, the response time is ~ 879 ms, and the carrier mobility is ~ 200000 [cm²/(V s)]. These properties will enforce the performance of the new proposed optical microfluidic device.

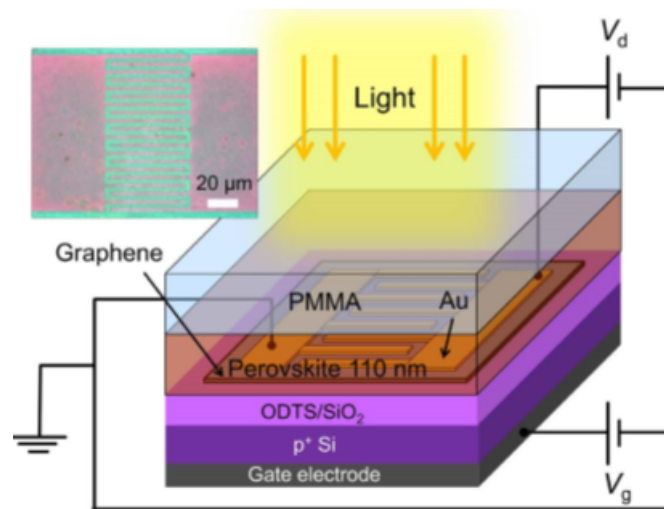


Fig. 5.5 Graphene- methylammonium lead iodide (MAPbI₃) perovskite hybrid phototransistor [26].

Chapter 6

Microfluidic device numerical simulation

Before to introduce the finite element analysis of the proposed device , by using the software COMSOL Multithysics 5.3.a, it is important to study the theory behind its work, for understanding well the problem treated.

6.1 Microfluidic theory

6.1.1 Non-Newtonian Fluid

One of the principal aspects of this work is the nature of the studied fluid; saliva can be considered to be a Non-Newtonian fluid time not-dependent, that is a fluid does not follow the Newtonian's law of viscosity in which the shear stress, τ , results to be directly proportional to the viscosity of the fluid μ and the shear rate $\dot{\gamma}$. For a fluid the shear stress represents the condition of shearing forces applied to a fluid at rest; this one cannot resist them and deforms continuously. The resistance to the action of shearing forces in a fluid appears only when the fluid is in motion, and this property of the fluid is called viscosity. For a Non-Newtonian fluid, the dynamic viscosity is dependent on the shear rate or on the time history of shear rate and it comports non-linear relations between shear stress and shear rate (figure 6.4). This not happens for Newtonian fluids for which the viscosity remains constant; the shear rate is the rate at which a progressive shearing deformation is applied to the fluid. Depending on this, the dynamic viscosity can change to a more robust or liquid state; fluids are shear thinning if the viscosity decreases as the shear rate increases, while the contrary is for shear thickening as shown in the figure 6.1.

From these considerations, the Carreau model [Equation(6.1)] was applied to calculate the value of μ . This model combines both the Newtonian and the Power law model and can represent both shear thinning and thickening materials [82]. The Power law fluid model

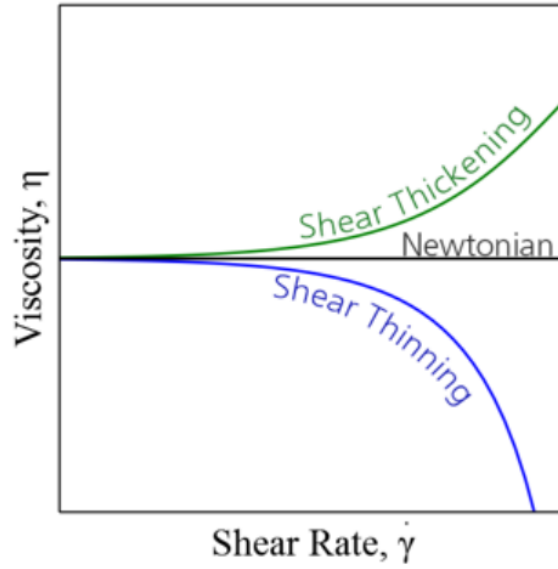


Fig. 6.1 Relation between viscosity and shear-rate for Newtonian and Non-Newtonian fluids [55].

gives a basic relation for dynamic viscosity and shear rate, while the Carreau law describes a four parameters model that is valid over the complete range of shear rates (equation 6.1). At very low shear rate and also at very high shear rate, Carreau fluid behaves as a Newtonian fluid. In the middle, there is a transition zone where the fluid follow the non proportionality between the shear rate and the dynamic viscosity. It becomes essential to incorporate the values of viscosity at zero shear, μ_0 and at infinite shear, μ_∞ into the formulation.

$$\mu = \mu_\infty + (\mu_0 - \mu_\infty) \left[1 + (\lambda \dot{\gamma})^2 \right]^{\frac{n-1}{2}} \quad (6.1)$$

In this equation, λ and n , are both parameters from the model where the first one is the relaxation time constant and the last one is the power law index. Saliva is considered to be a thinning material. In the figure 6.3 is possible to observe the development of the viscosity of unstimulated and stimulated human saliva (US, SS) depending on the shear rate. The profile development follows the characteristic profile of the Carreau fluids . The dynamic range, for saliva, appears to be 1-1000 [1/s], from this point the viscosity becomes constant, and the fluid has Newtonian behaviours.

It is said that 4 [1/s] is the shear rate to the flow of saliva in the tongue, 160 [1/s] for speech, and higher values till 500 [1/s] were found while eating.

In the Carreau model the n parameter changes due to the material as shown in figure 6.4. This parameter is defined for the thinning materials as $0 \leq n < 1$, for the thickening materials

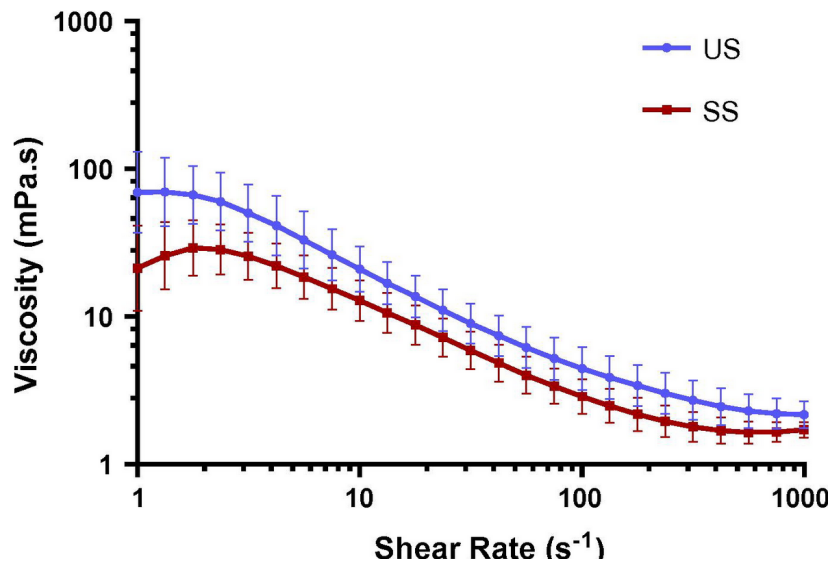


Fig. 6.2 Relation between viscosity and shear-rate for stimulated (SS) and unstimulated (US) saliva [55].

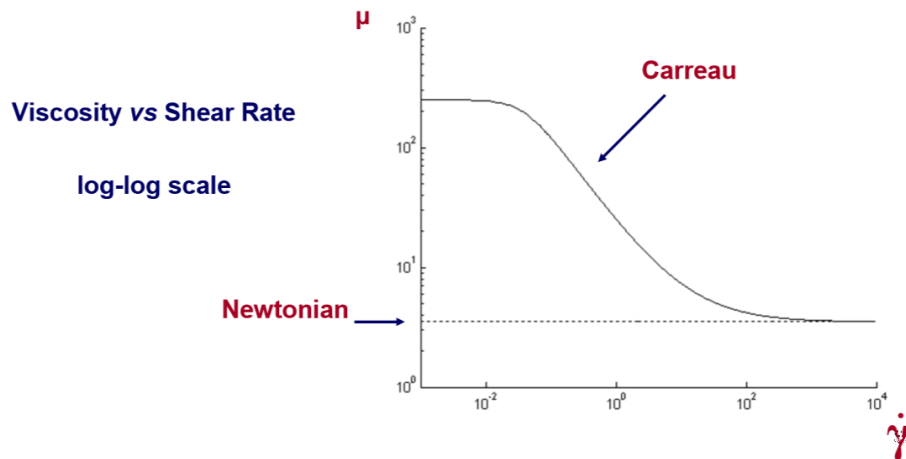


Fig. 6.3 Relation between viscosity and shear-rate for fluids that follow the Newtonian and the Carreau model.

$n > 1$, and for a Newtonian material as $n=1$. Saliva can be considered as a shear thinning material, in accordance with the results reported in the figure 6.3

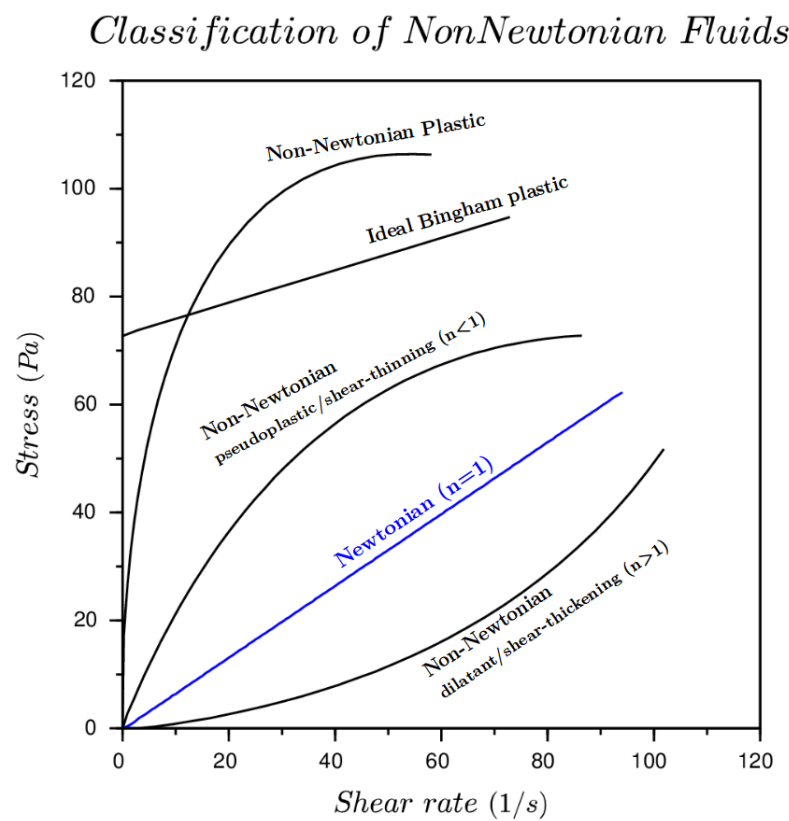


Fig. 6.4 Relation between shear stress and shear rate for Non-Newtonian fluids [55].

6.1.2 Pressure Drop

The proposed device wants that the sample moves horizontally into the microchannels and the chambers through capillary action. This physic event depends from an important variable that is the contact angle (θ) of the liquid upon a specific solid material, which considers the different superficial tensions between solid, liquid and gas phase for calculating how the capillary action will develop. Especially, if $\theta < 90^\circ$, the material is wettable and the capillary action will occur with a concave shape of the meniscus. Its value can be calculated from the equation (6.2) :

$$\cos \theta = \frac{\gamma_{sg} - \gamma_{sl}}{\gamma_{lg}} \quad (6.2)$$

where γ_{sg} represents the solid-vapour interfacial energy, γ_{lg} the liquid-vapour interfacial energy and γ_{sl} the solid-liquid interfacial energy.

Notwithstanding the contact angle, the fluid movement is a consequence of the pressure drop (ΔP) applied between the inlet and the outlet of the meniscus; the Young-Laplace pressure drop equation (6.3) describes this pressure gradient,

$$\Delta P = \Delta P_{surf} = \frac{2\gamma_{lg}}{h_{channel}} \cos \theta \quad (6.3)$$

That results constant along all the channel for creating a capillary pump; in this contest, the gravity force can be not considered because it loses its capability to limit the range of capillary action if the vertical dimension of the channel is of the order of 10^{-6} [m]. This is confirmed by calculating the dimensionless Bond number (equation 6.4) , that measures the importance of gravitational forces compared to surface tension forces. If its value is closer to zero it means that gravity force does not have a role.

$$Bo = \frac{\rho g h_{channel}^2}{\sigma} \quad (6.4)$$

where ρ is the density of the fluid, g the gravity force, h the channel height and σ the interfacial surface tension between saliva and air.

6.1.3 Laminar two-phase flow fluid model

The physic study can be modelled considering a laminar two-phase flow, in which phase field method can be chosen to study the interfacial motion of the multiphase flow; this approximation reveals to be good if the device design is structured for having laminar flow in the continuum domain. The continuum domain is satisfied when the value of the

dimensionless Knudsen number (equation 6.5) is less of 0.01. In its definition, λ represents the mean free path, that is the mean distance that a particle can travel before having an impact with another one. For a liquid, this variable is of the order of the intermolecular distance, that results being 0.3 [nm]. The variable D_H represents the hydraulic diameter, that is the dimension of interest for inflow problems.

$$Kn = \frac{\lambda}{D_H} \quad (6.5)$$

Furthermore, the laminar flow is verified for values of the dimensionless Reynolds Number (equation 6.6) less of 200:

$$Re = \frac{\rho u D_H}{\mu} \quad (6.6)$$

where D_H is the hydraulic diameter of the pipe (the inside diameter if the pipe is circular), u is the mean velocity of the fluid, μ is the dynamic viscosity of the fluid and ρ is the density of the fluid. As explained before, the saliva has Newtonian behaviours for high values of shear-rate. The basic equations governing fluid motion in microchannels under the continuum assumption are the Navier-Stokes equations for a non-compressible fluid coupled with the continuity equation. Furthermore, the inertial term is considered, because of the value of the dimensionless Capillary Number; this number is useful to describe multiphase flow behaviour in microchannels. It is defined as in equation 6.7, where μ is the viscosity, v is the average flow velocity, and σ is the interfacial tension between saliva and air. If its value is higher less than 1 but of the order of 10^{-3} , it means that inertial terms have to be considered and also that the distributed surface tension domains on viscous forces.

$$Ca = \frac{v \cdot \mu}{\sigma} \quad (6.7)$$

The Navier -Stokes equation (6.8) results to be:

$$\rho \frac{\delta u}{\delta t} + \rho(u \cdot \Delta)u = \Delta \cdot [-pI + \mu(\Delta u + (\Delta u)^T)] + F_{lg} \quad (6.8)$$

where $-\Delta p$ represents the inertial forces, p the fluid pressure, F_{lg} is related with the phase field surface tension, I is the identity tensor, μ is the viscosity, u is the velocity of the fluid and T is the temperature; in this way it is possible to simulate the capillary action. The phase field method also satisfies the conservation of mass, thanks the definition of the continuity equation [Equation (6.9)].

$$\rho \Delta \cdot (u) = 0 \quad (6.9)$$

The multiphase flow behaviour is described by a dimensionless phase field parameter φ that defines the interface as a region of transition from $\varphi = -1$ (gas phase) to $\varphi = 1$ (liquid phase), respecting the Cahn–Hilliard equation [Equation 6.10]. This is split up by COMSOL Multiphysics® into two other equations:

$$\frac{\delta \varphi}{\delta t} + u \Delta \varphi = \Delta \frac{\Gamma \chi}{\varepsilon^2} \Delta \psi \quad (6.10)$$

$$\psi = -\Delta \varepsilon^2 \Delta \varphi + (\varphi^2 - 1) \varphi$$

The surface tension coefficient in the liquid-air interface [Equation (6.11)] is calculated considering the dimensionless mixing energy density and interface thickness:

$$\gamma_g = \frac{2\sqrt{2}\chi}{3\varepsilon} \quad (6.11)$$

For maintaining a constant interfacial thickness along the model, χ is set to 50, while ε has the characteristic value of half mesh-size in the pressing interface region [63].

In the simulation, air is set as fluid 1, saliva as fluid 2, and their volume fractions are calculated from equations (6.12),

$$V_{f1} = \frac{1 - \varphi}{2} \quad (6.12)$$

$$V_{f2} = \frac{1 + \varphi}{2}$$

moreover, the density and viscosity of the mixture are defined as varying smoothly over the interface [Equation (6.13)]:

$$\rho = \rho_{saliva} + (\rho_{air} - \rho_{saliva})V_{f1} \quad (6.13)$$

$$\mu = \mu_{saliva} + (\mu_{air} - \mu_{saliva})V_{f1}$$

The software considers the phase field surface tension as an interfacial distributed force and provides its calculation by resorting the following equation (6.14):

$$F_{lg} = G \Delta \varphi \quad (6.14)$$

$$G = \chi \left[-\Delta^2 \varphi + \frac{\varphi(\varphi^2 - 1)}{\varepsilon^2} \right] = \frac{\chi}{\varepsilon^2} \psi$$

Where there is a direct proportionality to ψ and the gradient of φ .

6.2 Design proposal

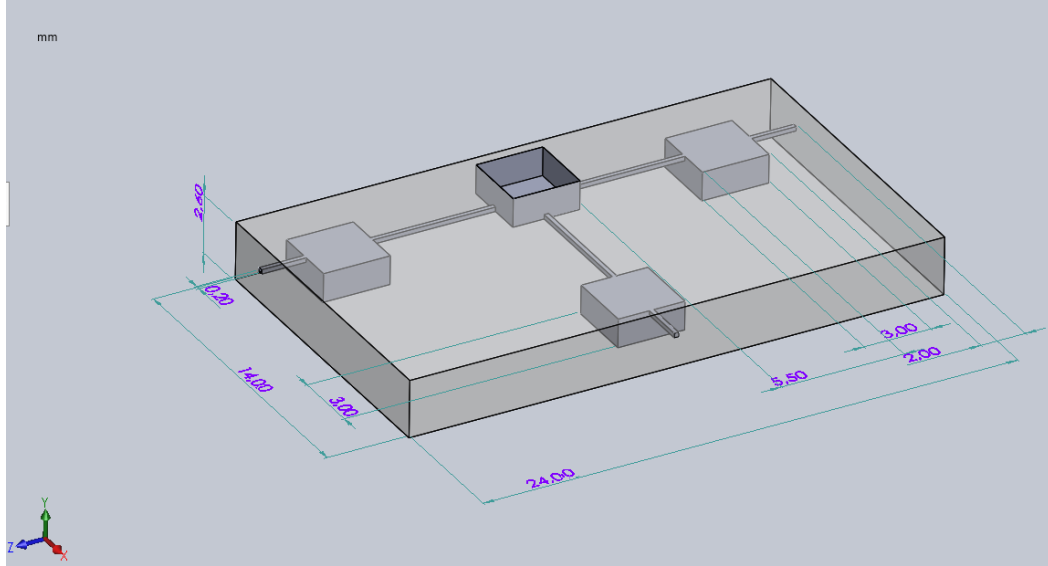


Fig. 6.5 Complete microfluidic model geometry.

In the proposed device (figure 6.5), the inlet chamber has a square shape of the dimensions of 3x3 [mm], a height of 1.3 [mm], and a top hole where the sample must be loaded; in this, symmetrically three rectangular microchannels depart from its bottom, of section area 0.2x0.2 [mm] and a length of 5.5 [mm]. The outlet of these channels is linked to the three rectangular reaction chambers, which position is a level less compared with the inlet chamber on the top; their depth is of 1.1 [mm]. The bottom of the model presents a thickness of 0.2 [mm] full of PMMA, that assures resistance and balance to the device; the rectangular shape of the PMMA base is 24 [mm] long, 14 [mm] width and 2.6 [mm] high. In the presented case, saliva is considered as non-compressible fluid, which density and viscosity are respectively approximated as 1000 [kg/m³] and 30 [mPa/s].

The material surface with which the fluid interacts is supposed to be PMMA. It is reported that the contact angle between water and PMMA is $\geq 70^\circ$ ($6 \cdot \pi/14$), so it can be considered as a hydrophilic surface but with a contact angle nearer to the hydrophobic properties [162]. Furthermore, according to these properties, the slip condition ($u \cdot n = 0$) can be applied to the wetted walls; experimental and molecular dynamics simulation studies have demonstrated that slip usually occurs on hydrophobic surfaces [158]. In different experiments reported in the literature, a minimum of the volume of 9 or 10 μL is indicated as the necessary inlet sample droplet for allowing the biomarkers detection in the sensitive area [63]. For this reason, the inlet chamber has the dimensions of 3*3*1.3 mm³, with a square surface area of 9 mm² and a volume of $\sim 10 \mu\text{L}$.

The device has a symmetrical design because the goal of the experiment is a symmetrical filling of the microchannels and chambers for all the time steps. Furthermore, a symmetrical inlet geometry produces a straight interface between saliva and air. The presence of a chamber in the center of the microfluidic channel is important to help to localise the biomarkers for the detection; the reactive chamber has the same dimensions of the inlet chamber.

A square cross-section for the microchannels is preferred because it is easier to fabricate [92]; the aspect ratio 1:1 for the microchannels respects the PMMA acceptable fabrication limits as shown in other works [84]. There are not specific requirements for the length of the channels, because it is supposed that the biomarkers concentration is homogeneous from the beginning of the motion; it is set as 5.5 [mm].

Usually the development of the laminar flow with straight parallel streamlines occurs between two parallel interfaces when the fluid velocity is very low, or the fluid has a high viscosity. It is reported that the flow is laminar in a microchannel with a rectangular cross section and hydraulic diameter less of 1 [mm]; in this case, the Reynolds number results to be $\ll 1$ [35]; furthermore, gravitational forces can be not considered if the Bond number is $\ll 1$ such as in the proposed case, so the viscous and inertial forces domain the motion. For the biomarkers detection, the mean fluid velocity should approximate to 0.003 [m/s] to allow the sufficient cells capture within the chambers [92]. From these considerations and after different sizes tried, in this site the hydraulic diameter is set as 200 μm and it is defined as the side dimension of the square for a square cross-section. In this application, capillary action is also allowed from the pressure drop value that guides the meniscus, together with the wettability conditions. The inlet surface is defined as a 0 [Pa] area, while the outlets are defined as pressure areas with a value of 10^5 Pa, because from the theory areas where air is still present will have this value of pressure; it is represented from the equations (6.2):

$$n^T [-pI + \mu(\Delta u + (\Delta u)^T)] n = -\hat{p}_0 n \quad (6.15)$$

$$\hat{p}_0 \leq p_0$$

In the simulation is assumed that the fluid is loaded with a normal inlet velocity of $15 \cdot 10^{-4}$ [m/s] in the inlet chamber, while the microchannel is filled with air; finally, this set of parameters is used (table 6.1):

Table 6.1 List of constants and values used in the simulation.

Name	Value	Description
ρ	1000 [kg/m^3]	Fluid density
μ_0	70 [$mPas$]	Zero shear rate viscosity
μ_∞	1 [$mPas$]	Infinite shear rate viscosity
v1	15e-4 [m/s]	INLET velocity
T	293 K	Temperature

On the base of the assumptions done, it is possible to calculate in the analytic way the dimensionless numbers cited before for a first approximation of the expected values in the problem. All the calculations are done for evaluating the worst condition that can occur. In the Kn number, the main free path considered is $0.3 \cdot 10^{-9}$ [m] and the hydraulic diameter is of $200 \cdot 10^{-6}$ [m]. It results to be approximately $0.0015 \cdot 10^{-3}$, so it respects the continuum domain. For calculating the Reynolds number, saliva is considered with a density of 1000 [Kg/m^3] and a dynamic viscosity of $1 \cdot 10^{-3}$ [Pa·s]. For the mean velocity is assumed the inlet velocity. The result is a Reynolds number of 0.3, that respects the laminar hypothesis. Furthermore, in this part saliva is approximated to water for considering the surface tension value in relation to air, which value is of $16 \cdot 10^{-3}$ [N/m]. The number results to be of 0.006, so lower than 1 but its order is of 10^{-3} . The assumption to consider the inertial terms in the problem results more accurate. Finally, with the same consideration on the fluid nature, the Bond number is of 0.024, so it is possible to not consider the gravitational contribute.

6.3 2D Cross-section FEM simulation

6.3.1 Geometry

The proposed device has a microfluidic geometry, where the saliva sample is loaded from the top of a central rectangular inlet chamber (3mm long, 1.3 mm height). From the bottom of this chamber a rectangular microfluidic channel departs (0.2 mm height, 5.5mm long); it is linked to the top of the detection chamber (3 mm long, 1.3 mm height), where the sample ideally flows in and the fluorescence reaction happens. It finally goes out from the outlet channel (0.2 mm diameter, 2 mm long) linked to the top of this last chamber. The dimensions of the microchannels, chambers, inlet and outlets were optimised according to the fluid flow arrangement using a finite-element method (*COMSOL Multiphysics 5.3.a*) and are visible in the figure 6.6.

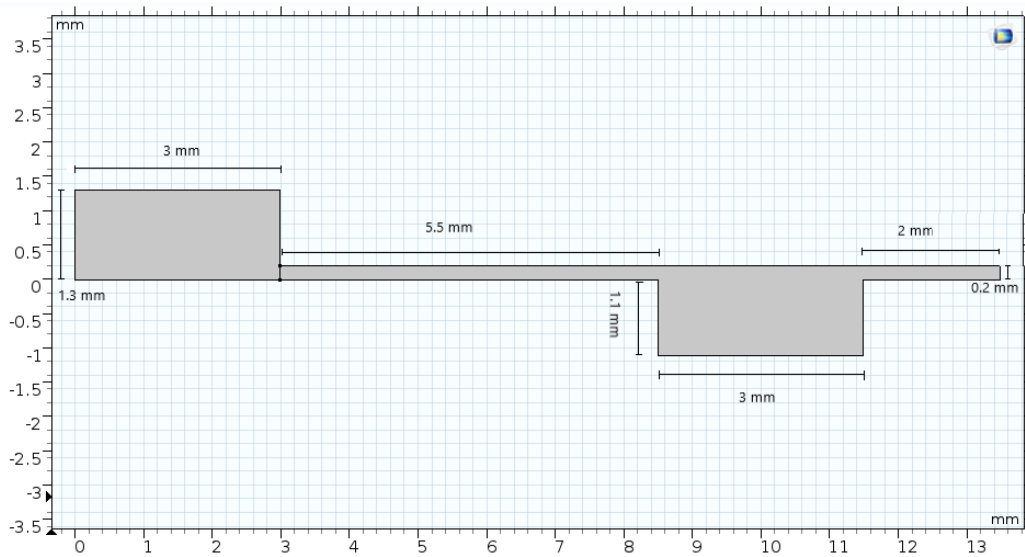


Fig. 6.6 Cross-section geometry.

6.3.2 Boundary conditions

In the simulation is assumed that the fluid is loaded with a normal inlet velocity of 0.0015 [m/s] in the inlet chamber, while the microchannel is filled with air. Regarding the wall conditions, the inlet walls have a no-slip condition ($u=0$) following the Dirichlet boundary conditions, while a slip condition ($u \cdot n=0$) was applied to the channel's walls and outlet chamber walls. The outlet is defined as a pressure area with a value of 10^5 [Pa].

6.3.3 Mesh

COMSOL Multiphysics 5.3.a provides automatic physics-controlled mesh generation, already adjusted for fluid flow and general physics. The manual mesh was defined with triangles, for a total of 5336 triangles. The mesh size was adjusted for having a manageable computing time; according to the finer design, the maximum element size is $0.0672 \text{ } [\mu\text{m}]$, the minimum is $9.6\text{E-}4 \text{ } [\mu\text{m}]$ and the curvature factor is of 0.25 . The mesh design is visible in figure 6.7.

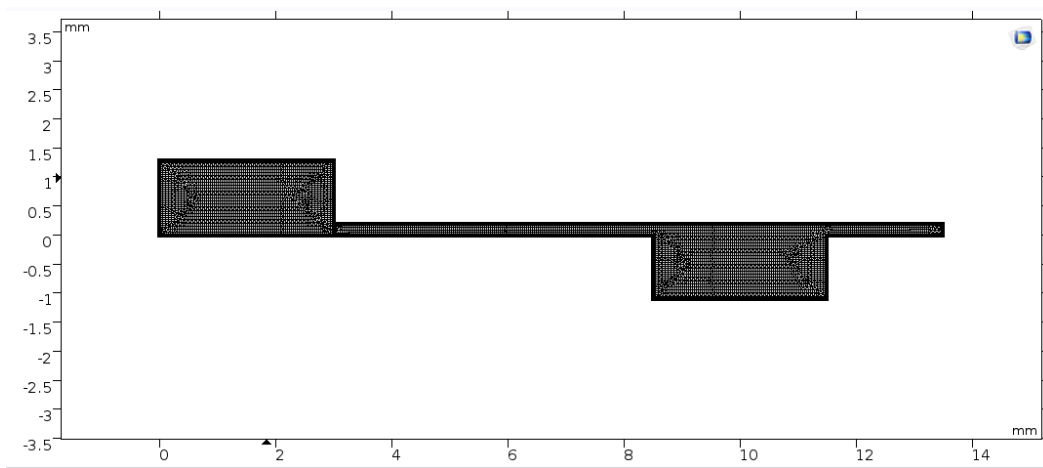


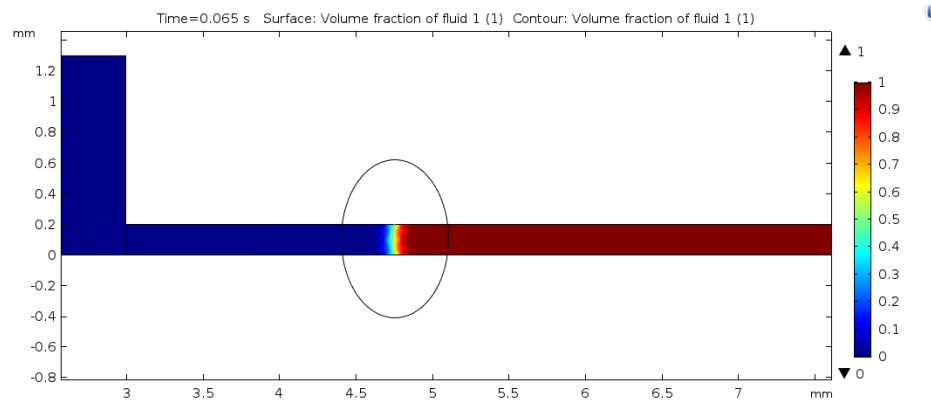
Fig. 6.7 Cross-section mesh.

6.3.4 Results

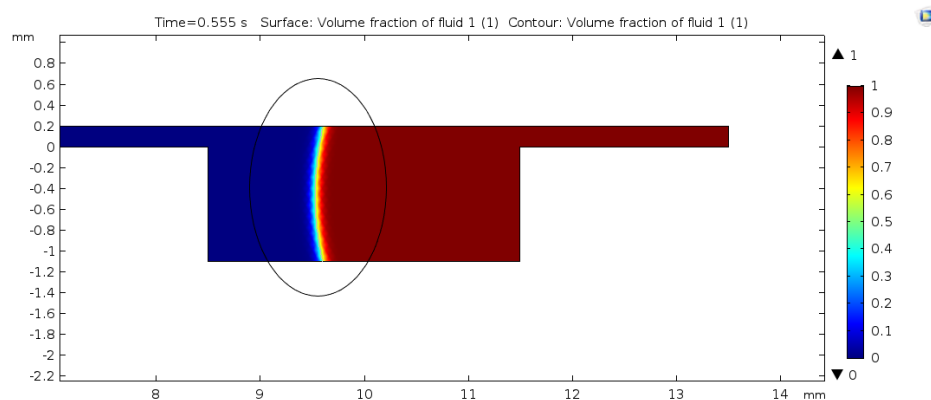
1. VOLUME FRACTION OF FLUID

Results show the formation of a meniscus along the channel and also along the reaction chamber, that moves uniformly as a piston along its way; furthermore, an interface between saliva and air is always present, demonstrating the correct phases separation. From the equations of the phase-field model (6.10,6.12) a constant value of 0 for the fraction volume of fluid one is obtained in areas filled with saliva; this condition is present along all the model, as is shown in the figures below 6.9. The meniscus has a concave shape, that usually occurs when the molecules of the liquid are more strongly attracted to the container than to each other, causing the liquid to fill the channel (figure 6.8) . The molecular forces that play a role in this contest are the adhesive inter-molecular forces between the liquid and the solid, and the cohesive inter-molecular forces inside the liquid. When the first ones are stronger than these last ones, the capillary phenomenon occurs with a concave shape of the meniscus.

Furthermore, the concave shape is not prominent, because of the contact angle that is near the hydrophobic properties of the surface in its hydrophilic nature. Finally, it is possible to see that the fluid takes 1.16 seconds to cross all the section of the microfluidic device. This time can bring several advantages for the POC devices since it will decrease the testing time.

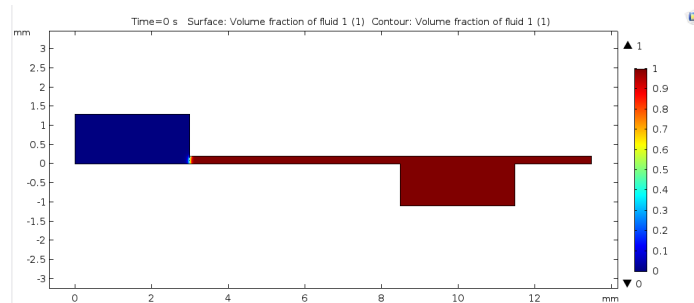


(a) Meniscus shape in the inlet channel.

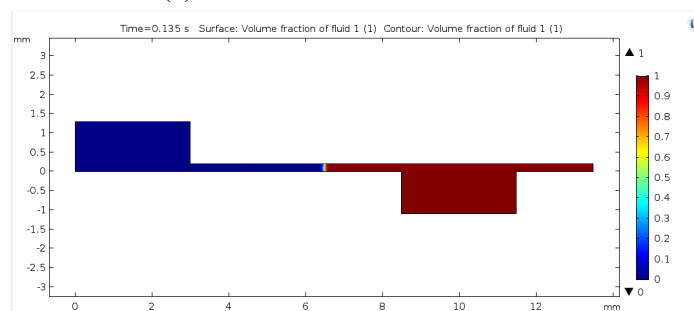


(b) Meniscus shape in the chamber.

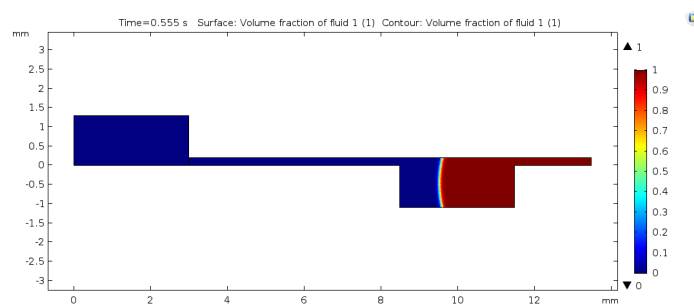
Fig. 6.8 Detail of the meniscus shape in the channel and in the detection chamber.



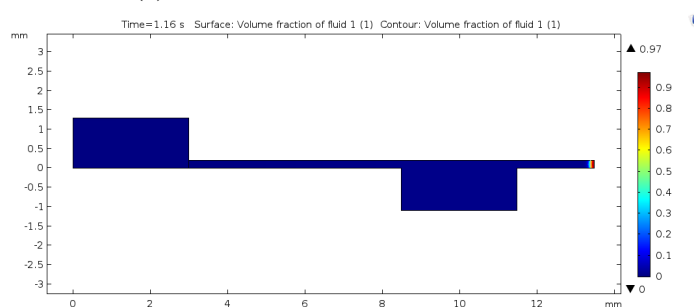
(a) Meniscus in the inlet chamber.



(b) Meniscus in the microchannel.



(c) Meniscus in the detection chamber.



(d) Meniscus in the outlet channel.

Fig. 6.9 Meniscus evolution between time 0 [s] and 1.16 [s].

2. VELOCITY

The fluid does not have the same velocity in every point of the simulation. By the analysis of the velocity from the input at time 0 [s], the initial condition is respected as shown from the maximum value of 15^{-4} [m/s] (figure 6.13a); the streaming lines from the start point show a laminar flow in the domain, in agreement with the Reynolds values obtained as well (figure 6.14a), for every section area along the model. The Reynolds values obtained are lower of the expected ones. The maximum value of the mean velocity in the channel is 0.03 [m/s] (figure 6.13b), then it drastically changes in the reaction chamber becoming of the order of $3 \cdot 10^{-3}$ [m/s] (figure 6.13c), respecting the guidelines for an accurate detection; this drop is visible in the line graph (6.10) also, and it allows the correct conditions for an accurate detection of the biomarkers of interest from the technological apparatus. Furthermore, Reynolds values become lower in the reaction chamber (figure 6.14c), changing from a maximum of 0.007 in the microchannel to 0.001 in the chamber; these values are also in agreement with the shear rate values, because a direct proportionality exists between the two parameters. In the reaction chamber, the shear rate values become lower, as it will be explained in the other section. Lower values of velocity could be obtained by making bigger geometrical sizes of the reaction chamber or by working on the surface hydrophobic behaviours of its walls. Finally, the velocity values rise when the meniscus enters in the outlet channel, reaching a maximum of 0.03 [m/s] (figure 6.13d). Considering the streaming lines shape until the saliva-air interface, the regime is laminar and the Stokes domain is respected. The velocity profile along the channel does not appear parabolic because of the slip condition and also maybe because it needs an higher length dimension of the microchannel for being completely developed; it appears to be trapezoidal (figure 6.11), with bigger values near the saliva-air interface. In the chamber the velocity appears to be homogenous along the y axes (figure 6.12, reaching the maximum value of 0.009 [m/s] in the middle and the lowest one of 0.003[m/s] at the border contact. It acts in the way that the meniscus seems to move like a piston.

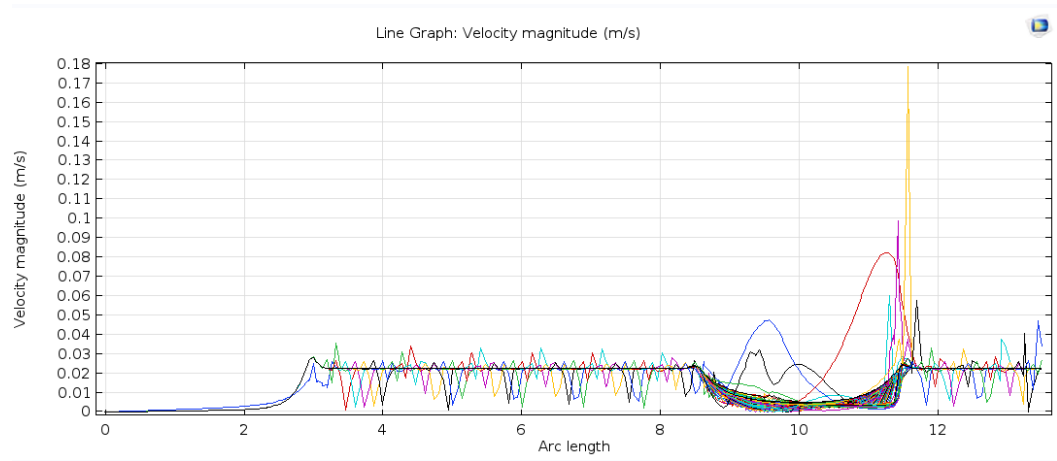


Fig. 6.10 Velocity drop in the reaction chamber.

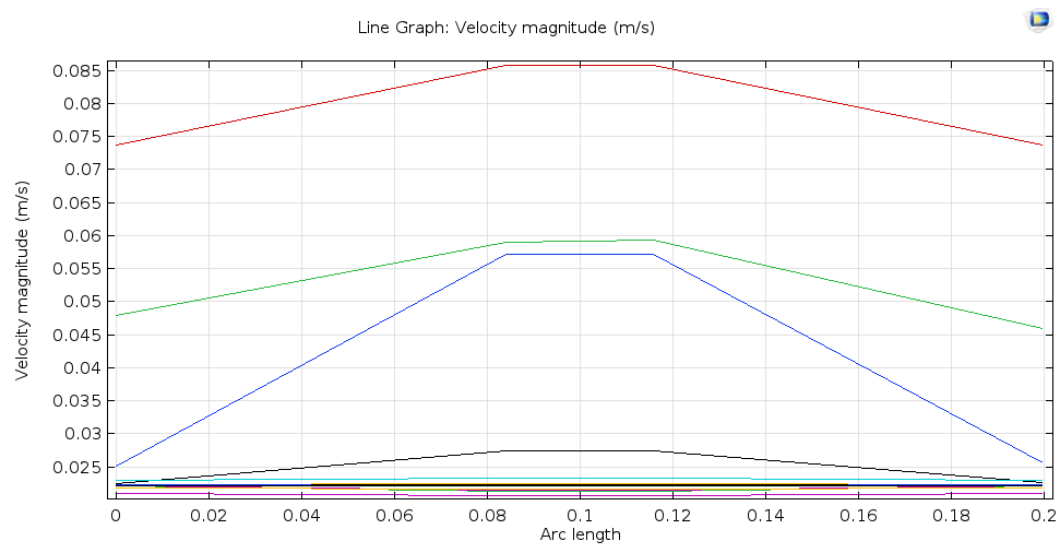


Fig. 6.11 Velocity profile in the microchannel.

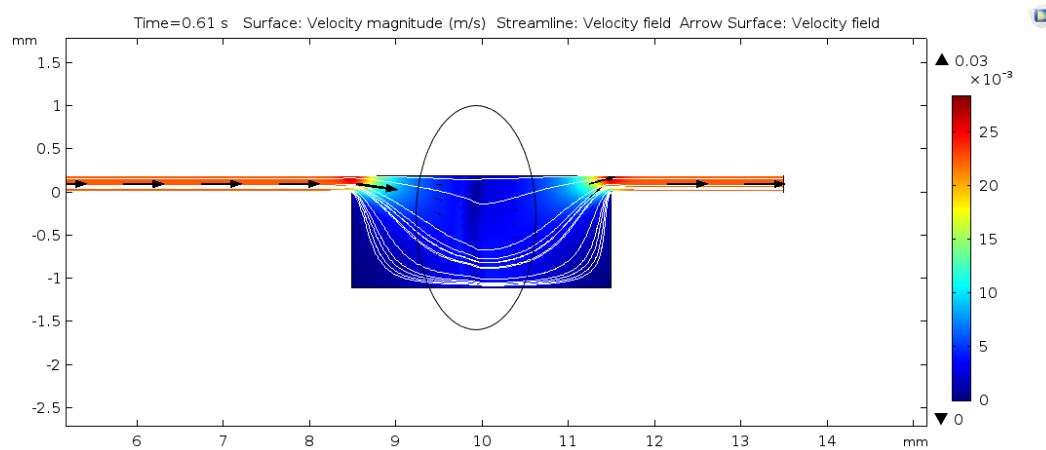
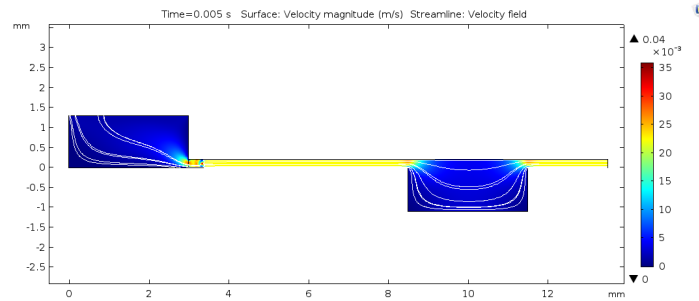
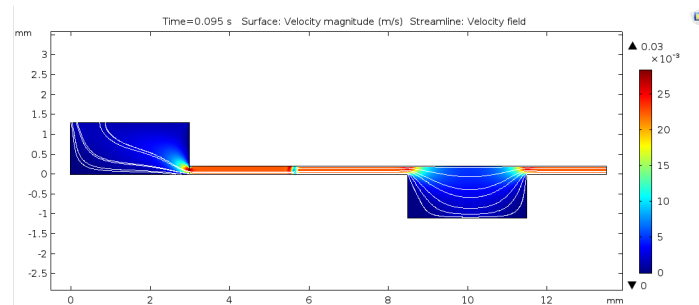


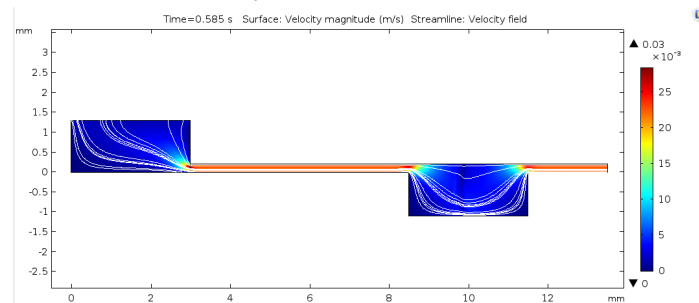
Fig. 6.12 Velocity profile in the reaction chamber.



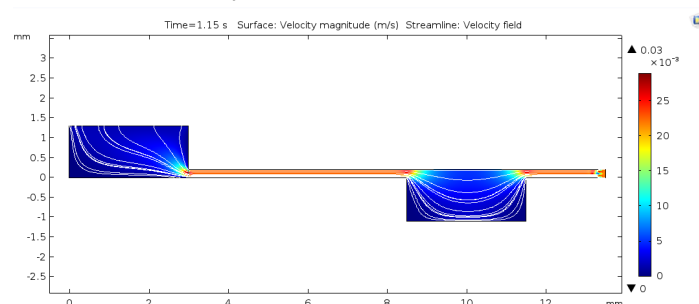
(a) Velocity values in the inlet chamber.



(b) Velocity values in the microchannel.

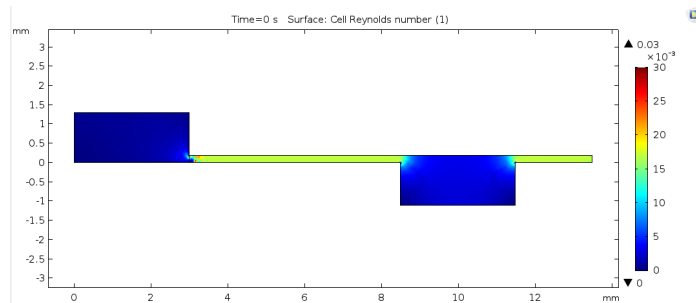


(c) Velocity values in the reaction chamber.

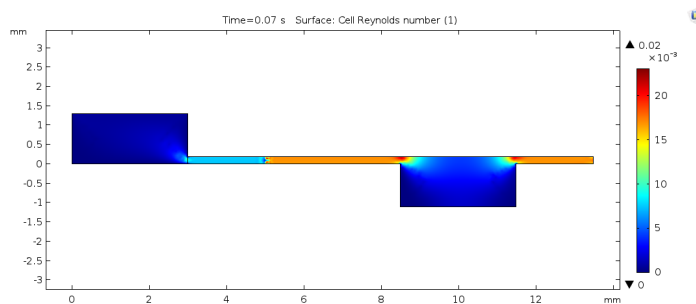


(d) Velocity values in the outlet channel.

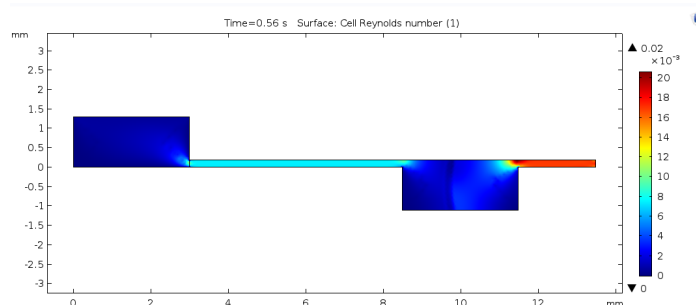
Fig. 6.13 Velocity values between time 0 [s] and 1.16 [s].



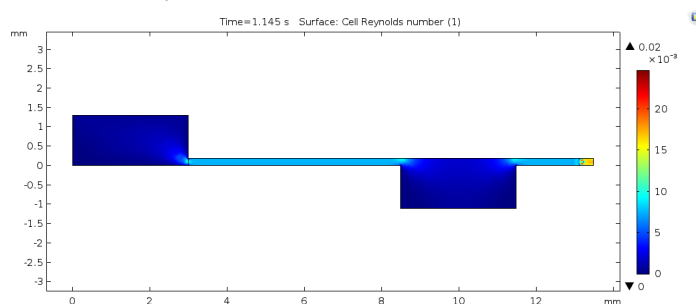
(a) Reynolds number in the inlet chamber.



(b) Reynolds number in the microchannel.



(c) Reynolds number in the reaction chamber.

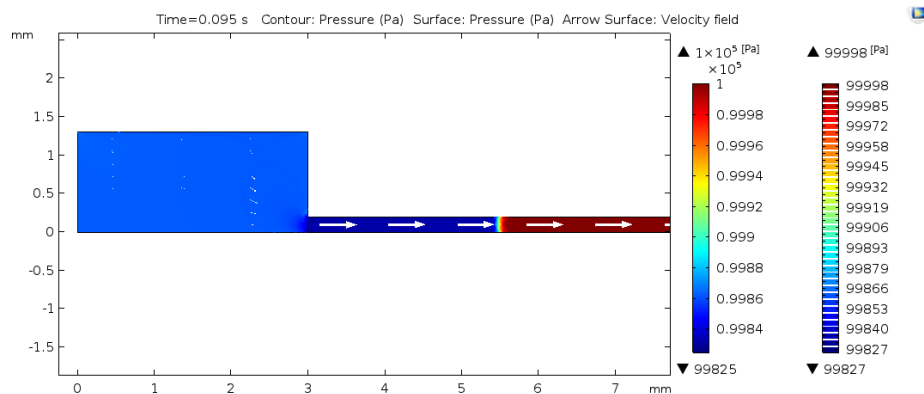


(d) Reynolds number in the outlet channel.

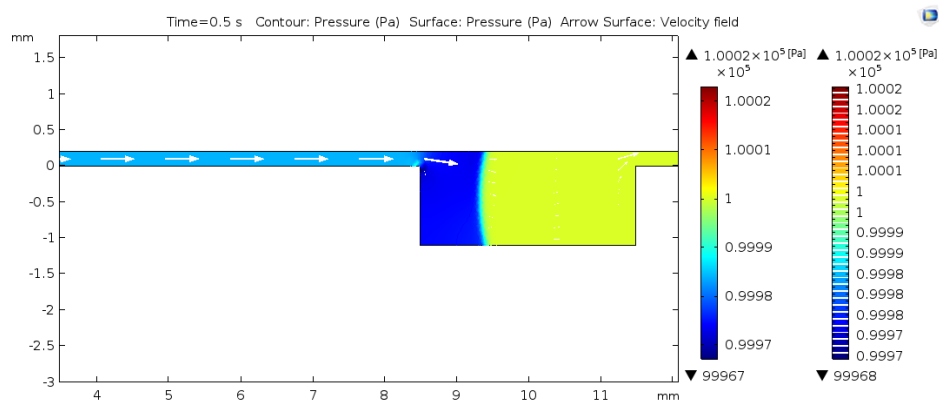
Fig. 6.14 Reynolds number values between time 0 [s] and 1.16 [s].

3. PRESSURE

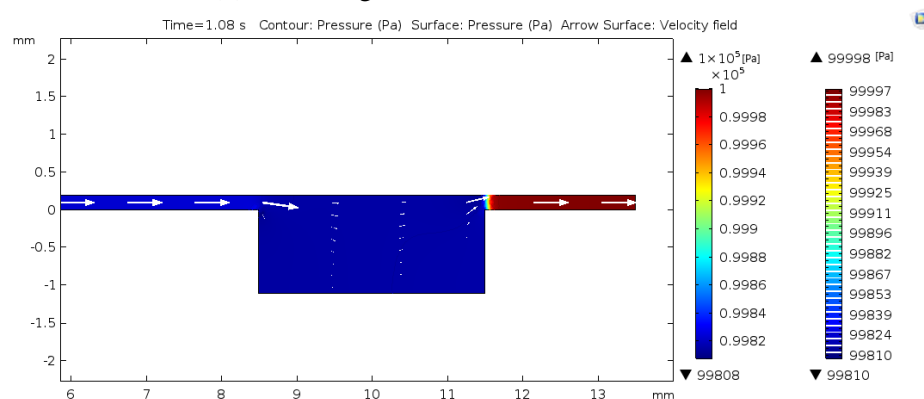
From the initial condition, a positive pressure gradient is present between the inlet and the outlet of the model, that drives the fluid as shown in the figures 6.15 . In the inlet, the initial condition is $P_o = 0$ Pa, while for the outlet where the air is still present the value is $P = 10^5$ Pa. In the zones where saliva is present, the value of pressure is lower, and it is $0.998 \cdot 10^5$ Pa (figure 6.16) . The value of ΔP is of almost 100 Pa and it remains constant along all the microchannel during the simulation, as shown from the figure 6.15 , where the scale is more accurate. Only when the meniscus is going to flow inside the reaction chamber and the outlet channel, all the values of pressure tend to 1 atm, and the pressure drop is lower, around 50 Pa. It rises again in the outlet channel, becoming of almost 200 Pa.



(a) Pressure gradient in the microchannel.

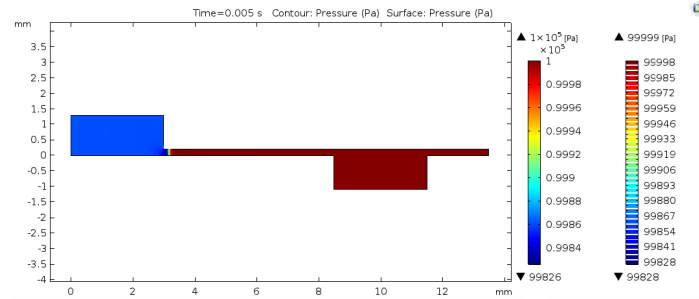


(b) Pressure gradient in the reaction chamber.

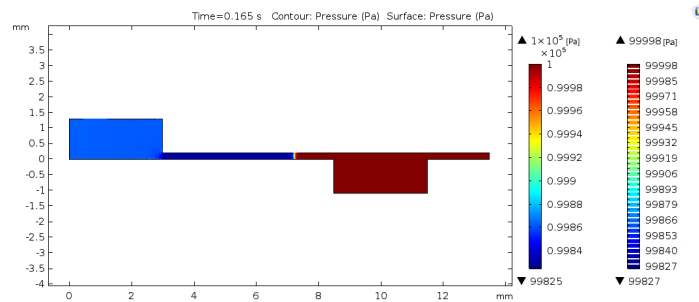


(c) Pressure gradient near the outlet microchannel.

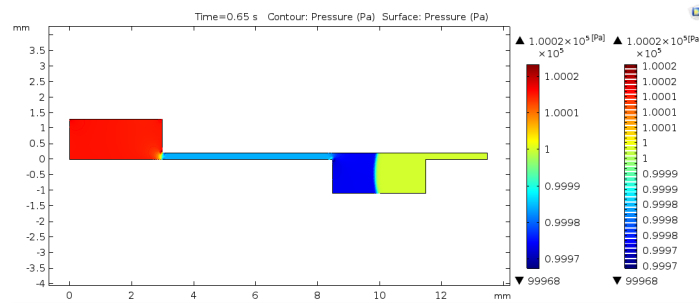
Fig. 6.15 Detail of the pressure drop along the model between time 0 [s] and 1.16 [s], measured in Pascal [Pa].



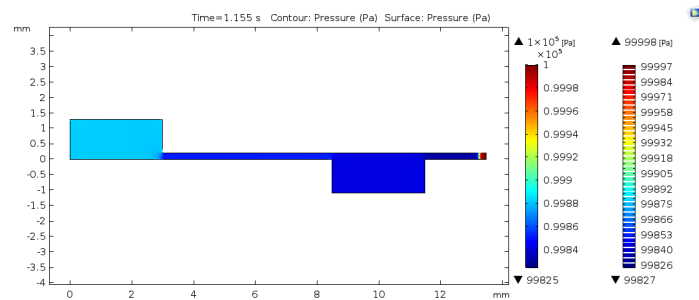
(a) Pressure in the inlet chamber.



(b) Pressure in the microchannel.



(c) Pressure in the reaction chamber.

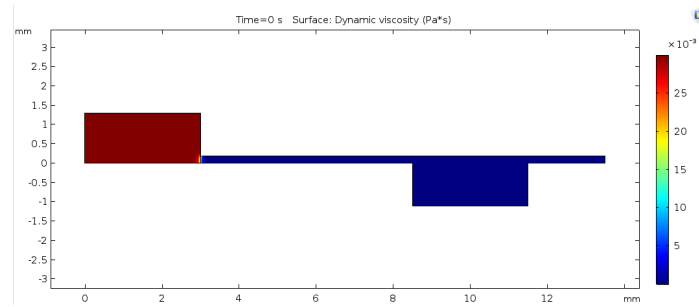


(d) Pressure in the outlet channel.

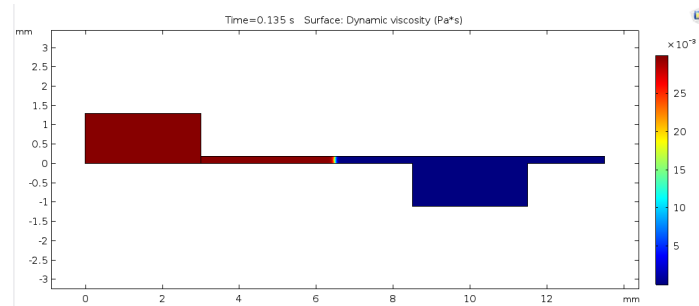
Fig. 6.16 Pressure values between time 0 [s] and 1.16 [s], measured in Pascal [Pa].

4. SHEAR RATE AND DYNAMIC VISCOSITY

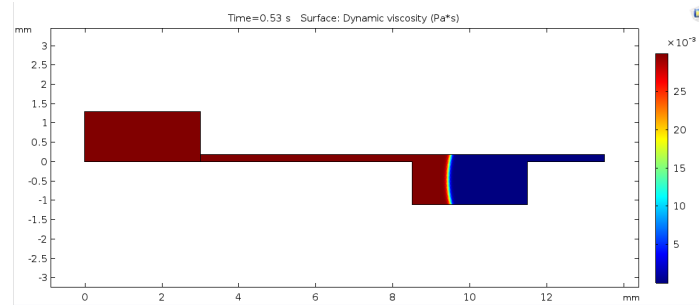
As explained before, referent values of shear rate for unstimulated saliva (US) are in the range of 1-1000 [1/s], in which the dynamic viscosity can change from a maximum value of 70 [mPa·s] to 1 [mPa·s]; the input values for the Carreau model were $\mu_0=70$ [mPa·s] and $\mu_\infty=1$ [mPa·s]. From the results an inverse relation between the shear rate and the dynamic viscosity is visible, having low values of dynamic viscosity around $25 \cdot 10^{-3}$ [Pa·s] (figure 6.17), for high values of shear rate, on the order of 10^3 [1/s] (figure 6.18). The dynamic viscosity values become lower at the two-fluid interface. The results confirm the Non-Newtonian nature of saliva. In the reaction chamber the values of shear rate are lower in confront of the ones in the microchannel, maybe because of the bigger sizes of the section; they resulted to increase from the borders to the centre varying in the range of 210÷250 [1/s]. These values are in accordance with ones obtained for Reynolds (figure 6.14), because they have a direct proportionality. Finally, maintaining the same input values for μ_0 and μ_∞ , new initial dynamic values were tested in different simulations for studying the device performance dependence from this parameter. The test range was from 1 [mPa·s] to 70 [mPa·s]. The results showed a maximum value for the dynamic viscosity along the model, of 18 [mPa·s] for initial values less of 20 [mPa·s]. For initial values bigger than 30 [mPa·s], the maximum value had a saturation to 45 [mPa·s]. The shear rate values remained comparable with the other ones of the initial simulation, as well for the pressure and velocity fields.



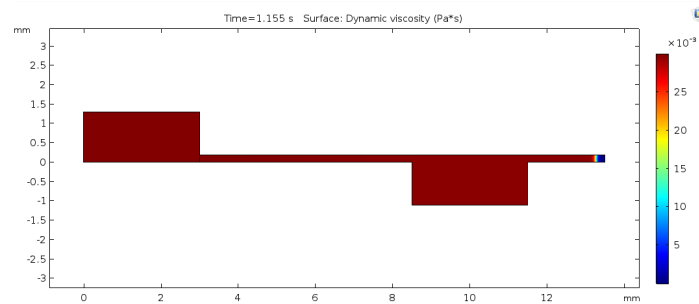
(a) Dynamic viscosity values in the inlet chamber.



(b) Dynamic viscosity values in the microchannel.

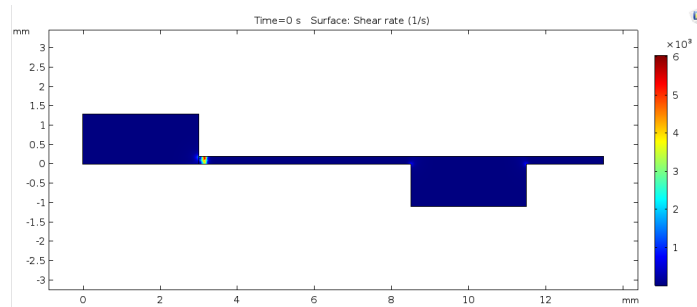


(c) Dynamic viscosity values in the reaction chamber.

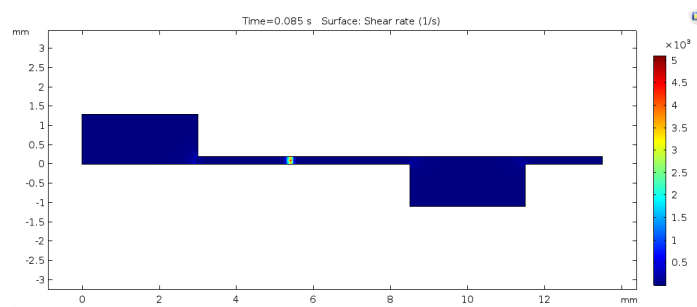


(d) Dynamic viscosity values in the outlet channel.

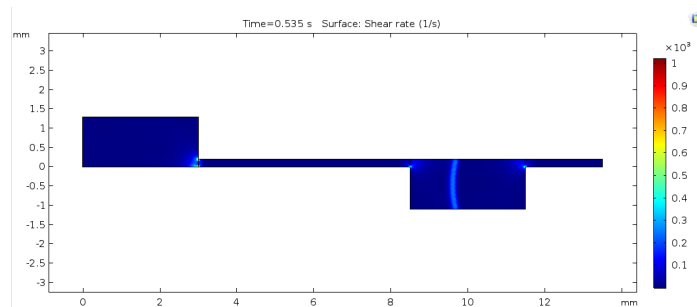
Fig. 6.17 Dynamic viscosity values between time 0 [s] and 1.16 [s], measured in Pascal for second [Pa · s].



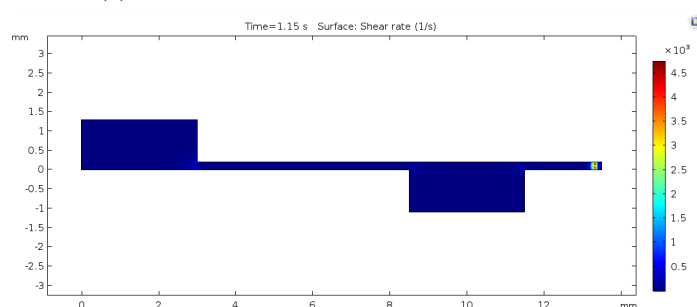
(a) Shear rate values in the inlet chamber.



(b) Shear rate values in the microchannel.



(c) Shear rate values in the reaction chamber.



(d) Shear rate values in the outlet channel.

Fig. 6.18 Shear rate for second values between time 0 [s] and 1.16 [s].

6.4 2D Top-section FEM simulation

6.4.1 Geometry

The proposed device has a microfluidic geometry, where the saliva sample is loaded from the top of a central rectangular inlet chamber (3 mm x 3 mm section); from this symmetrically three rectangular microfluidics channel depart (0.2 mm wide, 5.5 mm long); they are linked to the respective reaction chamber (3 mm x 3 mm section). It finally goes out from the outlet channel (0.2 mm width, 2 mm long) linked to this last chamber. The dimensions of the microchannels, chambers, inlet and outlets were optimized according to the fluid flow arrangement and to the dimensions of the first design model proposed, by using a finite-element method (*COMSOL Multiphysics 5.3.a*) (figure 6.19).

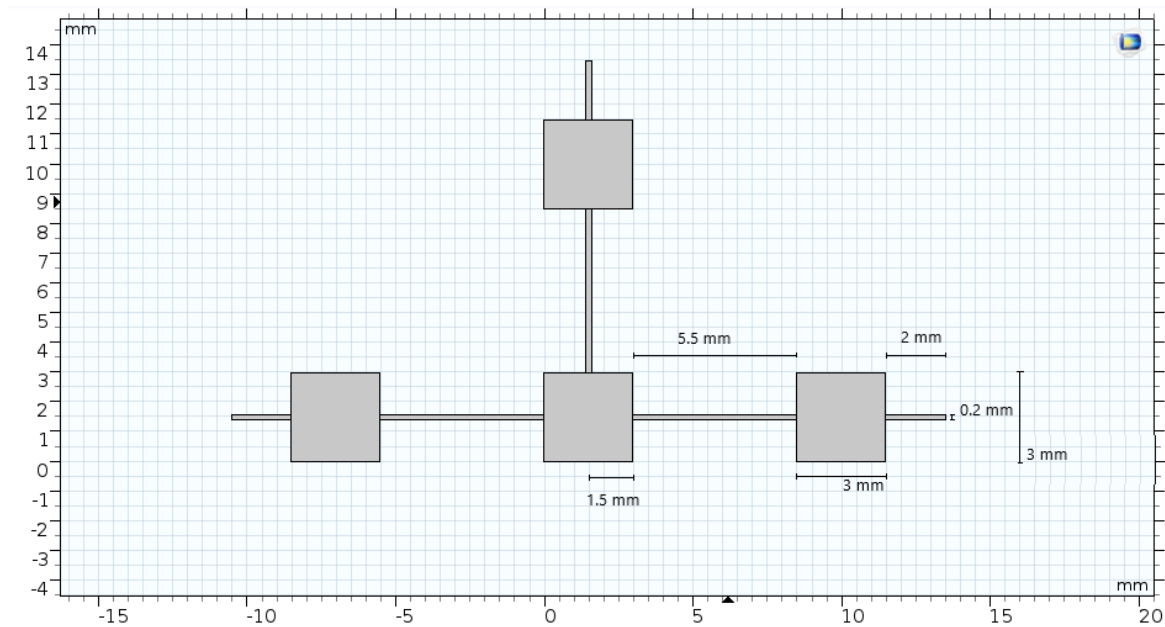


Fig. 6.19 2D model from the Top section.

6.4.2 Boundary conditions

All the input parameters used in the first simulation were respected regarding set up of walls and boundary conditions; also, materials properties were the same. For allowing the correct working of the software, the inlet boundary was supposed to be the bottom side of the model. The outlet was defined as a pressure area with a value of 10^5 Pa.

6.4.3 Mesh

In this model too was used the automatic physics-controlled mesh generation, already adjusted for fluid flow and general physics. The manual mesh was defined with triangles, for a total of 738 triangles. The mesh size was adjusted for having a manageable computing time; according to the coarser design, the maximum element size is $1.76\text{ }\mu\text{m}$, the minimum is $0.0675\text{ }\mu\text{m}$, and the curvature factor is of 0.8 (figure 6.20).

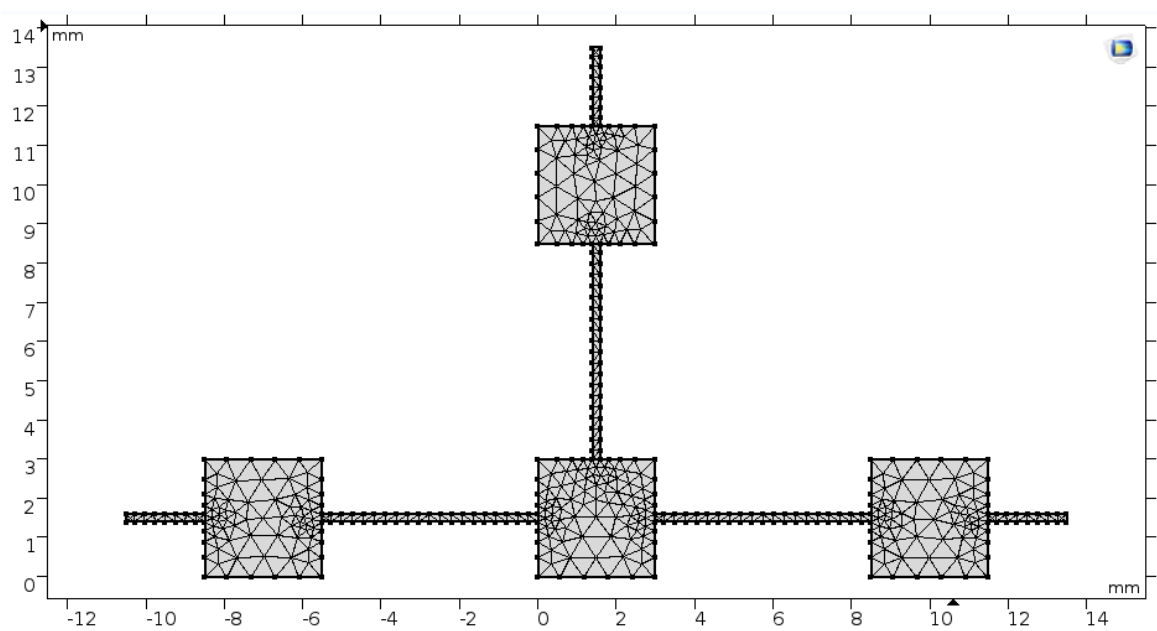
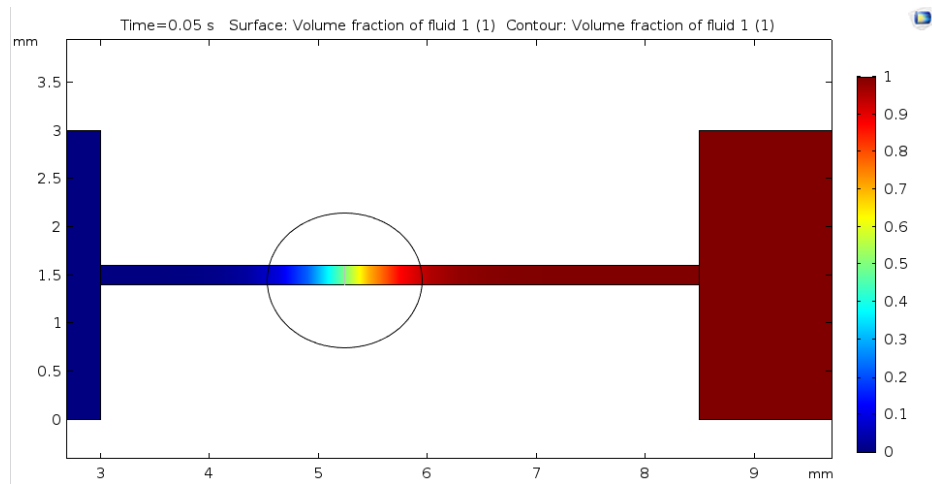


Fig. 6.20 2D model mesh from the Top section.

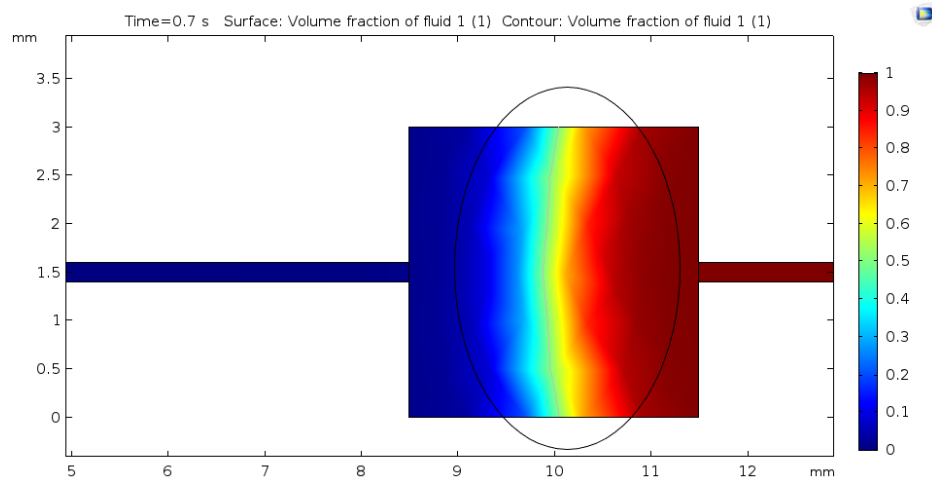
6.4.4 Results

1. VOLUME FRACTION OF FLUID

Results show the formation of a meniscus along the channels and also along the reaction chambers, that moves uniformly as a piston along its way; furthermore, an interface between saliva and air is always present, demonstrating the correct phases separation (figure 6.22). From the equations of the phase-field model (equations 6.10,6.12), a constant value of 0 for the fraction volume of fluid one is obtained in areas filled with saliva; this condition is present along all the model. Meniscus shape is concave, as result for the first simulation (figure 6.21). In this case too, it is possible to see that the fluid takes almost 1.16 seconds to cross all the section of the microuidic device.

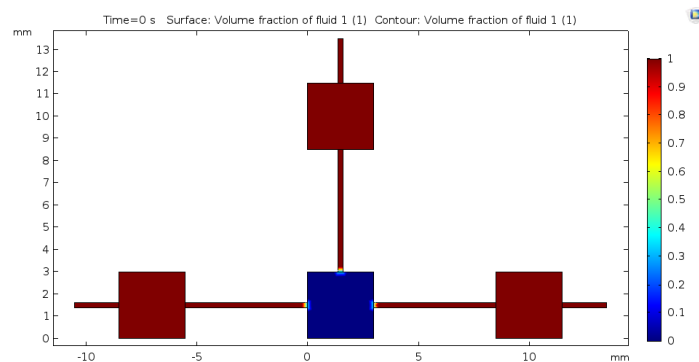


(a) Meniscus in the inlet channels.

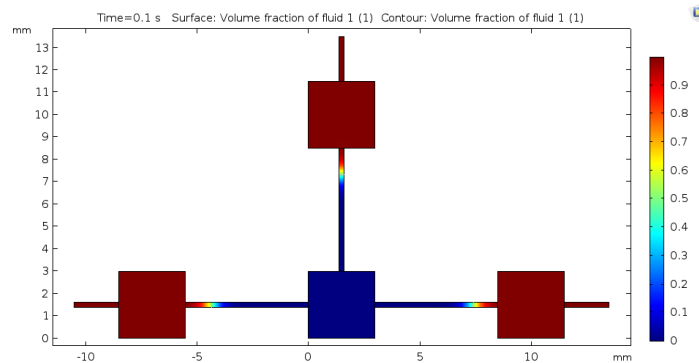


(b) Meniscus in the chambers.

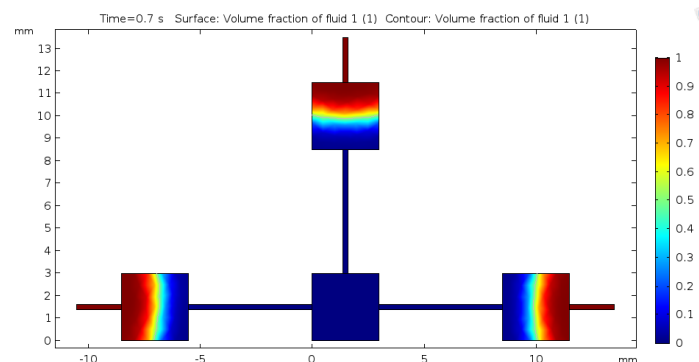
Fig. 6.21 Detail of the meniscus shape in the channel and in the reaction chamber.



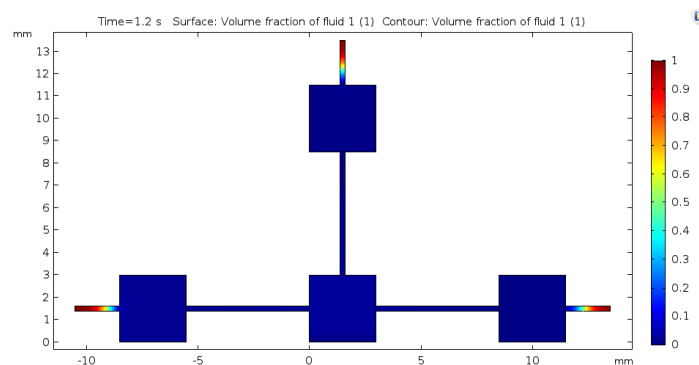
(a) Meniscus in the inlet chambers.



(b) Meniscus in the microchannels.



(c) Meniscus in the reaction chambers.



(d) Meniscus in the outlet channels.

Fig. 6.22 Meniscus evolution between time 0 [s] and 1.16 [s].

2. VELOCITY

The results are comparable with the ones obtained in the first design; the maximum value of velocity reached is 0.05 [m/s] in the microchannels while in the reaction chambers it drastically changes becoming of the order of $3 \cdot 10^{-3}$ [m/s], allowing the biomarkers detection (figure 6.25). The velocity rises again in the outlet channels. The fluid domain is laminar, in accordance with the Reynolds values obtained (figure 6.26). Furthermore these values result lower of the expected ones. The filling appears to develop with the same time steps of the first one. From this section model, it is possible to see the development of the meniscus in the microchannels during the time, while there is not possibility to see the velocity profile development as well. One explanation could be the bigger time step imposed for reducing the computational time, because of the bigger geometry. The velocity values seem to have a homogeneous value along all the microchannel geometry. However, the values respect the ones of the first simulation so for this reason, this factor does not change the consistency of the model. In the reaction chamber, from the contour line, it is possible to see that the fluid moves uniformly as in the first simulation. The streamlines occupy all the surface area uniformly (figure 6.23).

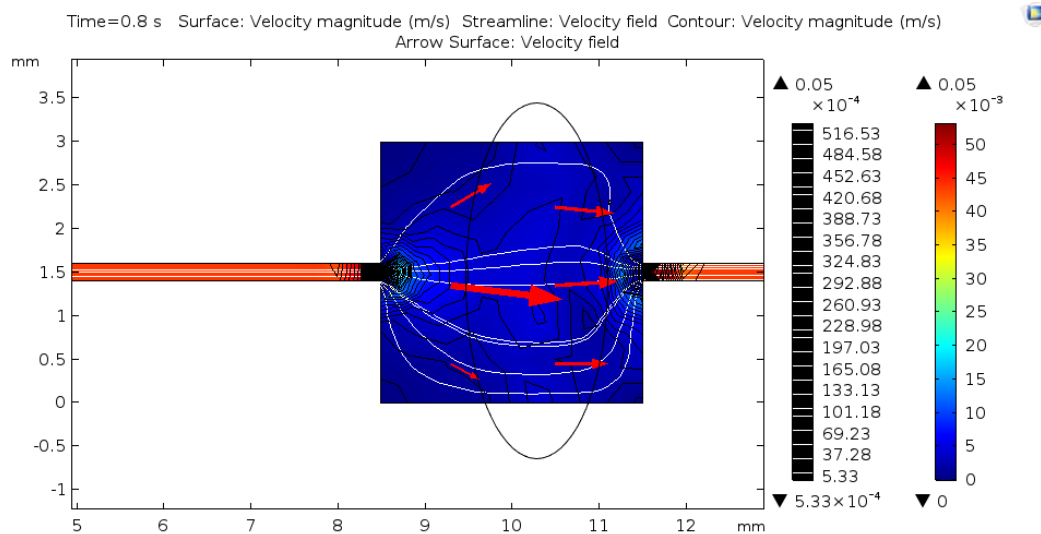
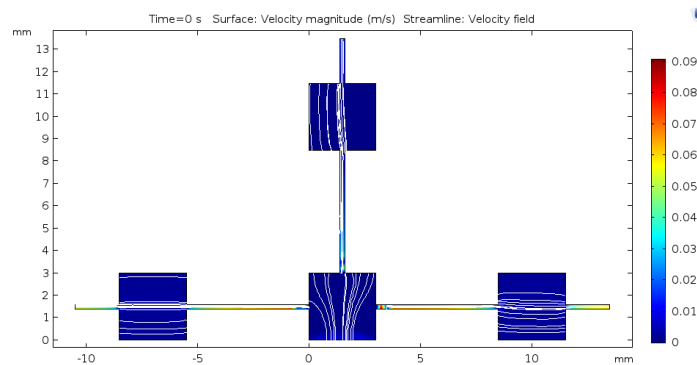
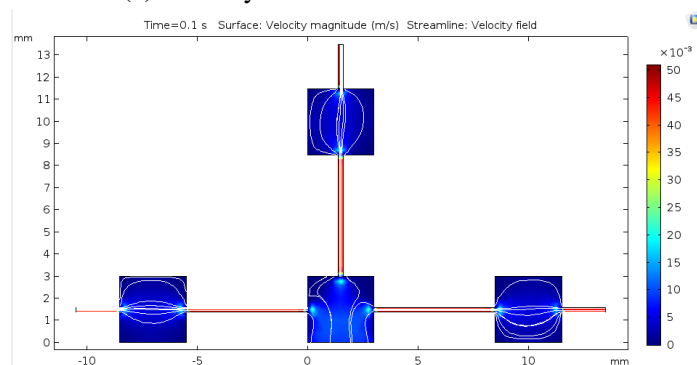


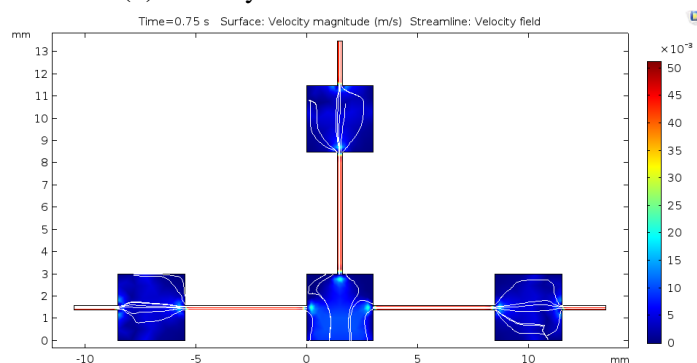
Fig. 6.23 Velocity profile in the reaction chambers.



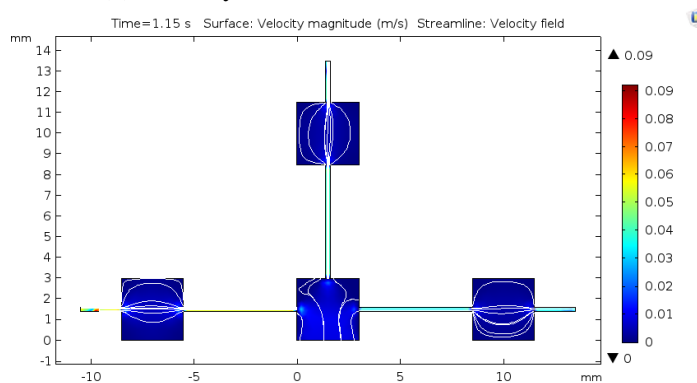
(a) Velocity values in the inlet chambers.



(b) Velocity values in the microchannels.

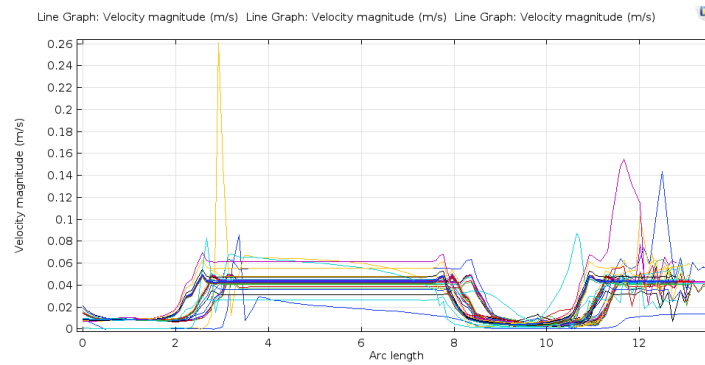


(c) Velocity values in the reaction chambers.

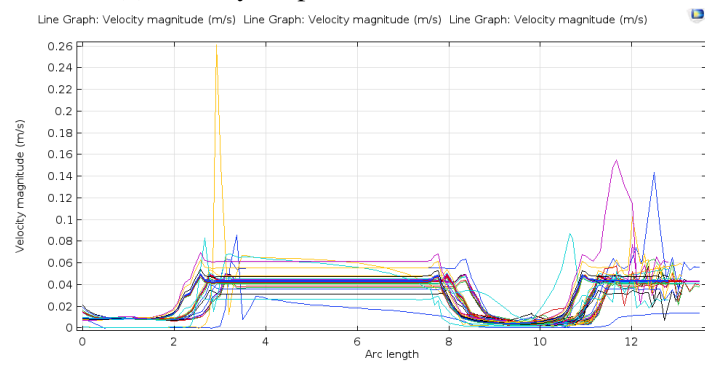


(d) Velocity values in the outlet channels.

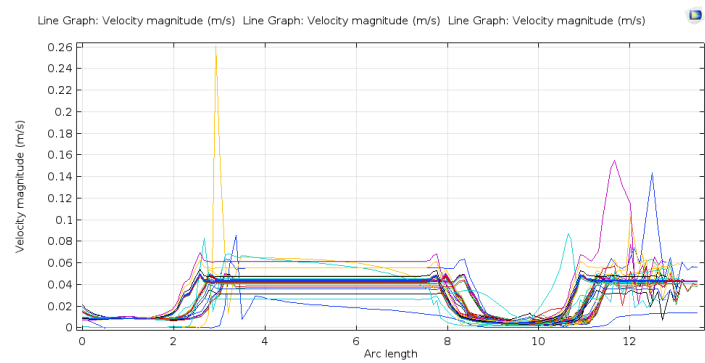
Fig. 6.24 Velocity values between time 0 [s] and 1.16 [s].



(a) Velocity drop in the reaction chamber 1.

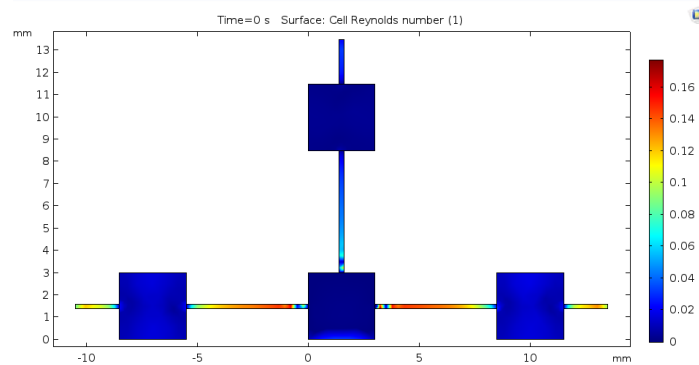


(b) Velocity drop in the reaction chamber 2.

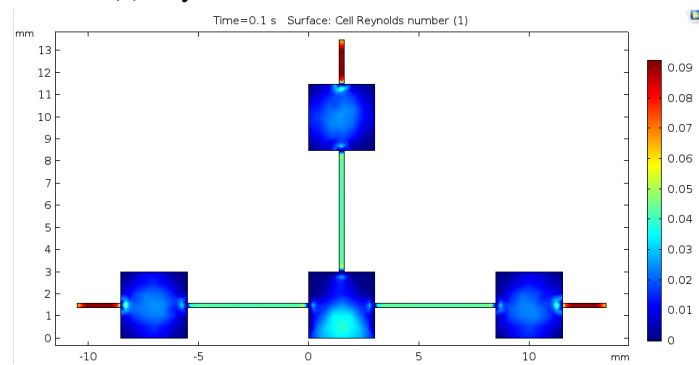


(c) Velocity drop in the reaction chamber 3.

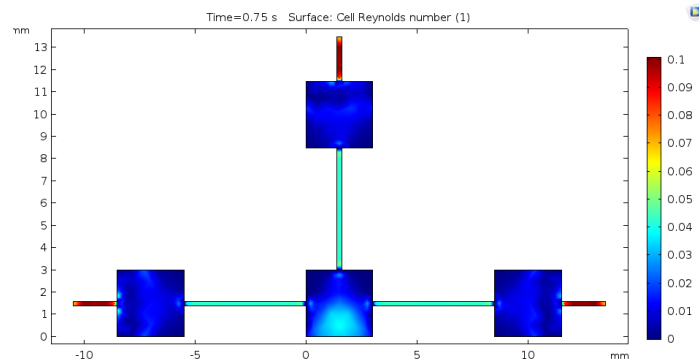
Fig. 6.25 Velocity drops between time 0 [s] and 1.16 [s].



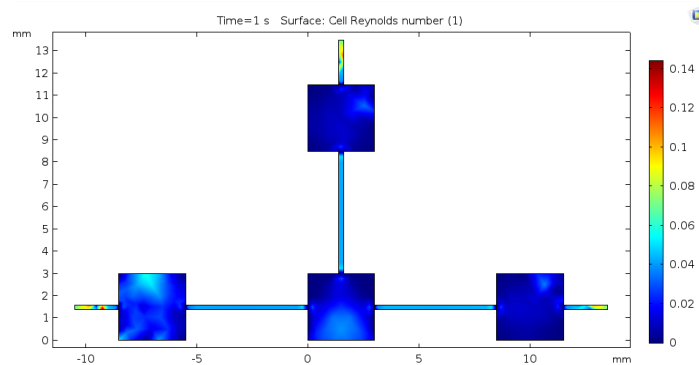
(a) Reynolds number in the inlet chambers.



(b) Reynolds number in the microchannels.



(c) Reynolds number in the reaction chambers.

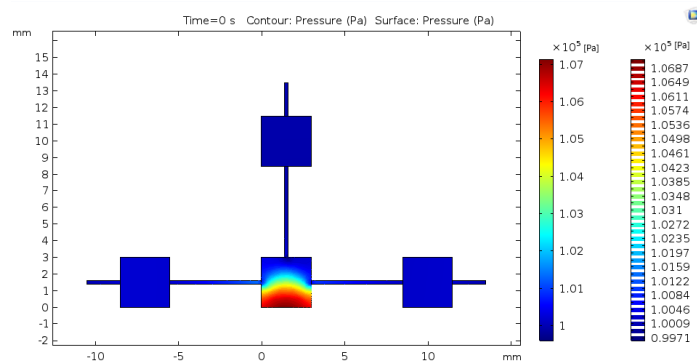


(d) Reynolds number in the outlet channels.

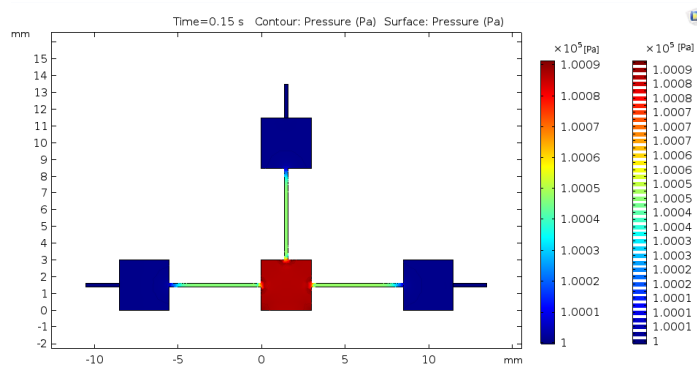
Fig. 6.26 Reynolds number values between time 0 [s] and 1.16 [s].

3. PRESSURE

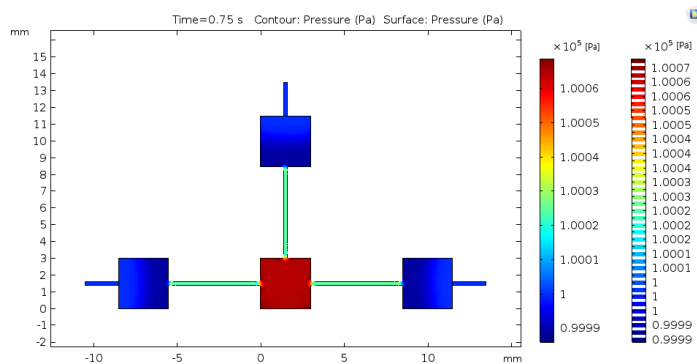
A pressure drop is evident at the beginning of the simulation; at time 0 [s] the drop pressure is different from the one obtained in the first design simulation because of the inlet side condition; values are around 10^5 [Pa]. However, during the fluid motion, all the values of pressure tend to be comparable with the ones of the first simulation. As for the velocity results, it is not possible to see the evolution of the pressure values along all the microchannel. The results become consistent and comparable from the observation of the meniscus pressure before entering the reaction chamber. In this point, the values tend to be higher in the microchannels and less in the rest of the model, as also verified in the first simulation (figure 6.27b). The comparison is visible in the figure 6.28. The pressure drop is ~ 10 [Pa] and drives the meniscus inside the chamber. From the theory, an area where air is still present, should be higher values of pressure compared with areas filled with saliva. Furthermore in the passage from a big section area to a lower one in a channel, expected values of pressure should be higher in the first one than in the second one. In addition, the expected velocity values should be lower in the area with the bigger section. Despite this, the inlet boundary condition and the hydrophilic surface properties can influence the pressure values in this point of the simulation. Furthermore, load losses can contribute to this phenomenon and for all these reasons, the pressure in this zone is lower, while the velocity values are as the expected. In the chamber both the results of velocity and pressure follow correctly the expected results (figure 6.29). The values of pressure tend to 1 [atm] (figure 6.24c), becoming higher in the side of the outlet channels; the gradient of pressure is minimum, less of 30 [Pa]. It remains constant along the chamber while in the outgoing it rises again, becoming bigger than 100 Pa. (figure 6.30) .



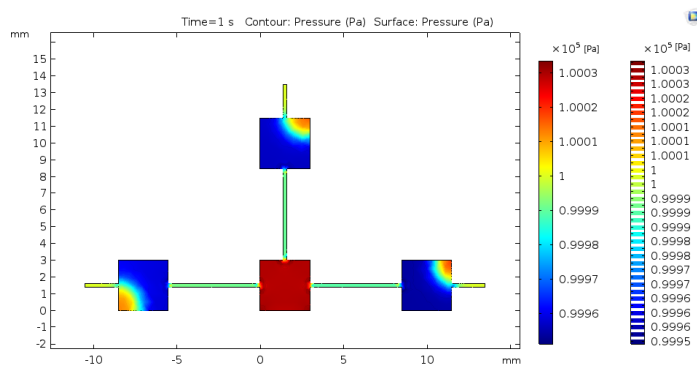
(a) Pressure in the inlet chambers.



(b) Pressure in the microchannels.

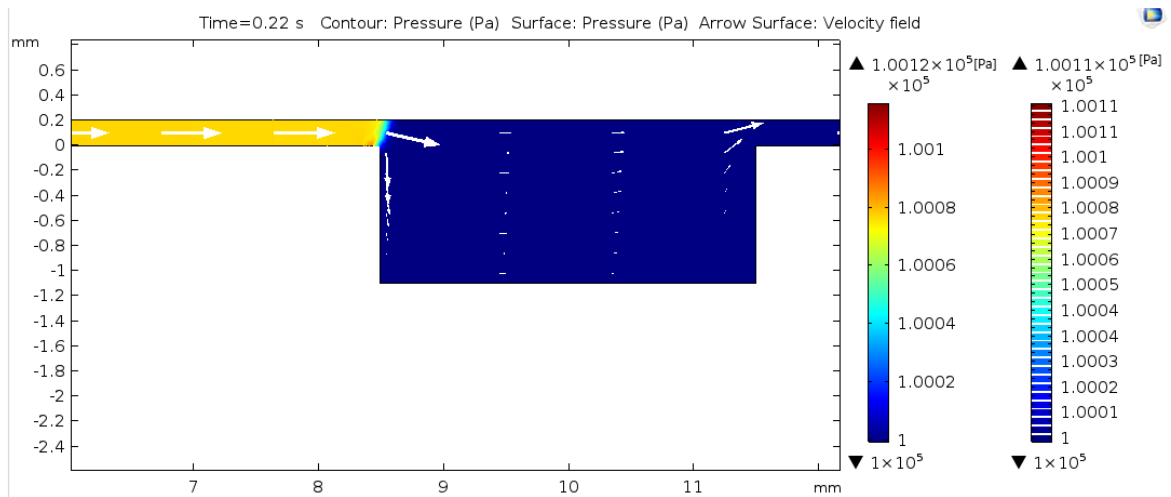


(c) Pressure in the reaction chambers.

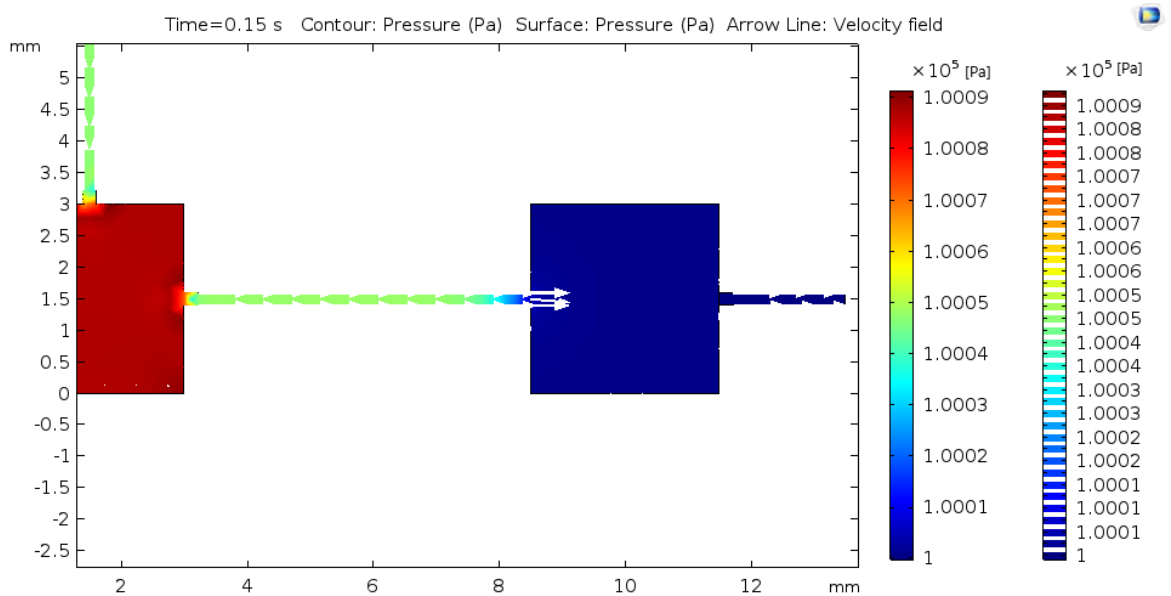


(d) Pressure in the outlet channels.

Fig. 6.27 Pressure values between time 0 [s] and 1.16 [s] measured in Pascal [Pa].

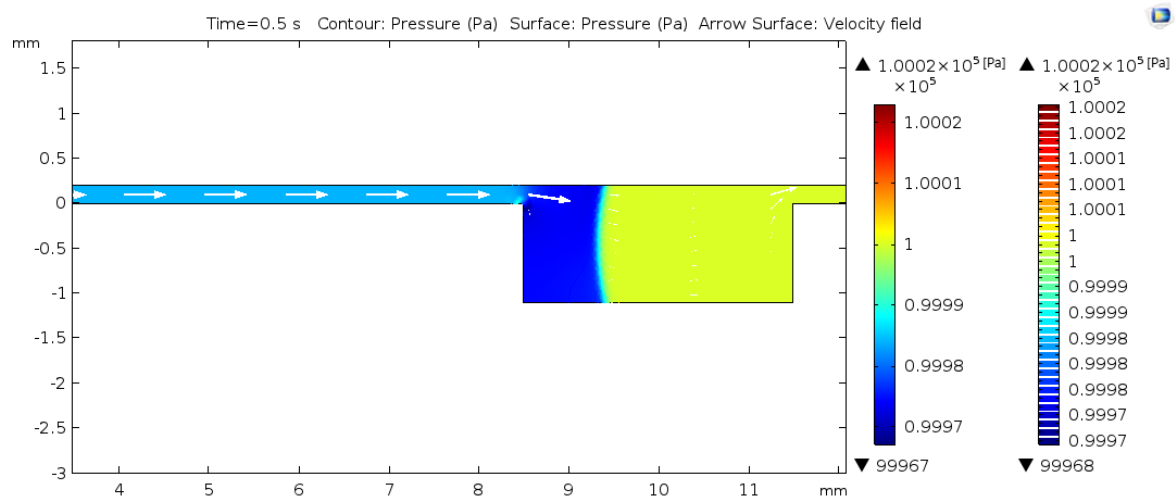


(a) Pressure gradient before the reaction chamber in the cross-section simulation.

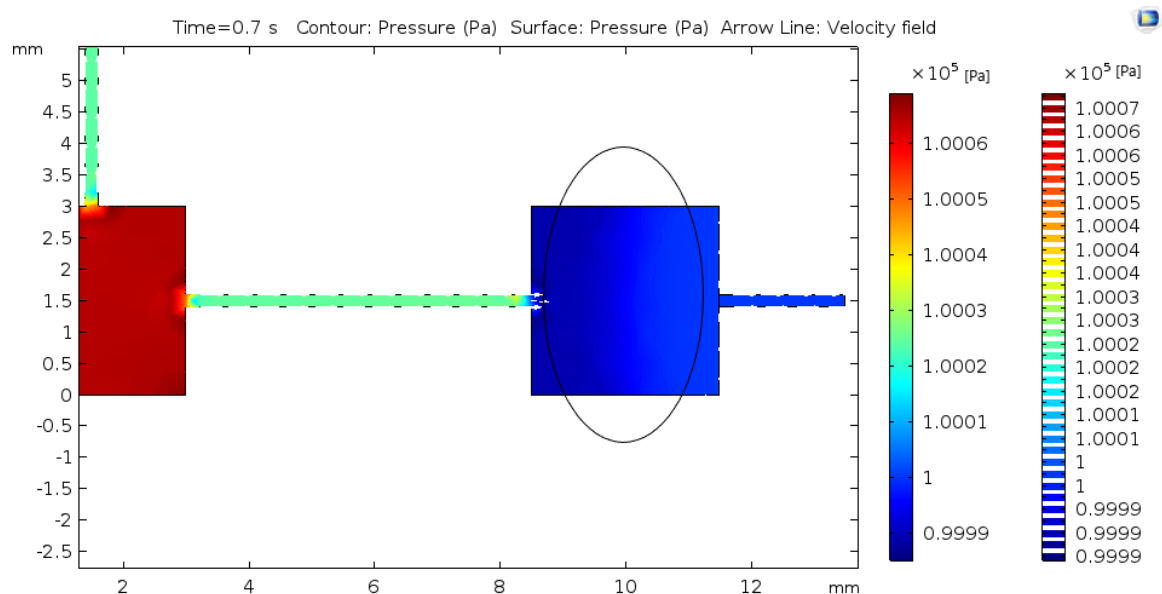


(b) Pressure gradient before the reaction chambers in the top-section simulation.

Fig. 6.28 Pressure gradient values in the microchannel.

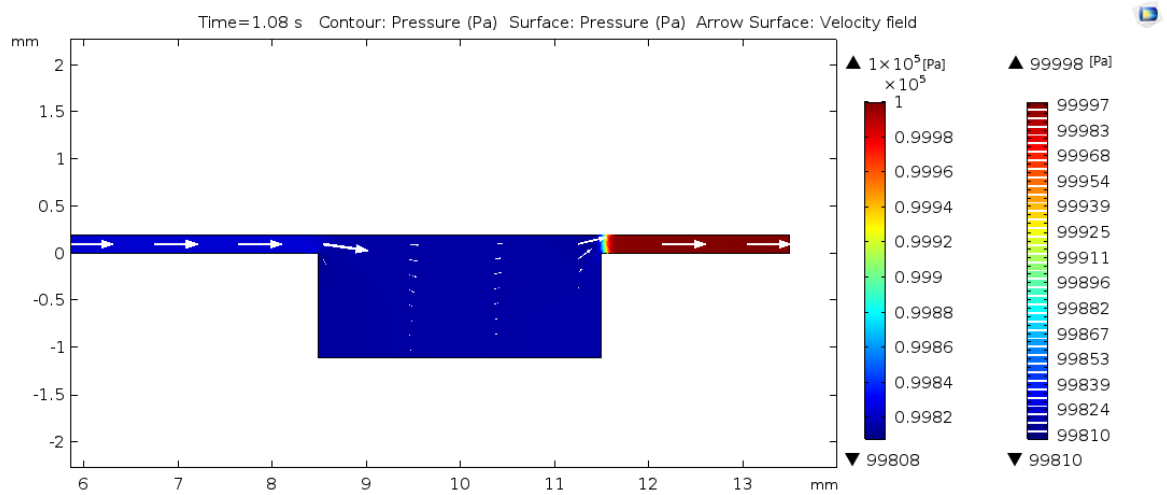


(a) Pressure gradient in the reaction chamber in the cross-section simulation.

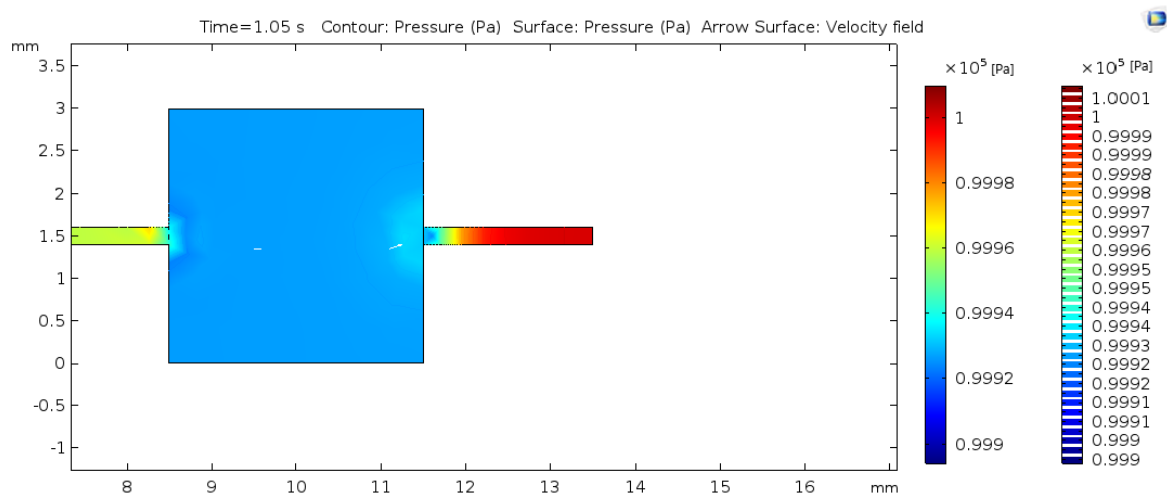


(b) Pressure gradient in the reaction chambers in the top-section simulation.

Fig. 6.29 Pressure gradient values in the reaction chamber.



(a) Pressure gradient near the outlet channel in the cross-section simulation.

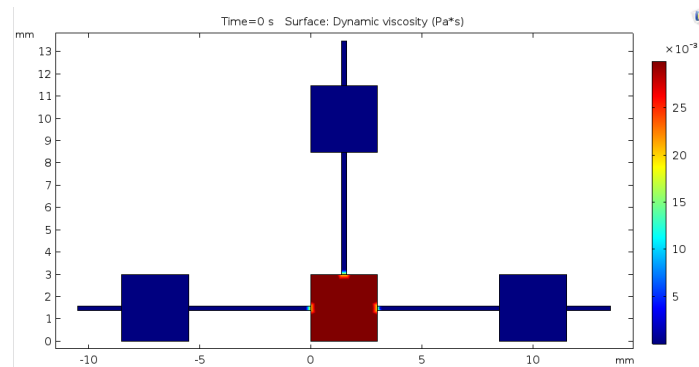


(b) Pressure gradient in the outlet channels in the top-section simulation.

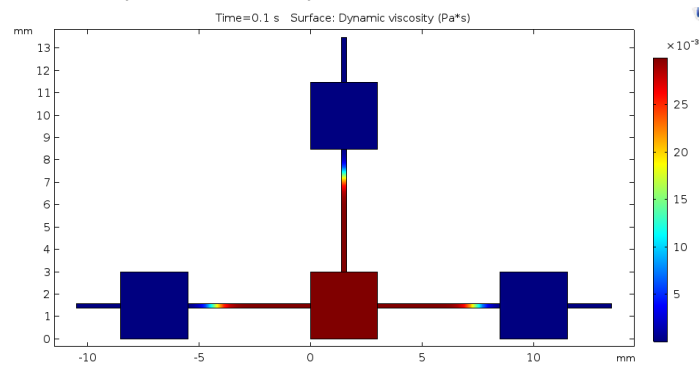
Fig. 6.30 Pressure gradient values in the outlet microchannel.

4. SHEAR RATE AND DYNAMIC VISCOSITY

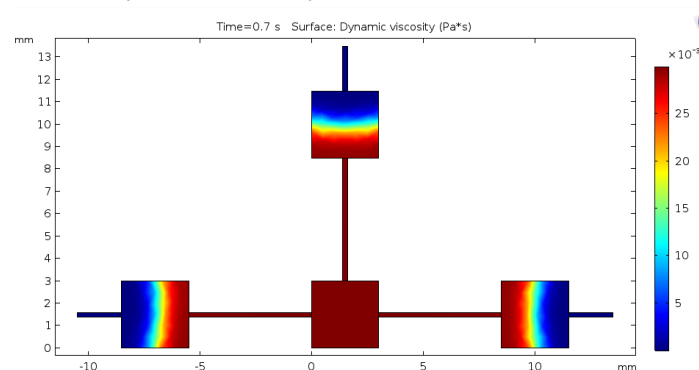
The results are the same as the first simulation design; an inverse relationship between the shear rate and the dynamic viscosity is visible, having values of dynamic viscosity around $25 \cdot 10^{-3}$ [Pa·s] (figure 6.32), for high values of shear rate, on the order of 10^3 [1/s] (figure 6.31). At the two fluid interface the dynamic viscosity values decrease. From the top, it is not visible the changing of the shear rate in the reaction chambers, that was verified in the first model.



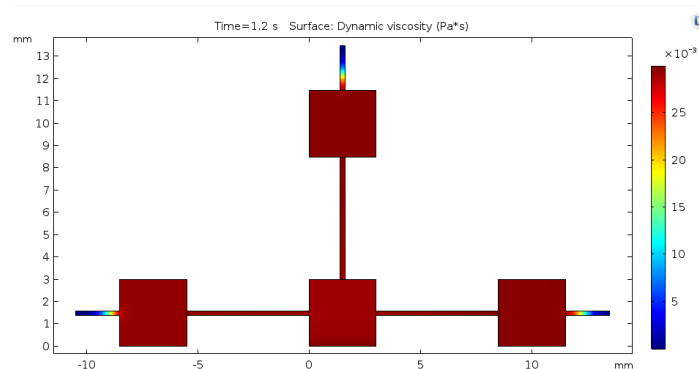
(a) Dynamic viscosity values in the inlet chambers.



(b) Dynamic viscosity values in the microchannels.

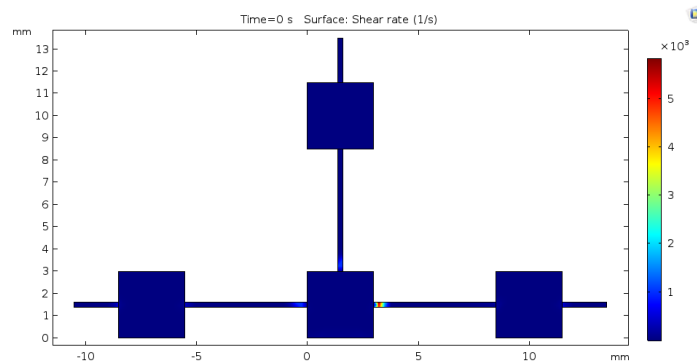


(c) Dynamic viscosity values in the reaction chambers.

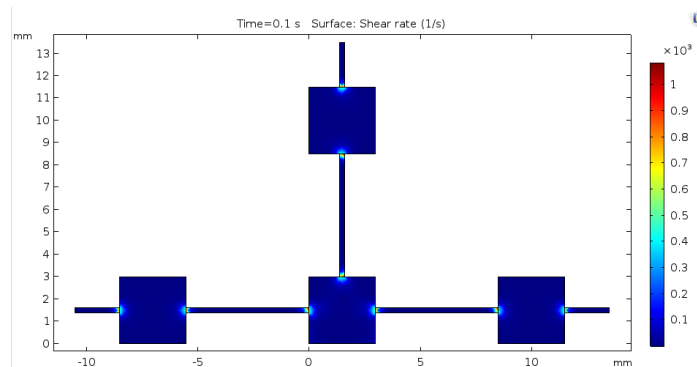


(d) Dynamic viscosity values in the outlet channels.

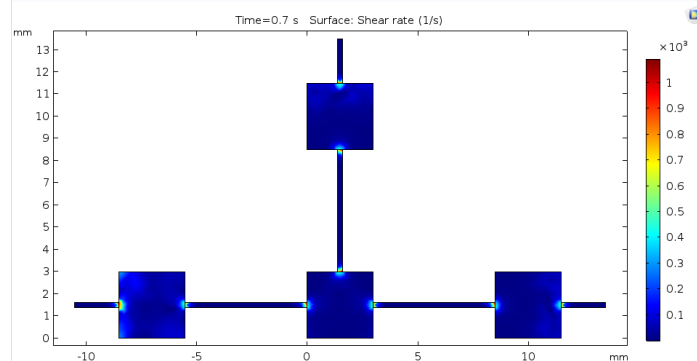
Fig. 6.31 Dynamic viscosity values measured in Pascal for second [Pa/s] between time 0 [s] and 1.16 [s]



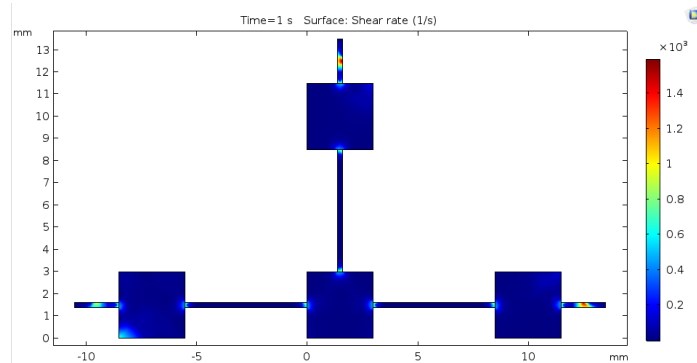
(a) Shear rate values in the inlet chambers.



(b) Shear rate values in the microchannels.



(c) Shear rate values in the reaction chambers.



(d) Shear rate values in the outlet channels.

Fig. 6.32 Shear rate values for second [1/s] between time 0 [s] and 1.16 [s].

Chapter 7

Building process experience: the Soft-lithography

In this chapter, the goal is to study the building process that could be used for the realization of the proposed PMMA microfluidic device.

7.1 Soft-lithography process

The soft-lithography is a building technique for micro and nano-structures included in the ‘top-down’ methods. It allows the realization of 2D and 3D structures by starting from a ‘bulk’ material. It includes two building steps; the first one is the photolithography process for the realization of the ‘master’, that reproduces the structure to transfer to the polymer substrate. The casting of a liquid polymer precursor on a master mould holding a pattern of photoresist, is the second step. The key materials for this technique are the wafer, the resist, the mask, and the incident radiation.

The wafer can be of different materials, such as gold or aluminum for metallization; furthermore, ceramic materials, such as SiO_2 , are used for dielectrics substrates. The resist is a photo-sensible material that changes its properties after being exposed to the irradiation. It can be defined as positive or negative. A positive photoresist increases the solubility in the irradiated zones; a developer solution will remove these. On the other hand, in a negative one, the cross linking between polymeric chains increases in the irradiates area, and the developer solution will delete the non-irradiated part of the photoresist.

The mask contains binary spatial information. The black zones correspond to 0 and the transparent ones to 1. It decides the photoresist area that will be irradiated (1) or not (0). Finally, the irradiation source can be of UV rays or X-rays. There are different approaches

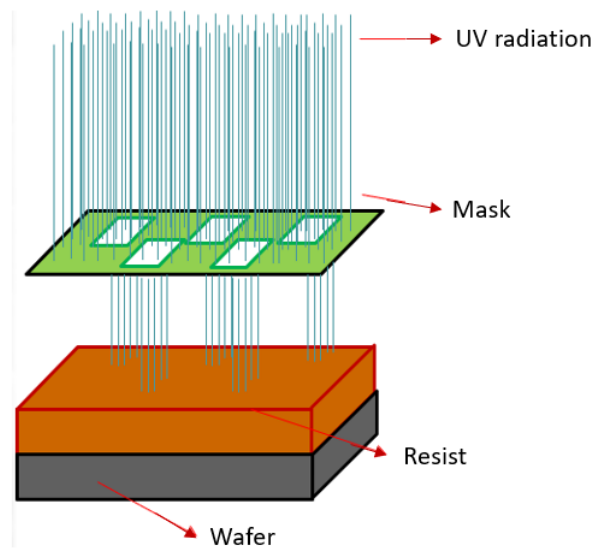


Fig. 7.1 Schematic explanation of the key materials used in the soft-lithography technique.

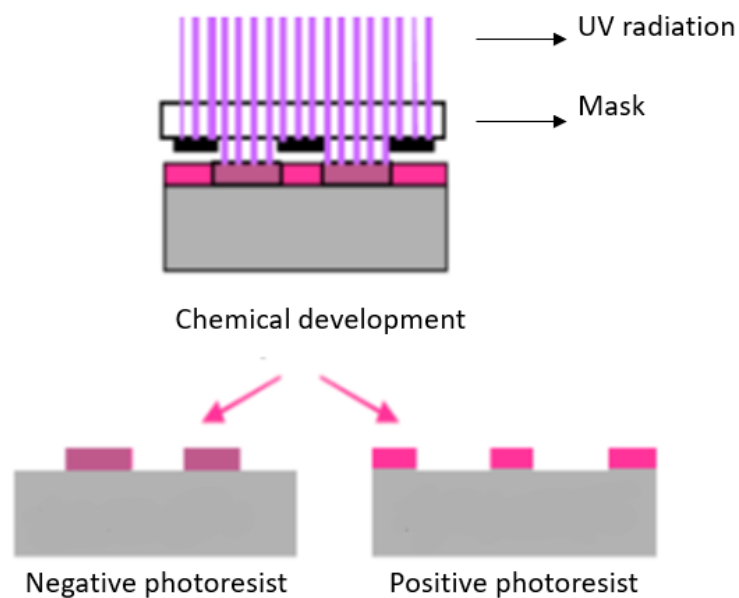


Fig. 7.2 Schematic explanation of the after exposure development for a respective positive and negative photoresist.

for the photolithography technique, that can be distinguished by the mask position. In the contact photolithography, the mask is in direct contact with the resist. In the soft-contact photolithography, there is a little ‘gap’ distance between the mask and the photoresist. The scale dimension of this gap must be less of the wavelength irradiation. The advantage of this solution is that the mask does not risk to be consumed. The disadvantage can be that the diffraction optical effects could influence the spatial resolution. For preventing this, the best solution is the ‘projection’ photolithography. The distance between the mask and the resist is bigger, but a lens system focuses the rays on the area to be irradiated. The traditional photolithography technique consists of different steps. In an example process firstly, the silicon wafer is treated for deleting all the impurities. After this, a homogeneous resist substrate is deposited on the wafer, that is fixed on the plate base of a spinning machine. Thanks to this machine, it is possible to control the photoresist thickness, by setting some initial parameters. The thickness is directly linked with the size of the desired structures. The parameters to be set are the spinning acceleration (rpm) and the spinning time (s). The next step is the soft-baking, in which the resist is usually backed at two different temperatures. This process allows to deleting the remaining solvent present in the resist. It influences the resolution of the final geometry. At this point, the resist is exposed to a UV source or X-rays, trough one of the processes explained before. Successively, the resist is backed again in the ‘post-baking- step’, at two different temperatures for increasing its quality. Finally, in the ‘development step’, the resist takes its shape and it is possible to observe the patterned structures called ‘master’. From this ‘master’ structure, it is possible to develop the microfluidic device with the desired material. The liquid state of the polymeric material is poured over the master. Finally, the complex is cured in the oven. The elastomeric stamp is obtained just from its peeling away from the master (figure 7.3).

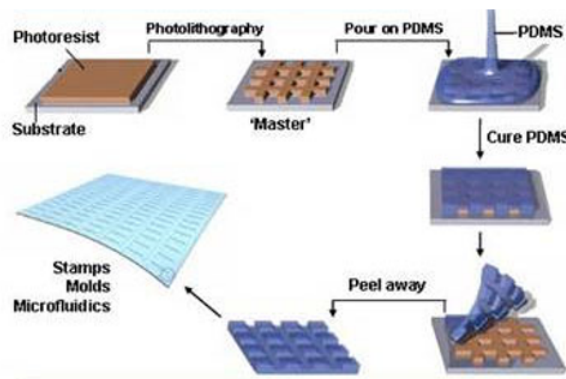


Fig. 7.3 Schematic explanation of the different steps of the soft-lithography process.

7.2 Work Methodology

The experiment consists in the manufacture of microfluidic structures, by casting PDMS on a master mould made from silicon wafer holding a pattern of SU-8 photoresist. This resist allows to obtain a thickness of 100 [μm] for a spin speed of 3000 [rpm] (figure 7.4); it is possible to obtain ticker substrates by adjusting the spin speed and the spin machine program. In this case, the goal was to obtain a maximum value of 100 [μm] which will be the size of the microchannels. All the process was performed in a clean room.

SU-8 Spin Speed Curve

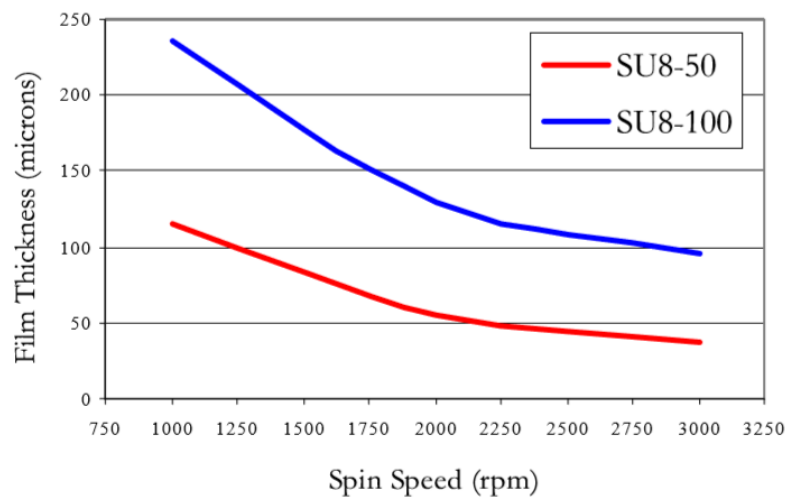


Fig. 7.4 Relation between the SU8-100 thickness and the spin speed.

In the experiment, the following chemicals were used:

- PDMS base- Sylgard 184 Silicone Elastomer (Dow Corning Corp., USA).
- PDMS curing agent- Sylgard 184 Curing Agent (Dow Corning Corp., USA).
- SU-8 100 photoresist

Furthermore, the following equipment was used:

- Balance
- Reactive Ion Etcher (RIE)- Plasma Therm SLR series
- Vacuum jar with a vacuum pump- Struers Epovac

- Oven- WTB Binder
- Glass plates (5x5 cm)
- Plastic plates
- Transfer pipette
- Glass stirring
- Gloves
- Protection glasses and cloths
- SI wafer (diameter 100 mm)
- Hot plates
- Mask
- Container (diameter > 100 mm)
- Surgical blade
- Blunt syringe needle and needles
- Spinning machine
- UV exposure machine
- Meshing machine Veeco machine (Dektat 150)
- Alpha Plasma machine

In the building process, the first step was the silicon (SI) wafer treatment; it was rinsed with DI water and Isopropyl alcohol for 6 minutes. Successively it was dried for 10 minutes on a hot plate at 200 °C (figure 7.6 a). The SI-wafer was positioned on the central base of the spinning machine, and the liquid resist precursor was poured over it (figure 7.6 b). The spinning machine was set to a program of three steps of different velocities, as shown in the table 7.10 and in figure 7.5; it reached a maximum of 3000 rpm. From this process, a homogeneous resist layer was obtained.

The soft-backing step deleted the impurities (bubbles) formed on the top of the substrate, and also the remaining solvent. The backing step consisted of two different temperatures:

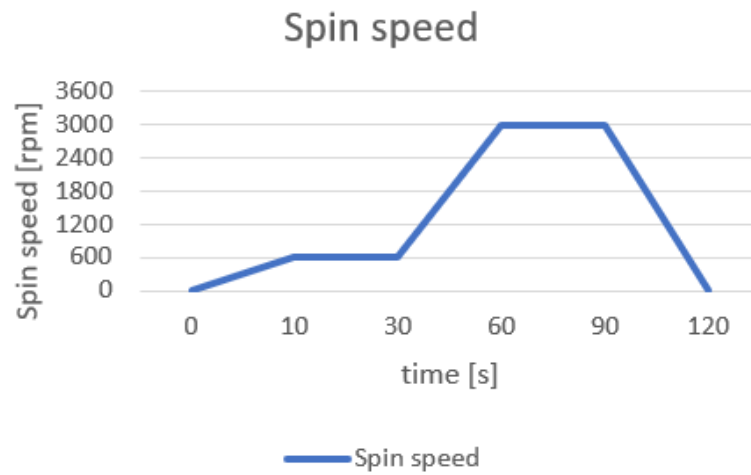
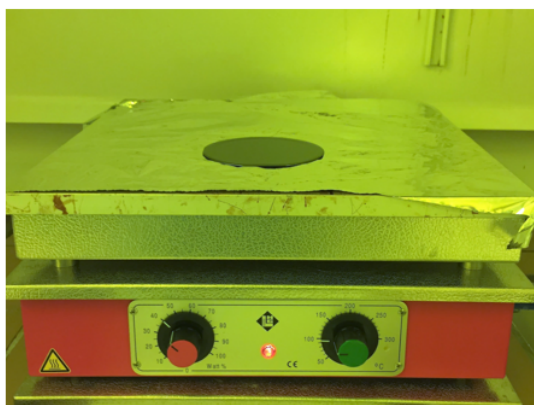
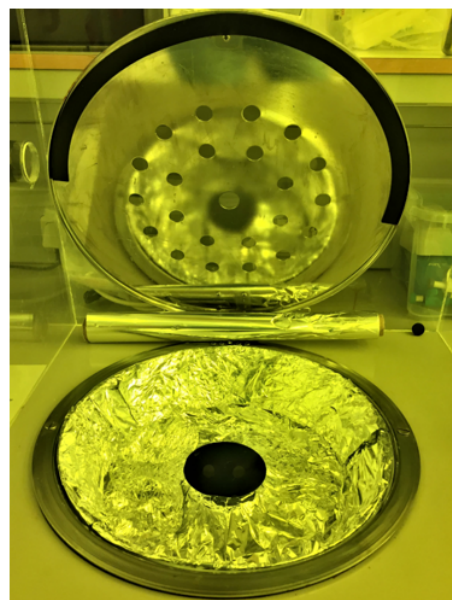


Fig. 7.5 Spin speed time evolution.



a)



b)

Fig. 7.6 a) Wafer drying on the hot plate; b) Wafer positioned in the spinning machine.

firstly the SI-resist wafer was backed at 65 °C for 15 minutes. After this, the hot plate was switched to 95°C and the complex was backed for other 30 minutes.

At this point, the SI-resist wafer was exposed to UV-source (350-450 nm) for 230 [s] (figure 7.7 b). The gap between the positive mask (figure 7.7 a) and the photoresist was of 30 [μm]. The successive step was the post-exposure backing at two temperatures, as before: 1 minute at 65 °C and 5 minutes at 95°C. Finally, the SI-resist wafer was rinsed with the SU8-100 developer for 6 minutes, and Isopropyl alcohol. The final master (figure 7.7 c) was dried with pressurized air for its final use.

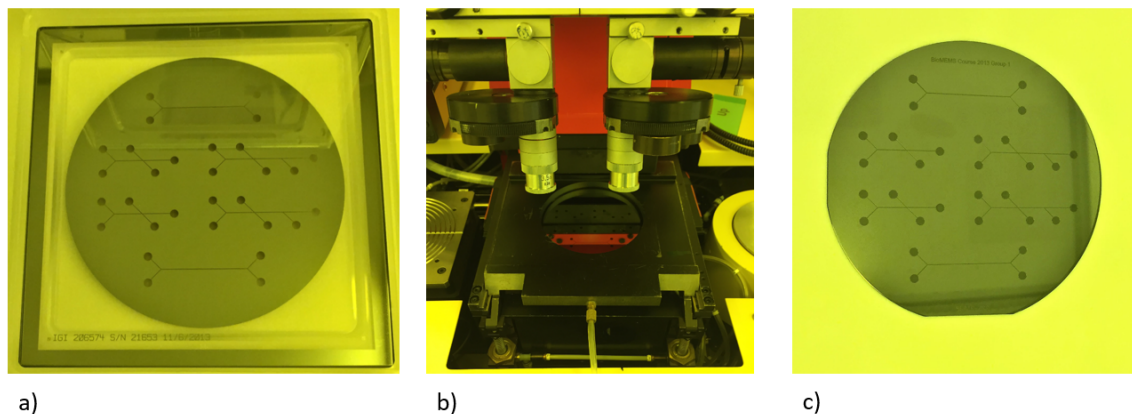


Fig. 7.7 a) Positive mask; b) UV-exposure machine; c) Master.

At this point started the step called 'micro-replica moulding'. It consists of pouring the liquid state of the polymeric material over the master. After this, the structure must be treated in the vacuum desiccators with a vacuum pump, for deleting the air bubbles. Finally, the complex must be backed in the oven. The elastomeric stamp can be obtained just from its peeling away from the master. The polymeric material used in this experiment was PDMS, because it was available in the laboratory. However the procedure would be the same by choosing PMMA. The PDMS prepolymer was prepared by mixing through a glass stirring into a plastic plate, 30 [g] of PDMS base with 3 [g] of PDMS curing agent (figure 7.8 a) added with a transfer pipette. This process was stopped when the mixture appeared almost white; this was a consequence of the air bubbles. The master was positioned into a grey container, and the mixture was poured on the top of it. Successively, the PDMS prepolymer was degassed for 30 minutes for getting rid it of air bubbles, until their complete disappearing (figure 7.8 b,c). Finally, it was cured in the oven at 65°C for 2 hours and left to rest at ambient temperature over night (figure 7.8 d). The curing occurs when vinyl groups ($-\text{CH}=\text{CH}_2$) present in the base react with a silicon hydride (Si-H) groups in the curing agent to form a cross-linked solid.

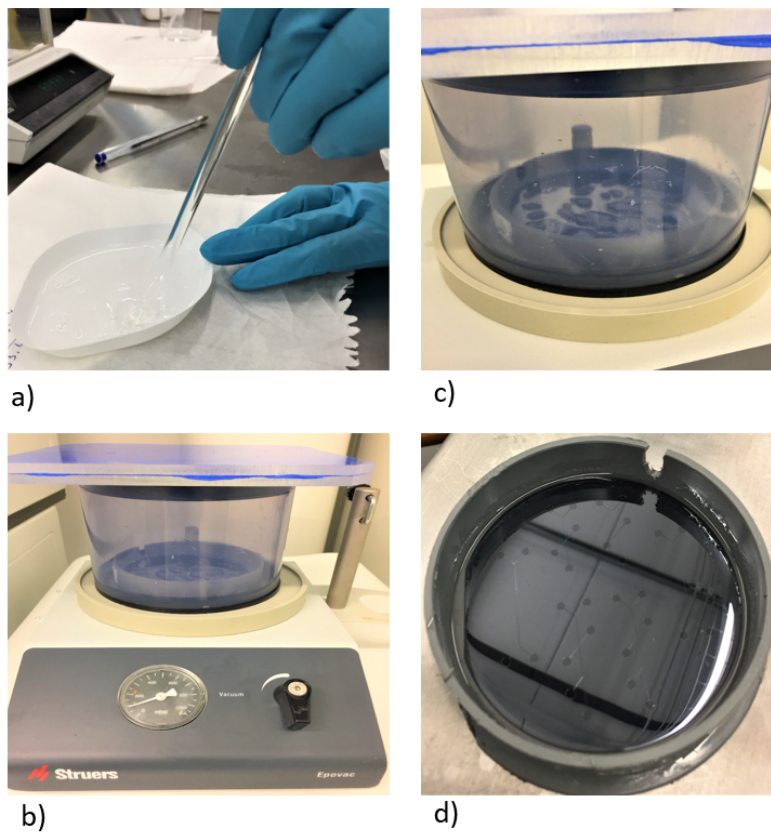
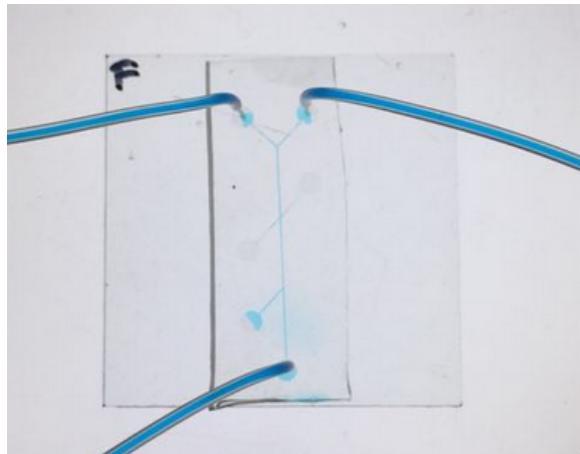


Fig. 7.8 a) PDMS mixing; b) Vacuum machine; c) PDMS curing d) PDMS after baking step.

All the parameters used in the different steps of photolithography are summarized in the table 7.10. In the second day, firstly the PDMS was cut from the master by using a surgical blade; the different microfluidic structures were separated. The plane was to test the correct development of the microfluidic channels and also the bounding between the PDMS and the glass material. For these purposes, the PDMS was punched out from the respective chambers by the use of a blunt syringe needle (diameter 0.5 [mm]). The glue plugs were removed by using tweezers, and needles (diameter 0.5 [mm]) were positioned in place of them. At this point, the PDMS structures and the glass were washed with DI water and dried under pressurized air. After this, they were pretreated with oxygen plasma (O_2 100 [sccm], Generator 100 [W], Timer 2 [min], Operating pressure 45 [Pa]) and then bounded together.



(a)



(b)

Fig. 7.9 a) Bounding between the PDMS structure and the glass layer. b) Test of the microchannels development through a colored solution.

SILICON (SI) WAFER PREPARATION			
Washing time: 3 [min]		1) Dry time: 10 [min] 2) Dry temperature: 200 [°C]	
NEGATIVE PHOTORESIST: SU8-100. Spinning machine: SP-100.			
Spinning acceleration [rpm]	Acceleration time [s]	Spinning time [s]	Deceleration time [s]
1) 0	0	0	0
2) 600	10	30	0
3) 3000	30	30	30
SOFT BAKING			
Temperature [°C]	Time [min]		
1) 65	15		
2) 95	30		
EXPOSURE TO MASK			
GAP [μm]	Time [s]		
30	230		
POST BAKING			
Temperature [°C]	Time [min]		
1) 65	1		
2) 95	10		
3) 0	5		
DEVELOPMENT			
Time [min]	Thikness [μm]		
6	100		
PDMS PREPARATION AND DEPOSITION			
PDMS base	30 [g]		
PDMS curing agent	3 [g]		
PDMS mix time	3 [min]		
PDMS degas time	30 [min]		
PDMS curing	1) Temperature: 65 [°C] 2) Ambient temperature	1) Time: 2 [h] 2) Time: 24 [h]	

Fig. 7.10 Soft-lithography parameters.

7.3 Results and final considerations

The final master structure was analyzed in the Veeco machine (Dektat 150) (figure 7.11), that allows to project the nanostructures on the desktop and to analyze the substrate thickness (in this case the high of the channels and of the chambers) thanks to its software.

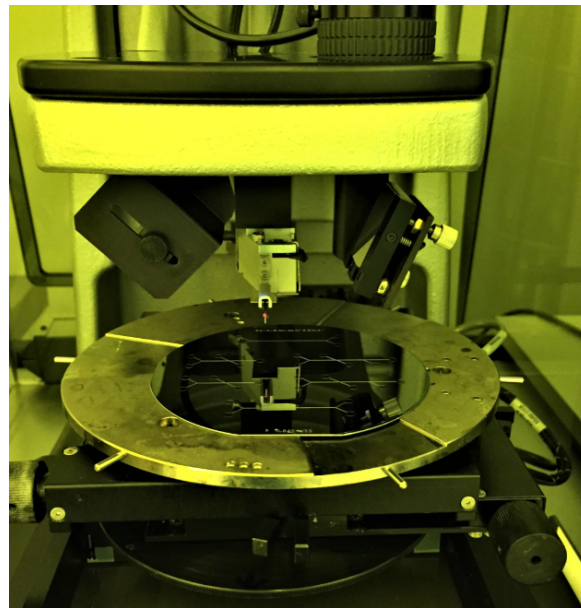


Fig. 7.11 Veeco machine (Dektat 150).

The thickness obtained was of $\sim 89[\mu\text{m}]$ for the channels (figure 7.12) and $\sim 89[\mu\text{m}]$ for the chambers (figure 7.13). It was calculated as the mean value of the meshing values; it resulted to be constant along the model.

For the device proposed in this thesis, this process could be used for its building. It results in an easy fabrication method, not expensive in terms of costs and time. From a simple costs analysis, the PDMS microfluidic device realized in this experiment costs less than 10 euro (Appendix1); this is a price estimated without considering that there is the chance to use more times the same master. For the work done in this thesis, the proposed device will require three different masks for the ‘master’ building, because the design is disposed in three levels. Furthermore, the experiment shows the possibility to realize multiple structures on the same wafer, during a single soft-lithography process. This is an important aspect to be considered, because the patient will use a different PMMA device for each day, while the transistor structure containing the electronic circuit will be permanent in the proposed PoC device. This means that the proposed PMMA chip could have great chances for the low-cost mass production.

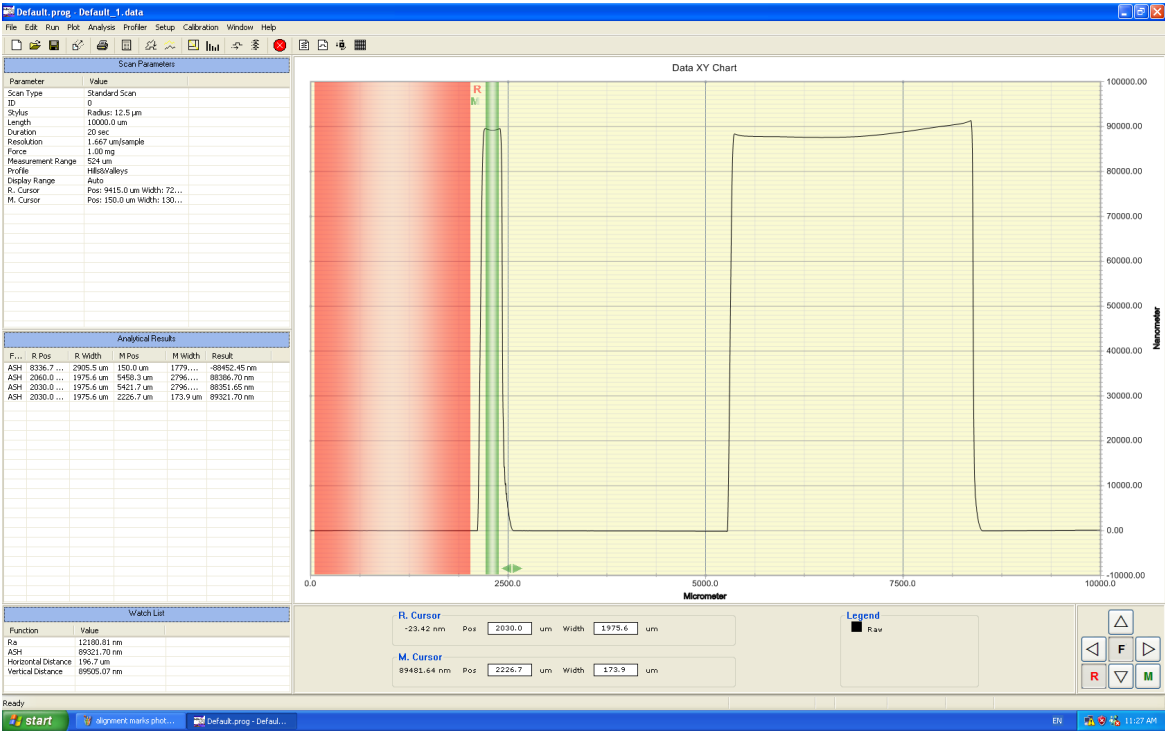


Fig. 7.12 Measurement of the Master channels thickness on the meshing machine.

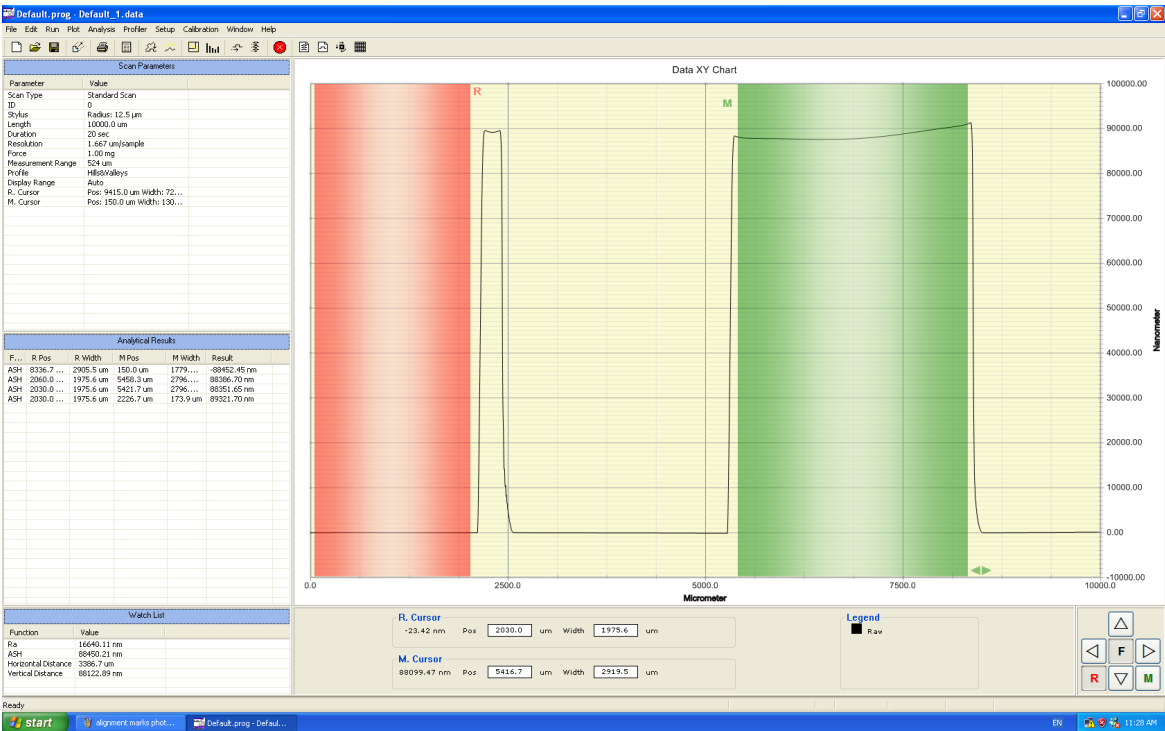


Fig. 7.13 Measurement of the Master chambers thickness on the meshing machine.

Finally, the bounding between the glass and PDMS resulted strong, showing the chance to dispose easily the proposed photodetectors onto a glass layer. The colored solution showed the correct development of the microfluidic channels.

Chapter 8

Conclusions and future work

The goal of this thesis was to propose a new salivary test method for the diagnosis and follow-up of COPD patients, for a friendly and daily use. The research was done by contemporary studying two different main tasks. The first one was to find the most relevant Biomarkers in saliva samples and also study the correlation with the diagnostic parameters of the Gold standard techniques relative to this case. The biomolecules that kept great attention were IL-8, IL-6, MMP-9, MMP-8, TNF- α , NE, and CRP, because of their prognostic role also found in other samples such as sputum and blood.

In this work, IL-8 was better evaluated by developing an ELISA test for a little cohort of healthy people. The results show its stability and the predictable advantage in terms of concentration during the day and along different days, so it is possible to be used as a test biomarker.

The second main task was to find an innovative solution for the development of a new salivary point-of-care device, on the base of state of the art for COPD. The device proposed is a compact optical microfluidic device in PMMA. It is thought for one-step processing of the sample, thanks to the introduction of the detection elements in a compact format. Graphene quantum dots and hybrid graphene-perovskite photodetectors are chosen for the optical detection, thanks to their excellent properties in terms of performance of the analysis and costs.

After the choose of the materials and the design, the device working was numerically tested through the FEM software Comsol *Multiphysics* 5.3.a. Two dimensional cross-section and top-section simulations were performed.

The results show the strong opportunity for this device for being built in the future. It is capable of performing the test in 1.16 seconds, and the values reported for the studied parameters confirm the ability to work through capillary action. The difficulty of this work was to find a numerical model that could approximate the real device working.

Finally, a possible building process for the proposed PMMA device was studied in the clean lab, by building a PDMS microfluidic device through the soft-lithography technique. The experiment was useful for having an idea about the costs in term of materials and time necessary for its building. From the obtained results, the proposed PoC device results to have great opportunities in terms of mass production. The general costs of the material is less of 10 euro and also after its use, the PMMA device could be chemically treated and used again thanks to its property to be a 'green material'.

With the contribution of this thesis, the future work will be to perform a new IL-8 ELISA test on a cohort of COPD patients for comparing the results with the ones obtained in this part. Furthermore, CRP and MMP-9 will be analyzed because, according to the literature research, they result to be relevant biomolecules capable of differentiating the stable state from the advent of an exacerbation. This cluster of biomarkers is chosen for its future application on the device.

The portable device will be improved with the addition of sophisticated technology for the detection such as graphene quantum dots and hybrid graphene photodetectors. It will be built and tested for the capillary action. Further the electronic component will transfer data by wireless to a smartphone APP, directly linked with the GP municipalities. The notification of biomarker-level increasing will allow to early start the prevention procedures for COPD patients. This solution will reduce the total cost over the insurance system and improve the quality life of the COPD patients.

References

- [1] (1996). Health effects of outdoor air pollution. committee of the environmental and occupational health assembly of the american thoracic society. *American Journal of Respiratory and Critical Care Medicine*, 153(1):3–50. PMID: 8542133.
- [2] (2008). A nanoparticle label/immunochromatographic electrochemical biosensor for rapid and sensitive detection of prostate-specific antigen. *Biosensors and Bioelectronics*, 23(11):1659 – 1665.
- [3] AARON, S., ANGEL, J., LUNAU, M., WRIGHT, K., FEX, C., LESAUX, N., and DALES, R. (2001). Granulocyte inflammatory markers and airway infection during acute exacerbation of chronic obstructive pulmonary disease. *American Journal of Respiratory and Critical Care Medicine*, 163(2):349–355. PMID: 11179105.
- [4] Aaron, S. D. (2014a). Management and prevention of exacerbations of copd. 349.
- [5] Aaron, S. D. (2014b). Management and prevention of exacerbations of copd. *bmj*, 349:g5237.
- [6] Aaron, S. D., Vandemheen, K. L., Ramsay, T., Zhang, C., Avnur, Z., Nikolcheva, T., and Quinn, A. (2010). Multi analyte profiling and variability of inflammatory markers in blood and induced sputum in patients with stable copd. *Respiratory Research*, 11(1):41.
- [7] Abe, K., Kotera, K., Suzuki, K., and Citterio, D. (2010). Inkjet-printed paperfluidic immuno-chemical sensing device. *Analytical and bioanalytical chemistry*, 398(2):885–893.
- [8] Abe, K., Suzuki, K., and Citterio, D. (2008). Inkjet-printed microfluidic multianalyte chemical sensing paper. *Analytical Chemistry*, 80(18):6928–6934. PMID: 18698798.
- [9] Álvarez-Diduk, R., Orozco, J., and Merkoçi, A. (2017). Paper strip-embedded graphene quantum dots: a screening device with a smartphone readout. *Scientific reports*, 7(1):976.
- [10] Awan, K. H., Siddiqi, K., Patil, S., and Hussain, Q. A. (2017). Assessing the effect of waterpipe smoking on cancer outcome-a systematic review of current evidence. *Asian Pacific journal of cancer prevention: APJCP*, 18(2):495.
- [11] Bafadhel, M., McKenna, S., Terry, S., Mistry, V., Reid, C., Haldar, P., McCormick, M., Haldar, K., Keadze, T., Duvoix, A., et al. (2011). Acute exacerbations of chronic obstructive pulmonary disease: identification of biologic clusters and their biomarkers. *American journal of respiratory and critical care medicine*, 184(6):662–671.

- [12] Barnes, P. J. (2004). Alveolar macrophages as orchestrators of copd. *COPD: Journal of Chronic Obstructive Pulmonary Disease*, 1(1):59–70.
- [13] Bhavsar, N. V., Dave, B. D., Brahmbhatt, N. A., and Parekh, R. (2015). Periodontal status and oral health behavior in hospitalized patients with chronic obstructive pulmonary disease. *Journal of natural science, biology, and medicine*, 6(Suppl 1):S93.
- [14] Bilan, R., Fleury, F., Nabiev, I., and Sukhanova, A. (2015). Quantum dot surface chemistry and functionalization for cell targeting and imaging. *Bioconjugate chemistry*, 26(4):609–624.
- [15] Blanco Ignacio, Diego Isidro, B. P.-F. E. C.-M. F. E. C. S. J. B. M. M. (2018). Geographical distribution of copd prevalence in europe, estimated by an inverse distance weighting interpolation technique. *PMC*, 13:57–67.
- [16] Blicharz, T. M., Siqueira, W. L., Helmerhorst, E. J., Oppenheim, F. G., Wexler, P. J., Little, F. F., and Walt, D. R. (2009). Fiber-optic microsphere-based antibody array for the analysis of inflammatory cytokines in saliva. *Analytical Chemistry*, 81(6):2106–2114. PMID: 19192965.
- [17] Bogart, L. K., Pourroy, G., Murphy, C. J., Puentes, V., Pellegrino, T., Rosenblum, D., Peer, D., and Lévy, R. (2014). Nanoparticles for imaging, sensing, and therapeutic intervention.
- [18] Bohara, R. A., Thorat, N. D., and Pawar, S. H. (2016). Role of functionalization: strategies to explore potential nano-bio applications of magnetic nanoparticles. *RSC Advances*, 6(50):43989–44012.
- [19] Bradford, E., Jacobson, S., Varasteh, J., Comellas, A. P., Woodruff, P., O’Neal, W., DeMeo, D. L., Li, X., Kim, V., Cho, M., et al. (2017). The value of blood cytokines and chemokines in assessing copd. *Respiratory research*, 18(1):180.
- [20] Carter, R. I., Ungurs, M. J., Mumford, R. A., and Stockley, R. A. (2013). A α -val360: a marker of neutrophil elastase and copd disease activity. *European Respiratory Journal*, 41(1):31–38.
- [21] Cavallès, A., Brinchault-Rabin, G., Dixmier, A., Goupil, F., Gut-Gobert, C., Marchand-Adam, S., Meurice, J.-C., Morel, H., Person-Tacnet, C., Leroyer, C., and Diot, P. (2013). Comorbidities of copd. *European Respiratory Review*, 22(130):454–475.
- [22] Cazzola, M. and Novelli, G. (2010). Biomarkers in copd. *Pulmonary pharmacology & therapeutics*, 23(6):493–500.
- [23] Ceylan, O., Mishra, G. K., Yazici, M., Niazi, J. H., Qureshi, A., and Gurbuz, Y. (2018). A hand-held point-of-care biosensor device for detection of multiple cancer and cardiac disease biomarkers using interdigitated capacitive arrays. *IEEE Transactions on Biomedical Circuits and Systems*, pages 1–1.
- [24] Chalmers, J. D., Moffitt, K. L., Suarez-Cuartin, G., Sibila, O., Finch, S., Furrie, E., Dicker, A., Wrobel, K., Elborn, J. S., Walker, B., Martin, S. L., Marshall, S. E., Huang, J. T.-J., and Fardon, T. C. (2017). Neutrophil elastase activity is associated with exacerbations

- and lung function decline in bronchiectasis. *American Journal of Respiratory and Critical Care Medicine*, 195(10):1384–1393. PMID: 27911604.
- [25] Chan, W. C., Maxwell, D. J., Gao, X., Bailey, R. E., Han, M., and Nie, S. (2002). Luminescent quantum dots for multiplexed biological detection and imaging. *Current opinion in biotechnology*, 13(1):40–46.
- [26] Chang, P.-H., Liu, S.-Y., Lan, Y.-B., Tsai, Y.-C., You, X.-Q., Li, C.-S., Huang, K.-Y., Chou, A.-S., Cheng, T.-C., Wang, J.-K., et al. (2017). Ultrahigh responsivity and detectivity graphene–perovskite hybrid phototransistors by sequential vapor deposition. *Scientific Reports*, 7:46281.
- [27] Chapman, K. R., Mannino, D. M., Soriano, J. B., Vermeire, P. A., Buist, A. S., Thun, M. J., Connell, C., Jemal, A., Lee, T. A., Miravittles, M., Aldington, S., and Beasley, R. (2006). Epidemiology and costs of chronic obstructive pulmonary disease. *European Respiratory Journal*, 27(1):188–207.
- [28] Chen, P., Chung, M. T., McHugh, W., Nidetz, R., Li, Y., Fu, J., Cornell, T. T., Shanley, T. P., and Kurabayashi, K. (2015). Multiplex serum cytokine immunoassay using nanoplasmonic biosensor microarrays. *ACS nano*, 9(4):4173–4181.
- [29] Chen, W., Lv, G., Hu, W., Li, D., Chen, S., and Dai, Z. (2018). Synthesis and applications of graphene quantum dots: A review. *Nanotechnology Reviews*, 7(2):157–185.
- [30] Chen, X., Chen, J., Wang, F., Xiang, X., Luo, M., Ji, X., and He, Z. (2012). Determination of glucose and uric acid with bienzyme colorimetry on microfluidic paper-based analysis devices. *Biosensors and Bioelectronics*, 35(1):363 – 368.
- [31] Chen, Z., Liang, R., Guo, X., Liang, J., Deng, Q., Li, M., An, T., Liu, T., and Wu, Y. (2017). Simultaneous quantitation of cytokeratin-19 fragment and carcinoembryonic antigen in human serum via quantum dot-doped nanoparticles. *Biosensors and Bioelectronics*, 91:60–65.
- [32] Chen X, Liu K, W. Z.-e. a. (2015). Computed tomography measurement of pulmonary artery for diagnosis of copd and its comorbidity pulmonary hypertension. *International Journal of Chronic Obstructive Pulmonary Disease*, 10:2525–2533.
- [33] Chivers, C. E., Koner, A. L., Lowe, E. D., and Howarth, M. (2011). How the biotin–streptavidin interaction was made even stronger: investigation via crystallography and a chimaeric tetramer. *Biochemical Journal*, 435(1):55–63.
- [34] Dahl, M., Vestbo, J., Lange, P., Bojesen, S. E., Tybjaerg-Hansen, A., and Nordestgaard, B. G. (2007). C-reactive protein as a predictor of prognosis in chronic obstructive pulmonary disease. *American journal of respiratory and critical care medicine*, 175(3):250–255.
- [35] Daniele, M. A., Boyd, D. A., Mott, D. R., and Ligler, F. S. (2015). 3d hydrodynamic focusing microfluidics for emerging sensing technologies. *Biosensors and Bioelectronics*, 67:25–34.

- [36] de Dieu Habimana, J., Ji, J., and Sun, X. (2018). Minireview: Trends in optical-based biosensors for point-of-care bacterial pathogen detection for food safety and clinical diagnostics.
- [37] De Torres, J., Cordoba-Lanus, E., Lopez-Aguilar, C., de Fuentes, M. M., De Garcini, A. M., Aguirre-Jaime, A., Celli, B., and Casanova, C. (2006). C-reactive protein levels and clinically important predictive outcomes in stable copd patients. *European Respiratory Journal*.
- [38] de Torres, J. P., Casanova, C., Pinto-Plata, V., Varo, N., Restituto, P., Cordoba-Lanus, E., Baz-Dávila, R., Aguirre-Jaime, A., and Celli, B. R. (2011). Gender differences in plasma biomarker levels in a cohort of copd patients: A pilot study. *PLOS ONE*, 6(1):1–5.
- [39] Di Nardo, F., Baggiani, C., Giovannoli, C., Spano, G., and Anfossi, L. (2017). Multi-color immunochromatographic strip test based on gold nanoparticles for the determination of aflatoxin b1 and fumonisins. *Microchimica Acta*, 184(5):1295–1304.
- [40] Diaclone (2019). Company of the group biotech investissment. <https://www.diaclone.com/uploads/File/downloads/851.860>.
- [41] Dillon, M. C., Opris, D. C., Kopanczyk, R., Lickliter, J., Cornwell, H. N., Bridges, E. G., Nazar, A. M., and Bridges, K. G. (2010). Detection of homocysteine and c-reactive protein in the saliva of healthy adults: Comparison with blood levels. *Biomarker Insights*, 5:BMI.S5305.
- [42] Dong, T. and Pires, N. M. M. (2017). Immunodetection of salivary biomarkers by an optical microfluidic biosensor with polyethylenimine-modified polythiophene-c70 organic photodetectors. *Biosensors and Bioelectronics*, 94:321–327.
- [43] Eickmeier, O., Huebner, M., Herrmann, E., Zissler, U., Rosewich, M., Baer, P. C., Buhl, R., Schmitt-Grohé, S., Zielen, S., and Schubert, R. (2010). Sputum biomarker profiles in cystic fibrosis (cf) and chronic obstructive pulmonary disease (copd) and association between pulmonary function. *Cytokine*, 50(2):152 – 157.
- [44] Elahi, N., Kamali, M., and Baghersad, M. H. (2018). Recent biomedical applications of gold nanoparticles: a review. *Talanta*.
- [45] Ellerbee, A. K., Phillips, S. T., Siegel, A. C., Mirica, K. A., Martinez, A. W., Striehl, P., Jain, N., Prentiss, M., and Whitesides, G. M. (2009). Quantifying colorimetric assays in paper-based microfluidic devices by measuring the transmission of light through paper. *Analytical Chemistry*, 81(20):8447–8452. PMID: 19722495.
- [46] Faner, R., Tal-Singer, R., Riley, J. H., Celli, B., Vestbo, J., MacNee, W., Bakke, P., Calverley, P. M., Coxson, H., Crim, C., et al. (2014). Lessons from eclipse: a review of copd biomarkers. *Thorax*, 69(7):666–672.
- [47] Fenton, E. M., Mascarenas, M. R., Lopez, G. P., and Sibbett, S. S. (2008). Multiplex lateral-flow test strips fabricated by two-dimensional shaping. *ACS applied materials & interfaces*, 1(1):124–129.

- [48] Fernández-Sánchez, C., McNeil, C. J., Rawson, K., and Nilsson, O. (2004). Disposable noncompetitive immunosensor for free and total prostate-specific antigen based on capacitance measurement. *Analytical Chemistry*, 76(19):5649–5656. PMID: 15456282.
- [49] Franciosi, L. G., Page, C. P., Celli, B. R., Cazzola, M., Walker, M. J., Danhof, M., Rabe, K. F., and Della Pasqua, O. E. (2006). Markers of disease severity in chronic obstructive pulmonary disease. *Pulmonary pharmacology & therapeutics*, 19(3):189–199.
- [50] Freeman, C. M., Martinez, C. H., Todt, J. C., Martinez, F. J., Han, M. K., Thompson, D. L., McCloskey, L., and Curtis, J. L. (2015). Acute exacerbations of chronic obstructive pulmonary disease are associated with decreased cd4+ & cd8+ t cells and increased growth & differentiation factor-15 (gdf-15) in peripheral blood. *Respiratory Research*, 16(1):94.
- [51] Fujimoto, K., Yasuo, M., Urushibata, K., Hanaoka, M., Koizumi, T., and Kubo, K. (2005). Airway inflammation during stable and acutely exacerbated chronic obstructive pulmonary disease. *European Respiratory Journal*, 25(4):640–646.
- [52] Gallardo Estrella, L., Pompe, E., Kuhnigk, J.-M., Lynch, D. A., Bhatt, S. P., van Ginneken, B., and van Rikxoort, E. M. (2017). Computed tomography quantification of tracheal abnormalities in copd and their influence on airflow limitation. *Medical Physics*, 44(7):3594–3603.
- [53] Gervais, L. and Delamarche, E. (2009). Toward one-step point-of-care immunodiagnostics using capillary-driven microfluidics and pdms substrates. *Lab Chip*, 9:3330–3337.
- [54] Ghasemiesfe, M., Ravi, D., Vali, M., Korenstein, D., Arjomandi, M., Frank, J., Austin, P. C., and Keyhani, S. (2018). Marijuana use, respiratory symptoms, and pulmonary function. *Annals of internal medicine*, 169(2):106–115.
- [55] Gittings, S., Turnbull, N., Henry, B., Roberts, C. J., and Gershkovich, P. (2015). Characterisation of human saliva as a platform for oral dissolution medium development. *European Journal of Pharmaceutics and Biopharmaceutics*, 91:16–24.
- [56] Goncharov, S., Krivenkov, V., Samokhvalov, P., Nabiev, I., and Rakovich, Y. (2018). Photoluminescence properties of thin-film nanohybrid material based on quantum dots and gold nanorods. *Optics and Spectroscopy*, 125(5):726–730.
- [57] Greene, C., D W Miller, S., Carroll, T., McLean, C., O’Mahony, M., Lawless, M., O’Neill, S., Taggart, C., and G McElvaney, N. (2008). Alpha-1 antitrypsin deficiency: A conformational disease associated with lung and liver manifestations. 31:21–34.
- [58] Han, Kwi Nam, C. J.-S.-K. J. (2016). Three-dimensional paper-based slip device for one-step point-of-care testing. 6.
- [59] Hanania, N. (2012). Chronic obstructive pulmonary disease (copd) is a major cause of morbidity and mortality worldwide. *Respiratory medicine*, 106:S1.
- [60] Health, N. (2019). Nucleus medical media. <http://hlp.nucleushealth.com/copd/view-item?ItemID=75505>.
- [61] Henson, B. S. and Wong, D. T. (2010). Collection, storage, and processing of saliva samples for downstream molecular applications. In *Oral Biology*, pages 21–30. Springer.

- [62] Hogg, J. C. (2004). Pathophysiology of airflow limitation in chronic obstructive pulmonary disease. *The Lancet*, 364(9435):709 – 721.
- [63] Honrado, C. and Dong, T. (2014). Development and optimization of an integrated capillary-based opto-microfluidic device for chemiluminescence quantitative detection. *Journal of Micromechanics and Microengineering*, 24(12):125023.
- [64] Hou, Y., Wang, K., Xiao, K., Qin, W., Lu, W., Tao, W., and Cui, D. (2017). Smartphone-based dual-modality imaging system for quantitative detection of color or fluorescent lateral flow immunochromatographic strips. *Nanoscale research letters*, 12(1):291.
- [65] Hu, G., Sheng, W., Li, S., Zhang, Y., Wang, J., and Wang, S. (2017). Quantum dot based multiplex fluorescence quenching immune chromatographic strips for the simultaneous determination of sulfonamide and fluoroquinolone residues in chicken samples. *RSC Advances*, 7(49):31123–31128.
- [66] Hurst, J. R., Donaldson, G. C., Perera, W. R., Wilkinson, T. M., Bilello, J. A., Hagan, G. W., Vessey, R. S., and Wedzicha, J. A. (2006). Use of plasma biomarkers at exacerbation of chronic obstructive pulmonary disease. *American Journal of Respiratory and Critical Care Medicine*, 174(8):867–874.
- [67] Hyun, J., Zhu, Y., Liebmman-Vinson, A., Beebe, T. P., and Chilkoti, A. (2001). Microstamping on an activated polymer surface: Patterning biotin and streptavidin onto common polymeric biomaterials. *Langmuir*, 17(20):6358–6367.
- [68] Ilumets Helen, Ryttilä Paula, D. I.-B. G. G.-S. A. M. M. S. T. K. V. (2018). Matrix metalloproteinases -8, -9 and -12 in smokers and patients with stage 0 copd. *Dove Medical Press*, 12.
- [69] Jamieson, T., Bakhshi, R., Petrova, D., Pocock, R., Imani, M., and Seifalian, A. M. (2007). Biological applications of quantum dots. *Biomaterials*, 28(31):4717–4732.
- [70] Javaid, M. A., Ahmed, A. S., Durand, R., and Tran, S. D. (2016). Saliva as a diagnostic tool for oral and systemic diseases. *Journal of Oral Biology and Craniofacial Research*, 6(1):67 – 76.
- [71] Ji, J., von Schéele, I., Bergström, J., Billing, B., Dahlén, B., Lantz, A.-S., Larsson, K., and Palmberg, L. (2014). Compartment differences of inflammatory activity in chronic obstructive pulmonary disease. *Respiratory research*, 15(1):104.
- [72] Karadeniz, G., Polat, G., Senol, G., and Buyuksirin, M. (2013). C-reactive protein measurements as a marker of the severity of chronic obstructive pulmonary disease exacerbations. *Inflammation*, 36(4):948–953.
- [73] Kawde, A.-N., Mao, X., Xu, H., Zeng, Q., He, Y., and Liu, G. (2010). Moving enzyme-linked immunosorbent assay to the point-of-care dry-reagent strip biosensors. *Am. J. Biomed. Sci*, 2(1):23–32.
- [74] Keatings, V. M., Collins, P. D., Scott, D. M., and Barnes, P. J. (1996). Differences in interleukin-8 and tumor necrosis factor-alpha in induced sputum from patients with chronic obstructive pulmonary disease or asthma. *American Journal of Respiratory and Critical Care Medicine*, 153(2):530–534. PMID: 8564092.

- [75] Kelly, E., Greene, C. M., Carroll, T. P., McElvaney, N. G., and O'Neill, S. J. (2011). Alpha-1 antitrypsin deficiency. *Respiratory Medicine CME*, 4(1):1–8.
- [76] Kemmler, M., Sauer, U., Schleicher, E., Preininger, C., and Brandenburg, A. (2014). Biochip point-of-care device for sepsis diagnostics. *Sensors and Actuators B: Chemical*, 192:205–215.
- [77] Kent Brian, Mitchell Patrick, M. W. T. (2011). Hypoxemia in patients with copd: cause, effects, and disease progression. *International Journal of Chronic Obstructive Pulmonary Disease*, 6:199–208.
- [78] Khan, R. S., Khurshid, Z., and Yahya Ibrahim Asiri, F. (2017). Advancing point-of-care (poc) testing using human saliva as liquid biopsy. *Diagnostics*, 7(3).
- [79] Khansili, N., Rattu, G., and Krishna, P. M. (2018). Label-free optical biosensors for food and biological sensor applications. *Sensors and Actuators B: Chemical*.
- [80] Kim, W.-J., Choi, J. B., Kim, S., Kim, A. R., and Yoo, D. J. (2015). Preparation and characterization of a triple layered au-pmma-pbse hybrid nanocomposite: Manipulation of pmma spacer layer by oxygen plasma etching. *Bulletin of the Korean Chemical Society*, 36(8):1966–1973.
- [81] Kleniewska, A., Walusiak-Skorupa, J., Piotrowski, W., Nowakowska-Świrta, E., and Wiszniewska, M. (2016). Comparison of biomarkers in serum and induced sputum of patients with occupational asthma and chronic obstructive pulmonary disease. *Journal of occupational health*, 58(4):333–339.
- [82] Koh, K. S., Wong, V. L., and Ren, Y. (2018). Microdroplets advancement in newtonian and non-newtonian microfluidic multiphase system. In *Microfluidics and Nanofluidics*. IntechOpen.
- [83] Kong, F.-Y., Zhang, J.-W., Li, R.-F., Wang, Z.-X., Wang, W.-J., and Wang, W. (2017). Unique roles of gold nanoparticles in drug delivery, targeting and imaging applications. *Molecules*, 22(9):1445.
- [84] Lake, M., Narciso, C., Cowdrick, K., Storey, T., Zhang, S., Zartman, J., and Hoelzle, D. (2015). Microfluidic device design, fabrication, and testing protocols. *Protoc. Exch*, 10.
- [85] LEBOWITZ, M. D., KNUDSON, R. J., and BURROWS, B. (1975). Tucson epidemiologic study of obstructive lung diseases: I: methodology and prevalence of disease. *American journal of epidemiology*, 102(2):137–152.
- [86] Li, C.-z., Vandenberg, K., Prabhulkar, S., Zhu, X., Schneper, L., Methee, K., Rosser, C. J., and Almeida, E. (2011). Paper based point-of-care testing disc for multiplex whole cell bacteria analysis. *Biosensors and Bioelectronics*, 26(11):4342–4348.
- [87] Li, N., Zhao, P., and Astruc, D. (2014). Anisotropic gold nanoparticles: synthesis, properties, applications, and toxicity. *Angewandte Chemie International Edition*, 53(7):1756–1789.

- [88] Li, S., Wang, J., Sheng, W., Wen, W., Gu, Y., and Wang, S. (2018). Fluorometric lateral flow immunochromatographic zearalenone assay by exploiting a quencher system composed of carbon dots and silver nanoparticles. *Microchimica Acta*, 185(8):388.
- [89] Li, X., Wei, J., Aifantis, K. E., Fan, Y., Feng, Q., Cui, F.-Z., and Watari, F. (2016). Current investigations into magnetic nanoparticles for biomedical applications. *Journal of Biomedical Materials Research Part A*, 104(5):1285–1296.
- [90] Linder, R., Rönmark, E., Pourazar, J., Behndig, A., Blomberg, A., and Lindberg, A. (2015). Serum metalloproteinase-9 is related to copd severity and symptoms-cross-sectional data from a population based cohort-study. *Respiratory research*, 16(1):28.
- [91] Liu, J. and Duan, Y. (2012). Saliva: a potential media for disease diagnostics and monitoring. *Oral oncology*, 48(7):569–577.
- [92] Low, W. S., Kadri, N. A., Abas, W., et al. (2014). Computational fluid dynamics modelling of microfluidic channel for dielectrophoretic biomems application. *The Scientific World Journal*, 2014.
- [93] Lozano, R., Naghavi, M., Foreman, K., Lim, S., Shibuya, K., Aboyans, V., Abraham, J., Adair, T., Aggarwal, R., Ahn, S. Y., AlMazroa, M. A., Alvarado, M., Anderson, H. R., Anderson, L. M., Andrews, K. G., Atkinson, C., Baddour, L. M., Barker-Collo, S., Bartels, D. H., Bell, M. L., Benjamin, E. J., Bennett, D., Bhalla, K., Bikbov, B., Abdulhak, A. B., Birbeck, G., Blyth, F., Bolliger, I., Boufous, S., Bucello, C., Burch, M., Burney, P., Carapetis, J., Chen, H., Chou, D., Chugh, S. S., Coffeng, L. E., Colan, S. D., Colquhoun, S., Colson, K. E., Condon, J., Connor, M. D., Cooper, L. T., Corriere, M., Cortinovis, M., de Vaccaro, K. C., Couser, W., Cowie, B. C., Criqui, M. H., Cross, M., Dabhadkar, K. C., Dahodwala, N., Leo, D. D., Degenhardt, L., Delossantos, A., Denenberg, J., Jarlais, D. C. D., Dharmaratne, S. D., Dorsey, E. R., Driscoll, T., Duber, H., Ebel, B., Erwin, P. J., Espindola, P., Ezzati, M., Feigin, V., Flaxman, A. D., Forouzanfar, M. H., Fowkes, F. G. R., Franklin, R., Fransen, M., Freeman, M. K., Gabriel, S. E., Gakidou, E., Gaspari, F., Gillum, R. F., Gonzalez-Medina, D., Halasa, Y. A., Haring, D., Harrison, J. E., Havmoeller, R., Hay, R. J., Hoen, B., Hotez, P. J., Hoy, D., Jacobsen, K. H., James, S. L., Jasrasaria, R., Jayaraman, S., Johns, N., Karthikeyan, G., Kassebaum, N., Keren, A., Khoo, J.-P., Knowlton, L. M., Kobusingye, O., Koranteng, A., Krishnamurthi, R., Lipnick, M., Lipshultz, S. E., Ohno, S. L., Mabweijano, J., MacIntyre, M. F., Mallinger, L., March, L., Marks, G. B., Marks, R., Matsumori, A., Matzopoulos, R., Mayosi, B. M., McAnulty, J. H., McDermott, M. M., McGrath, J., Memish, Z. A., Mensah, G. A., Merriman, T. R., Michaud, C., Miller, M., Miller, T. R., Mock, C., Mocumbi, A. O., Mokdad, A. A., Moran, A., Mulholland, K., Nair, M. N., Naldi, L., Narayan, K. M. V., Nasser, K., Norman, P., O'Donnell, M., Omer, S. B., Ortblad, K., Osborne, R., Ozgediz, D., Pahari, B., Pandian, J. D., Rivero, A. P., Padilla, R. P., Perez-Ruiz, F., Perico, N., Phillips, D., Pierce, K., Pope, C. A., Porrini, E., Pourmalek, F., Raju, M., Ranganathan, D., Rehm, J. T., Rein, D. B., Remuzzi, G., Rivara, F. P., Roberts, T., León, F. R. D., Rosenfeld, L. C., Rushton, L., Sacco, R. L., Salomon, J. A., Sampson, U., Sanman, E., Schwebel, D. C., Segui-Gomez, M., Shepard, D. S., Singh, D., Singleton, J., Sliwa, K., Smith, E., Steer, A., Taylor, J. A., Thomas, B., Tleyjeh, I. M., Towbin, J. A., Truelsen, T., Undurraga, E. A., Venketasubramanian, N., Vijayakumar, L., Vos, T., Wagner, G. R., Wang, M., Wang, W., Watt, K., Weinstock, M. A., Weintraub, R., Wilkinson, J. D., Woolf, A. D., Wulf, S., Yeh, P.-H., Yip, P., Zabetian, A., Zheng, Z.-J., Lopez, A. D., and Murray, C. J. (2012).

- Global and regional mortality from 235 causes of death for 20 age groups in 1990 and 2010: a systematic analysis for the global burden of disease study 2010. *The Lancet*, 380(9859):2095 – 2128.
- [94] Lytras, T., Kogevinas, M., Kromhout, H., Carsin, A.-E., Antó, J. M., Bentouhami, H., Weyler, J., Heinrich, J., Nowak, D., Urrutia, I., et al. (2018). Occupational exposures and 20-year incidence of copd: the european community respiratory health survey. *Thorax*, pages thoraxjnl–2017.
- [95] Malhotra, R., Patel, V., Vaqué, J. P., Gutkind, J. S., and Rusling, J. F. (2010). Ultrasensitive electrochemical immunosensor for oral cancer biomarker il-6 using carbon nanotube forest electrodes and multilabel amplification. *Analytical Chemistry*, 82(8):3118–3123. PMID: 20192182.
- [96] Mannino, D. M. and Buist, A. S. (2007). Global burden of copd: risk factors, prevalence, and future trends. *The Lancet*, 370(9589):765 – 773.
- [97] Marçôa, R., Rodrigues, D. M., Dias, M., Ladeira, I., Vaz, A. P., Lima, R., and Guimarães, M. (2018). Classification of chronic obstructive pulmonary disease (copd) according to the new global initiative for chronic obstructive lung disease (gold) 2017: comparison with gold 2011. *COPD: Journal of Chronic Obstructive Pulmonary Disease*, 15(1):21–26.
- [98] Martinez, A. W., Phillips, S. T., Butte, M. J., and Whitesides, G. M. (2007). Patterned paper as a platform for inexpensive, low-volume, portable bioassays. *Angewandte Chemie International Edition*, 46(8):1318–1320.
- [99] Martinez, A. W., Phillips, S. T., Carrilho, E., Thomas III, S. W., Sindi, H., and Whitesides, G. M. (2008). Simple telemedicine for developing regions: camera phones and paper-based microfluidic devices for real-time, off-site diagnosis. *Analytical chemistry*, 80(10):3699–3707.
- [100] Marçôa, R., Rodrigues, D. M., Dias, M., Ladeira, I., Vaz, A. P., Lima, R., and Guimarães, M. (2018). Classification of chronic obstructive pulmonary disease (copd) according to the new global initiative for chronic obstructive lung disease (gold) 2017: Comparison with gold 2011. *COPD: Journal of Chronic Obstructive Pulmonary Disease*, 15(1):21–26. PMID: 29161163.
- [101] Miller, C. S., Foley, J. D., Bailey, A. L., Campell, C. L., Humphries, R. L., Christodoulides, N., Floriano, P. N., Simmons, G., Bhagwandin, B., Jacobson, J. W., Redding, S. W., Ebersole, J. L., and McDevitt, J. T. (2010). Current developments in salivary diagnostics. *Biomarkers in Medicine*, 4(1):171–189. PMID: 20387312.
- [102] Mirabelli MC, Beavers SF, C. A. (2014). Active asthma and the prevalence of physician-diagnosed copd. 192:693–700.
- [103] Mirza, S., Clay, R. D., Koslow, M. A., and Scanlon, P. D. (2018). Copd guidelines: A review of the 2018 gold report. In *Mayo Clinic Proceedings*, volume 93, pages 1488–1502. Elsevier.
- [104] Mitchell, J. (2015a). Pathophysiology of copd: Part 1. *Practice Nursing*, 26(4):172–178.

- [105] Mitchell, J. (2015b). Pathophysiology of copd: Part 2. *Practice Nursing*, 26(9):444–449.
- [106] Mohammed, M. and Desmulliez, M. (2014). Autonomous capillary microfluidic system with embedded optics for improved troponin i cardiac biomarker detection. *Biosensors and Bioelectronics*, 61:478 – 484.
- [107] Mulyadi, Sunnati, and Azhary, M. (2016). The correlation between pulmonary function tests and the salivary mmp-9 activity among chronic obstructive pulmonary disease (copd) patients. *Procedia Chemistry*, 18:194 – 198. Molecular and Cellular Life Sciences: Infectious Diseases, Biochemistry and Structural Biology 2015 Conference.
- [108] Murray, C. J. L., Vos, T., Lozano, R., Naghavi, M., Flaxman, A. D., Michaud, C., Ezzati, M., Shibuya, K., Salomon, J. A., Abdalla, S., Aboyans, V., Abraham, J., Ackerman, I., Aggarwal, R., Ahn, S. Y., Ali, M. K., AlMazroa, M. A., Alvarado, M., Anderson, H. R., Anderson, L. M., Andrews, K. G., Atkinson, C., Baddour, L. M., Bahalim, A. N., Barker-Collo, S., Barrero, L. H., Bartels, D. H., Basáñez, M.-G., Baxter, A., Bell, M. L., Benjamin, E. J., Bennett, D., Bernabé, E., Bhalla, K., Bhandari, B., Bikbov, B., Abdulhak, A. B., Birbeck, G., Black, J. A., Blencowe, H., Blore, J. D., Blyth, F., Bolliger, I., Bonaventure, A., Boufous, S., Bourne, R., Boussinesq, M., Braithwaite, T., Brayne, C., Bridgett, L., Brooker, S., Brooks, P., Brugha, T. S., Bryan-Hancock, C., Bucello, C., Buchbinder, R., Buckle, G., Budke, C. M., Burch, M., Burney, P., Burstein, R., Calabria, B., Campbell, B., Canter, C. E., Carabin, H., Carapetis, J., Carmona, L., Cella, C., Charlson, F., Chen, H., Cheng, A. T.-A., Chou, D., Chugh, S. S., Coffeng, L. E., Colan, S. D., Colquhoun, S., Colson, K. E., Condon, J., Connor, M. D., Cooper, L. T., Corriere, M., Cortinovis, M., de Vaccaro, K. C., Couser, W., Cowie, B. C., Criqui, M. H., Cross, M., Dabhadkar, K. C., Dahiya, M., Dahodwala, N., Damsere-Derry, J., Danaei, G., Davis, A., Leo, D. D., Degenhardt, L., Dellavalle, R., Delossantos, A., Denenberg, J., Derrett, S., Jarlais, D. C. D., Dharmaratne, S. D., Dherani, M., Diaz-Torne, C., Dolk, H., Dorsey, E. R., Driscoll, T., Duber, H., Ebel, B., Edmond, K., Elbaz, A., Ali, S. E., Erskine, H., Erwin, P. J., Espindola, P., Ewoigbokhan, S. E., Farzadfar, F., Feigin, V., Felson, D. T., Ferrari, A., Ferri, C. P., Fèvre, E. M., Finucane, M. M., Flaxman, S., Flood, L., Foreman, K., Forouzanfar, M. H., Fowkes, F. G. R., Fransen, M., Freeman, M. K., Gabbe, B. J., Gabriel, S. E., Gakidou, E., Ganatra, H. A., Garcia, B., Gaspari, F., Gillum, R. F., Gmel, G., Gonzalez-Medina, D., Gosselin, R., Grainger, R., Grant, B., Groeger, J., Guillemin, F., Gunnell, D., Gupta, R., Haagsma, J., Hagan, H., Halasa, Y. A., Hall, W., Haring, D., Haro, J. M., Harrison, J. E., Havmoeller, R., Hay, R. J., Higashi, H., Hill, C., Hoen, B., Hoffman, H., Hotez, P. J., Hoy, D., Huang, J. J., Ibeanusi, S. E., Jacobsen, K. H., James, S. L., Jarvis, D., Jasrasaria, R., Jayaraman, S., Johns, N., Jonas, J. B., Karthikeyan, G., Kassebaum, N., Kawakami, N., Keren, A., Khoo, J.-P., King, C. H., Knowlton, L. M., Kobusingye, O., Koranteng, A., Krishnamurthi, R., Laden, F., Lalloo, R., Laslett, L. L., Lathlean, T., Leasher, J. L., Lee, Y. Y., Leigh, J., Levinson, D., Lim, S. S., Limb, E., Lin, J. K., Lipnick, M., Lipshultz, S. E., Liu, W., Loane, M., Ohno, S. L., Lyons, R., Mabweijano, J., MacIntyre, M. F., Malekzadeh, R., Mallinger, L., Manivannan, S., Marcenes, W., March, L., Margolis, D. J., Marks, G. B., Marks, R., Matsumori, A., Matzopoulos, R., Mayosi, B. M., McAnulty, J. H., McDermott, M. M., McGill, N., McGrath, J., Medina-Mora, M. E., Meltzer, M., Memish, Z. A., Mensah, G. A., Merriman, T. R., Meyer, A.-C., Miglioli, V., Miller, M., Miller, T. R., Mitchell, P. B., Mock, C., Mocumbi, A. O., Moffitt, T. E., Mokdad, A. A., Monasta, L., Montico, M., Moradi-Lakeh, M., Moran, A., Morawska, L., Mori,

- R., Murdoch, M. E., Mwaniki, M. K., Naidoo, K., Nair, M. N., Naldi, L., Narayan, K. M. V., Nelson, P. K., Nelson, R. G., Nevitt, M. C., Newton, C. R., Nolte, S., Norman, P., Norman, R., O'Donnell, M., O'Hanlon, S., Olives, C., Omer, S. B., Ortblad, K., Osborne, R., Ozgediz, D., Page, A., Pahari, B., Pandian, J. D., Rivero, A. P., Patten, S. B., Pearce, N., Padilla, R. P., Perez-Ruiz, F., Perico, N., Pesudovs, K., Phillips, D., Phillips, M. R., Pierce, K., Pion, S., Polanczyk, G. V., Polinder, S., Pope, C. A., Popova, S., Porrini, E., Pourmalek, F., Prince, M., Pullan, R. L., Ramaiah, K. D., Ranganathan, D., Razavi, H., Regan, M., Rehm, J. T., Rein, D. B., Remuzzi, G., Richardson, K., Rivara, F. P., Roberts, T., Robinson, C., Leòn, F. R. D., Ronfani, L., Room, R., Rosenfeld, L. C., Rushton, L., Sacco, R. L., Saha, S., Sampson, U., Sanchez-Riera, L., Sanman, E., Schwebel, D. C., Scott, J. G., Segui-Gomez, M., Shahraz, S., Shepard, D. S., Shin, H., Shivakoti, R., Silberberg, D., Singh, D., Singh, G. M., Singh, J. A., Singleton, J., Sleet, D. A., Sliwa, K., Smith, E., Smith, J. L., Stapelberg, N. J., Steer, A., Steiner, T., Stolk, W. A., Stovner, L. J., Sudfeld, C., Syed, S., Tamburlini, G., Tavakkoli, M., Taylor, H. R., Taylor, J. A., Taylor, W. J., Thomas, B., Thomson, W. M., Thurston, G. D., Tleyjeh, I. M., Tonelli, M., Towbin, J. A., Truelsen, T., Tsilimbaris, M. K., Ubeda, C., Undurraga, E. A., van der Werf, M. J., van Os, J., Vavilala, M. S., Venketasubramanian, N., Wang, M., Wang, W., Watt, K., Weatherall, D. J., Weinstock, M. A., Weintraub, R., Weisskopf, M. G., Weissman, M. M., White, R. A., Whiteford, H., Wiebe, N., Wiersma, S. T., Wilkinson, J. D., Williams, H. C., Williams, S. R., Witt, E., Wolfe, F., Woolf, A. D., Wulf, S., Yeh, P.-H., Zaidi, A. K., Zheng, Z.-J., Zonies, D., and Lopez, A. D. (2012). Disability-adjusted life years (dalys) for 291 diseases and injuries in 21 regions, 1990–2010: a systematic analysis for the global burden of disease study 2010. *The Lancet*, 380(9859):2197 – 2223.
- [109] Nelson, Eric E Guyer, A. E. (2012). A bio-abiotic interface constructed by nanoscale dna-dendrimer and conducting polymer for ultra-sensitive bio-molecular diagnosis. 1:233–245.
- [110] Nie, S., Henley, W. H., Miller, S. E., Zhang, H., Mayer, K. M., Dennis, P. J., Oblath, E. A., Alarie, J. P., Wu, Y., Oppenheim, F. G., Little, F. F., Uluer, A. Z., Wang, P., Ramsey, J. M., and Walt, D. R. (2014). An automated integrated platform for rapid and sensitive multiplexed protein profiling using human saliva samples. *Lab Chip*, 14:1087–1098.
- [111] Nor, N. M., Razak, K. A., Tan, S. C., and Noordin, R. (2012). Properties of surface functionalized iron oxide nanoparticles (ferrofluid) conjugated antibody for lateral flow immunoassay application. *Journal of Alloys and Compounds*, 538:100–106.
- [112] NR, A., JJ, M., CW, W., ES, H., GM, H., and NA, N. (1987). Antibiotic therapy in exacerbations of chronic obstructive pulmonary disease. *Annals of Internal Medicine*, 106(2):196–204.
- [113] Nunna, B. B., Mandal, D., Zhuang, S., and Lee, E. S. (2017). A standalone micro biochip to monitor the cancer progression by measuring cancer antigens as a point-of-care (poc) device for enhanced cancer management. In *2017 IEEE Healthcare Innovations and Point of Care Technologies (HI-POCT)*, pages 212–215.
- [114] Oba, Y, K. E. G. N. and Dias, S. (2018). Dual combination therapy versus long-acting bronchodilators alone for chronic obstructive pulmonary disease (copd): a systematic review and network meta-analysis. *Cochrane Database of Systematic Reviews*, (12).

- [115] Ojeda, I., M.-G. M. G.-C. A. e. a. (2014).
- [116] Oliveira, J., Brito-Pereira, R., Gonçalves, B., Etxebarria, I., and Lanceros-Mendez, S. (2018). Recent developments on printed photodetectors for large area and flexible applications. *Organic Electronics*.
- [117] Pakchin, P. S., Nakhjavani, S. A., Saber, R., Ghanbari, H., and Omid, Y. (2017). Recent advances in simultaneous electrochemical multi-analyte sensing platforms. *TrAC Trends in Analytical Chemistry*, 92:32 – 41.
- [118] Panahi, Y., Mohammadhosseini, M., Nejati-Koshki, K., Abadi, A. J. N., Moafi, H. F., Akbarzadeh, A., and Farshbaf, M. (2017). Preparation, surface properties, and therapeutic applications of gold nanoparticles in biomedicine. *Drug research*, 11(02):77–87.
- [119] Paone, G., Conti, V., Vestri, A., Leone, A., Puglisi, G., Benassi, F., Brunetti, G., Schmid, G., Cammarella, I., and Terzano, C. (2011). Analysis of sputum markers in the evaluation of lung inflammation and functional impairment in symptomatic smokers and copd patients. *Disease markers*, 31(2):91–100.
- [120] Papi, A., Bellettato, C. M., Braccioni, F., Romagnoli, M., Casolari, P., Caramori, G., Fabbri, L. M., and Johnston, S. L. (2006). Infections and airway inflammation in chronic obstructive pulmonary disease severe exacerbations. *American Journal of Respiratory and Critical Care Medicine*, 173(10):1114–1121. PMID: 16484677.
- [121] Patel, N., Belcher, J., Thorpe, G., Forsyth, N. R., and Spiteri, M. A. (2015). Measurement of c-reactive protein, procalcitonin and neutrophil elastase in saliva of copd patients and healthy controls: correlation to self-reported wellbeing parameters. *Respiratory research*, 16(1):62.
- [122] Pawar, R. S. and Abhang, S. A. (2015). Evaluation of serum level of neutrophil 3 elastase, superoxide dismutase and nitric 4 oxide in copd patients and its correlation with 5 lung function test 6.
- [123] Pedersen, B. K. and Toft, A. D. (2000). Effects of exercise on lymphocytes and cytokines. *British Journal of Sports Medicine*, 34(4):246–251.
- [124] Perera, W. R., Hurst, J. R., Wilkinson, T. M., Sapsford, R. J., Müllerova, H., Donaldson, G. C., and Wedzicha, J. A. (2007). Inflammatory changes, recovery and recurrence at copd exacerbation. *European Respiratory Journal*, 29(3):527–534.
- [125] Pilavaki, E. and Demosthenous, A. (2017). Optimized lateral flow immunoassay reader for the detection of infectious diseases in developing countries. *Sensors*, 17(11):2673.
- [126] Pilavaki, E., Valente, V., and Demosthenous, A. (2018). Cmos image sensor for lateral flow immunoassay readers. *IEEE Transactions on Circuits and Systems II: Express Briefs*, 65(10):1405–1409.
- [127] Pinto-Plata, V. M., Müllerova, H., Toso, J. F., Feudjo-Tepie, M., Soriano, J. B., Vessey, R. S., and Celli, B. R. (2006). C-reactive protein in patients with copd, control smokers and non-smokers. *Thorax*, 61(1):23–28.

- [128] Pires, N. M. M. and Dong, T. (2013). Multiplexed detection of waterborne pathogens with an array of microfluidic integrated high-sensitivity organic photodiodes. In *2013 IEEE Biomedical Circuits and Systems Conference (BioCAS)*, pages 105–108.
- [129] Pires, N. M. M. and Dong, T. (2015). On-site, parallel detection of bio-analytes in water by an integrated capillary flow based opto-microfluidic device. In *Medical Measurements and Applications (MeMeA), 2015 IEEE International Symposium on*, pages 100–105. IEEE.
- [130] Pu, Y., Cai, F., Wang, D., Wang, J.-X., and Chen, J.-F. (2018). Colloidal synthesis of semiconductor quantum dots toward large-scale production: a review. *Industrial & Engineering Chemistry Research*, 57(6):1790–1802.
- [131] Punjiya, M., Mostafalu, P., and Sonkusale, S. (2014). Low-cost paper-based electrochemical sensors with cmos readout ic. In *2014 IEEE Biomedical Circuits and Systems Conference (BioCAS) Proceedings*, pages 324–327.
- [132] Punter-Villagrasa, J., Cid, J., Pérez-Avilés, C., Rodríguez-Villarreal, I., Juanola-Feliu, E., Colomer-Farrarons, J., and Miribel-Català, P. L. (2015). An instantaneous low-cost point-of-care anemia detection device. *Sensors*, 15(2):4564–4577.
- [133] Putcha Nirupama, Drummond M. Bradley, W. R. H. N. N. (2015). Comorbidities and chronic obstructive pulmonary disease: Prevalence, influence on outcomes, and management. 36.
- [134] Qiu, X., T. J. C. Z. e. a. (2009).
- [135] Rabe, K. F., Hurd, S., Anzueto, A., Barnes, P. J., Buist, S. A., Calverley, P., Fukuchi, Y., Jenkins, C., Rodriguez-Roisin, R., Van Weel, C., et al. (2007). Global strategy for the diagnosis, management, and prevention of chronic obstructive pulmonary disease: Gold executive summary. *American journal of respiratory and critical care medicine*, 176(6):532–555.
- [136] Raghavan, D., Varkey, A., and Bartter, T. (2017). Chronic obstructive pulmonary disease: the impact of gender. *Current opinion in pulmonary medicine*, 23(2):117–123.
- [137] Rahimi, R., Ochoa, M., Donaldson, A., Parupudi, T., Dokmeci, M. R., Khademhosseini, A., Ghaemmaghami, A., and Ziaie, B. (2015). A janus-paper pdms platform for air–liquid interface cell culture applications. *Journal of Micromechanics and Microengineering*, 25(5):055015.
- [138] Rajeev, G., Xifre-Perez, E., Simon, B. P., Cowin, A. J., Marsal, L. F., and Voelcker, N. H. (2018). A label-free optical biosensor based on nanoporous anodic alumina for tumour necrosis factor-alpha detection in chronic wounds. *Sensors and Actuators B: Chemical*, 257:116–123.
- [139] Ran, B., Xianyu, Y., Dong, M., Chen, Y., Qian, Z., and Jiang, X. (2017). Bioorthogonal reaction-mediated elisa using peroxide test strip as signal readout for point-of-care testing. *Analytical chemistry*, 89(11):6113–6119.

- [140] Rathnayake, N., Gieselmann, D.-R., Heikkinen, A. M., Tervahartiala, T., and Sorsa, T. (2017). Salivary diagnostics—point-of-care diagnostics of mmp-8 in dentistry and medicine. *Diagnostics*, 7(1).
- [141] Rennard, S. I. and Drummond, M. B. (2015). Early chronic obstructive pulmonary disease: definition, assessment, and prevention. *The Lancet*, 385(9979):1778 – 1788.
- [142] Rivas, L., de la Escosura-Muñiz, A., Serrano, L., Altet, L., Francino, O., Sánchez, A., and Merkoçi, A. (2015). Triple lines gold nanoparticle-based lateral flow assay for enhanced and simultaneous detection of leishmania dna and endogenous control. *Nano Research*, 8(11):3704–3714.
- [143] Rocha-Santos, T. A. (2014). Sensors and biosensors based on magnetic nanoparticles. *TrAC Trends in Analytical Chemistry*, 62:28–36.
- [144] Rosenberg, S., Kalhan, R., and Mannino, D. M. (2015). Epidemiology of chronic obstructive pulmonary disease: Prevalence, morbidity, mortality, and risk factors. *Seminars in respiratory and critical care medicine*, 36 4:457–69.
- [145] Rosenthal, S. J., Chang, J. C., Kovtun, O., McBride, J. R., and Tomlinson, I. D. (2011). Biocompatible quantum dots for biological applications. *Chemistry & biology*, 18(1):10–24.
- [146] Rossi, A., Butorac-Petanjek, B., Chilosi, M., Cosío, B. G., Flezar, M., Koulouris, N., Marin, J., Miculinic, N., Polese, G., Samaržija, M., et al. (2017). Chronic obstructive pulmonary disease with mild airflow limitation: current knowledge and proposal for future research—a consensus document from six scientific societies. *International journal of chronic obstructive pulmonary disease*, 12:2593.
- [147] Sakao, S., Voelkel, N. F., and Tatsumi, K. (2014). The vascular bed in copd: pulmonary hypertension and pulmonary vascular alterations. *European Respiratory Review*, 23(133):350–355.
- [148] Sanjay, S. T., Fu, G., Dou, M., Xu, F., Liu, R., Qi, H., and Li, X. (2015). Biomarker detection for disease diagnosis using cost-effective microfluidic platforms. *Analyst*, 140:7062–7081.
- [149] Santos, A., Malaguti, C., Corso, S., and Silva, C. (2009). Expressão das metaloproteinases da matriz 2 e 9 na saliva de pacientes com doença pulmonar obstrutiva crônica. *Fisioterapia e Pesquisa*, 16(4):299–305.
- [150] Sardesai, N. P., Barron, J. C., and Rusling, J. F. (2011). Carbon nanotube microwell array for sensitive electrochemiluminescent detection of cancer biomarker proteins. *Analytical chemistry*, 83(17):6698–6703.
- [151] SCALE, M. M. R. C. (2019). <http://www.csc.unc.edu/spir/public/UNLICOMMMRCModifiedMedicalResearchCouncilDyspneaScale08252011.pdf>.
- [152] Sears, M. R. (2015). Smoking, asthma, chronic airflow obstruction and copd. *European Respiratory Journal*, 45(3):586–588.

- [153] Sethi, S. and Murphy, T. F. (2001). Bacterial infection in chronic obstructive pulmonary disease in 2000: a state-of-the-art review. *Clinical Microbiology Reviews*, 14(2):336–363.
- [154] Sethi, S., Wrona, C., Eschberger, K., Lobbins, P., Cai, X., and Murphy, T. F. (2008). Inflammatory profile of new bacterial strain exacerbations of chronic obstructive pulmonary disease. *American Journal of Respiratory and Critical Care Medicine*, 177(5):491–497. PMID: 18079493.
- [155] Shaw, J. G., Vaughan, A., Dent, A. G., O'Hare, P. E., Goh, F., Bowman, R. V., Fong, K. M., and Yang, I. A. (2014). Biomarkers of progression of chronic obstructive pulmonary disease (copd). *Journal of thoracic disease*, 6(11):1532.
- [156] Shen, L., Ratterman, M., Klotzkin, D., and Papautsky, I. (2011). A cmos optical detection system for point-of-use luminescent oxygen sensing. *Sensors and actuators B: Chemical*, 155(1):430–435.
- [157] Silva, G. E., Sherrill, D. L., Guerra, S., and Barbee, R. A. (2004). Asthma as a risk factor for copd in a longitudinal study. *Chest*, 126(1):59 – 65.
- [158] Sochi, T. (2011). Slip at fluid-solid interface. *Polymer Reviews*, 51(4):309–340.
- [159] Song, X. and Knotts, M. (2008). Time-resolved luminescent lateral flow assay technology. *Analytica chimica acta*, 626(2):186–192.
- [160] Soriano, J. B., Abajobir, A. A., Abate, K. H., Abera, S. F., Agrawal, A., Ahmed, M. B., Aichour, A. N., Aichour, I., Aichour, M. T. E., Alam, K., Alam, N., Alkaabi, J. M., Al-Maskari, F., Alvis-Guzman, N., Amberbir, A., Amoako, Y. A., Ansha, M. G., Antó, J. M., Asayesh, H., Atey, T. M., Avokpaho, E. F. G. A., Barac, A., Basu, S., Bedi, N., Bensenor, I. M., Berhane, A., Beyene, A. S., Bhutta, Z. A., Biryukov, S., Boneya, D. J., Brauer, M., Carpenter, D. O., Casey, D., Christopher, D. J., Dandona, L., Dandona, R., Dharmaratne, S. D., Do, H. P., Fischer, F., Gebrehiwot, T. T., Geleto, A., Ghoshal, A. G., Gillum, R. F., Ginawi, I. A. M., Gupta, V., Hay, S. I., Hedayati, M. T., Horita, N., Hosgood, H. D., Jakovljevic, M. M. B., James, S. L., Jonas, J. B., Kasaeian, A., Khader, Y. S., Khalil, I. A., Khan, E. A., Khang, Y.-H., Khubchandani, J., Knibbs, L. D., Kosen, S., Koul, P. A., Kumar, G. A., Leshargie, C. T., Liang, X., Razek, H. M. A. E., Majeed, A., Malta, D. C., Manhertz, T., Marquez, N., Mehari, A., Mensah, G. A., Miller, T. R., Mohammad, K. A., Mohammed, K. E., Mohammed, S., Mokdad, A. H., Naghavi, M., Nguyen, C. T., Nguyen, G., Nguyen, Q. L., Nguyen, T. H., Ningrum, D. N. A., Nong, V. M., Obi, J. I., Odeyemi, Y. E., Ogbo, F. A., Oren, E., PA, M., Park, E.-K., Patton, G. C., Paulson, K., Qorbani, M., Quansah, R., Rafay, A., Rahman, M. H. U., Rai, R. K., Rawaf, S., Reinig, N., Safiri, S., Sarmiento-Suarez, R., Sartorius, B., Savic, M., Sawhney, M., Shigematsu, M., Smith, M., Tadese, F., Thurston, G. D., Topor-Madry, R., Tran, B. X., Ukwaja, K. N., van Boven, J. F. M., Vlassov, V. V., Vollset, S. E., Wan, X., Werdecker, A., Hanson, S. W., Yano, Y., Yimam, H. H., Yonemoto, N., Yu, C., Zaidi, Z., Zaki, M. E. S., Lopez, A. D., Murray, C. J. L., and Vos, T. (2017). Global, regional, and national deaths, prevalence, disability-adjusted life years, and years lived with disability for chronic obstructive pulmonary disease and asthma, 1990–2015: a systematic analysis for the global burden of disease study 2015. *The Lancet Respiratory Medicine*, 5(9):691 – 706.

- [161] Suárez, I., Larrue, A., Rodríguez-Cantó, P., Almuneau, G., Abargues, R., Chirvony, V., and Martínez-Pastor, J. (2014). Efficient excitation of photoluminescence in a two-dimensional waveguide consisting of a quantum dot-polymer sandwich-type structure. *Optics letters*, 39(16):4962–4965.
- [162] Suk, J. W. and Cho, J.-H. (2007). Capillary flow control using hydrophobic patterns. *Journal of micromechanics and microengineering*, 17(4):N11.
- [163] Suzuki, K., Yamada, M., Kurakake, S., Okamura, N., Yamaya, K., Liu, Q., Kudoh, S., Kowatari, K., Nakaji, S., and Sugawara, K. (2000). Circulating cytokines and hormones with immunosuppressive but neutrophil-priming potentials rise after endurance exercise in humans. *European Journal of Applied Physiology*, 81(4):281–287.
- [164] Syedmoradi, L., Daneshpour, M., Alvandipour, M., Gomez, F. A., Hajghassem, H., and Omidfar, K. (2017). Point of care testing: the impact of nanotechnology. *Biosensors and Bioelectronics*, 87:373–387.
- [165] Taton, K., Johnson, D., Guire, P., Lange, E., and Tondra, M. (2009). Lateral flow immunoassay using magnetoresistive sensors. *Journal of Magnetism and Magnetic Materials*, 321(10):1679–1682.
- [166] Test, C. A. (2019). <http://www.catestonline.org/>.
- [167] Torrente-Rodríguez, R., Campuzano, S., Montiel, V. R.-V., Gamella, M., and Pingarrón, J. (2016). Electrochemical bioplatfroms for the simultaneous determination of interleukin (il)-8 mrna and il-8 protein oral cancer biomarkers in raw saliva. *Biosensors and Bioelectronics*, 77:543 – 548.
- [168] Tufvesson, E., Ekberg, M., and Bjermer, L. (2013). Inflammatory biomarkers in sputum predict copd exacerbations. *Lung*, 191(4):413–416.
- [169] Tzortzaki, E. G., Lambiri, I., Vlachaki, E., and Siafakas, N. M. (2007). Biomarkers in copd. *Current medicinal chemistry*, 14(9):1037–1048.
- [170] Uchino, E., Sonoda, S., Kinukawa, N., and Sakamoto, T. (2006). Alteration pattern of tear cytokines during the course of a day: Diurnal rhythm analyzed by multicytokine assay. *Cytokine*, 33(1):36 – 40.
- [171] Vernooy, J. H., Lindeman, J. H., Jacobs, J. A., Hanemaaijer, R., and Wouters, E. F. (2004). Increased activity of matrix metalloproteinase-8 and matrix metalloproteinase-9 in induced sputum from patients with copd. *Chest*, 126(6):1802 – 1810.
- [172] Vestbo, J., Hurd, S. S., Agustí, A. G., Jones, P. W., Vogelmeier, C., Anzueto, A., Barnes, P. J., Fabbri, L. M., Martinez, F. J., Nishimura, M., Stockley, R. A., Sin, D. D., and Rodriguez-Roisin, R. (2013). Global strategy for the diagnosis, management, and prevention of chronic obstructive pulmonary disease. *American Journal of Respiratory and Critical Care Medicine*, 187(4):347–365. PMID: 22878278.
- [173] Viniol, C. and Vogelmeier, C. F. (2018). Exacerbations of copd. 27(147).

- [174] Wan, Y., Deng, W., Su, Y., Zhu, X., Peng, C., Hu, H., Peng, H., Song, S., and Fan, C. (2011). Carbon nanotube-based ultrasensitive multiplexing electrochemical immunosensor for cancer biomarkers. *Biosensors and Bioelectronics*, 30(1):93 – 99.
- [175] Wang, H., Ma, Z., Qin, J., Shen, Z., Liu, Q., Chen, X., Wang, H., An, Z., Liu, W., and Li, M. (2019). A versatile loop-mediated isothermal amplification microchip platform for streptococcus pneumoniae and mycoplasma pneumoniae testing at the point of care. *Biosensors and Bioelectronics*, 126:373–380.
- [176] Wang, J., Ahmad, H., Ma, C., Shi, Q., Vermesh, O., Vermesh, U., and Heath, J. (2010). A self-powered, one-step chip for rapid, quantitative and multiplexed detection of proteins from pinpricks of whole blood. *Lab Chip*, 10:3157–3162.
- [177] Wang, K.-Y. and Chau, T.-T. (2013). An association between air pollution and daily outpatient visits for respiratory disease in a heavy industry area. *PloS one*, 8(10):e75220.
- [178] Wang, X., Li, M., Zhang, B., Wang, H., Zhao, Y., and Wang, B. (2018). Recent progress in organometal halide perovskite photodetectors. *Organic Electronics*, 52:172–183.
- [179] Wang, Y., Zhang, Y., Lu, Y., Xu, W., Mu, H., Chen, C., Qiao, H., Song, J., Li, S., Sun, B., et al. (2015). Hybrid graphene–perovskite phototransistors with ultrahigh responsivity and gain. *Advanced Optical Materials*, 3(10):1389–1396.
- [180] Wignarajah, S., Suaifan, G. A. R. Y., Bizzarro, S., Bikker, F. J., Kaman, W. E., and Zourob, M. (2015). Colorimetric assay for the detection of typical biomarkers for periodontitis using a magnetic nanoparticle biosensor. *Analytical Chemistry*, 87(24):12161–12168. PMID: 26631371.
- [181] Wilson, M. S. and Nie, W. (2006). Multiplex measurement of seven tumor markers using an electrochemical protein chip. *Analytical Chemistry*, 78(18):6476–6483. PMID: 16970323.
- [182] Wright, P. (1977). The natural history of chronic bronchitis and emphysema: Charles fletcher, richard peto, cecily tinker and frank e. speizer oxford: Oxford university press. 1976. *British Journal of Diseases of the Chest*, 71:215 – 216.
- [183] Wu, J., Dong, M., Santos, S., Rigatto, C., Liu, Y., and Lin, F. (2017). Lab-on-a-chip platforms for detection of cardiovascular disease and cancer biomarkers. *Sensors*, 17(12):2934.
- [184] Wu, J., Hillier, C., Komenda, P., Lobato de Faria, R., Levin, D., Zhang, M., and Lin, F. (2015). A microfluidic platform for evaluating neutrophil chemotaxis induced by sputum from copd patients. *PLOS ONE*, 10(5):1–13.
- [185] Xiao, K., Wang, K., Qin, W., Hou, Y., Lu, W., Xu, H., Wo, Y., and Cui, D. (2017). Use of quantum dot beads-labeled monoclonal antibody to improve the sensitivity of a quantitative and simultaneous immunochromatographic assay for neuron specific enolase and carcinoembryonic antigen. *Talanta*, 164:463–469.
- [186] Yaghi, A. and Dolovich, M. B. (2016). Airway epithelial cell cilia and obstructive lung disease. *Cells*, 5(4).

- [187] Yang, Q., Gong, X., Song, T., Yang, J., Zhu, S., Li, Y., Cui, Y., Li, Y., Zhang, B., and Chang, J. (2011). Quantum dot-based immunochromatography test strip for rapid, quantitative and sensitive detection of alpha fetoprotein. *Biosensors and Bioelectronics*, 30(1):145–150.
- [188] Yoshizawa, J. M., Schafer, C. A., Schafer, J. J., Farrell, J. J., Paster, B. J., and Wong, D. T. W. (2013). Salivary biomarkers: Toward future clinical and diagnostic utilities. *Clinical Microbiology Reviews*, 26(4):781–791.
- [189] Zemans, R. L., Jacobson, S., Keene, J., Kechris, K., Miller, B. E., Tal-Singer, R., and Bowler, R. P. (2017). Multiple biomarkers predict disease severity, progression and mortality in copd. *Respiratory research*, 18(1):117.
- [190] Zhang, L., Farrell, J. J., Zhou, H., Elashoff, D., Akin, D., Park, N.-H., Chia, D., and Wong, D. T. (2010). Salivary transcriptomic biomarkers for detection of resectable pancreatic cancer. *Gastroenterology*, 138(3):949–957.
- [191] Zhao, C., Thuo, M. M., and Liu, X. (2015). Corrigendum: A microfluidic paper-based electrochemical biosensor array for multiplexed detection of metabolic biomarkers (2013 sci. technol. adv. mater. 14 [http://dx.doi.org/10.1088/1468-6996/14/5/054402] 054402). *Science and Technology of Advanced Materials*, 16(4):049501.
- [192] Zheng, C., Wang, X., Lu, Y., and Liu, Y. (2012). Rapid detection of fish major allergen parvalbumin using superparamagnetic nanoparticle-based lateral flow immunoassay. *Food Control*, 26(2):446–452.
- [193] Zhu, S., Song, Y., Zhao, X., Shao, J., Zhang, J., and Yang, B. (2015). The photoluminescence mechanism in carbon dots (graphene quantum dots, carbon nanodots, and polymer dots): current state and future perspective. *Nano research*, 8(2):355–381.
- [194] Zuo, P., Li, X., Dominguez, D. C., and Ye, B.-C. (2013). A pdms/paper/glass hybrid microfluidic biochip integrated with aptamer-functionalized graphene oxide nano-biosensors for one-step multiplexed pathogen detection. *Lab on a Chip*, 13(19):3921–3928.

Appendix A

Costs analysis

PDMS microfluidic device

Cost of the principal elements used for the Soft-lithography building process, referred to the price of a single kit or piece for each one. Data were purchase from the laboratory database.

- SI Wafer (1 piece): 12.80 euro
- 0.5 [L] SU8-100 photoresist: 859 euro
- 2.2 [Kg] Sylgard 184 Silicone KIT: 383 euro
- 5 [L] SU8-100 developer: 105 euro
- Glass (1 piece) : < 1 euro

Material quantities utilized in the PDMS device realization

- Wafer (1 piece diameter 100 [mm])
- 0.02 [L] SU8-100 photoresist
- 0.3 [L] SU8-100 developer
- 30 [g] PDMS base-Sylgard 184 Silicone Elastomer
- 3 [g] PDMS curing agent- Sylgard 184 Curing Agent
- Glass (1 piece)

The cost for the production of one microfluidic device is approximately less of 10 euro, considering the draft of a maximum of six microfluidic structures onto a piece of wafer for the studied case.

Acknowledgements

Con parole molto semplici, arrivata alla fine di questo percorso, voglio ringraziare le persone che ci sono sempre state, nonostante la distanza e i silenzi.

Innanzitutto ringrazio i miei genitori e mia sorella Chiara, per avermi sostenuta moralmente ed economicamente, per avermi permesso di realizzare la mia passione con determinazione e forza. L'amore è stato ed è la nostra roccia.

Ringrazio quindi la mia famiglia, la mia bussola nella vita.

Ringrazio Benedetta e Simona, la mia seconda famiglia qui a Torino. Le prime persone che ho incontrato in una nuova città per iniziare una nuova avventura. Con la loro lealtà e spensieratezza, si sono dimostrate delle amiche preziose.

Ringrazio Azzurra, Ilaria e Betta, le amiche che hanno condiviso con me una parte di vita a Roma. Ho cambiato città, ma ho portato con me una piccola parte di ognuna di loro e ne ho fatto tesoro. Mi hanno insegnato a combattere per arrivare dove sono ora.

Ringrazio le mie amiche d'infanzia Debora e Federica, distanti perchè come me sono persone ambiziose, ma sempre vicine nel mio cuore.

Ringrazio tutti i miei amici qui a Torino, che hanno condiviso momenti di ansia ma soprattutto momenti di felicità e gioia, cantando una canzone arrangiata con una chitarra sul momento o giocando al parco godendosi le belle giornate.

Ringrazio i miei amici del liceo che hanno sempre trovato il modo di organizzare un incontro ed essere felici insieme.

Ringrazio gli amici della Norvegia che mi hanno accompagnata in questi ultimi mesi. Persone con culture e idee diverse che mi hanno insegnato ad avere un nuovo sguardo della vita.

Infine ringrazio Alexei, un punto di riferimento fondamentale per arrivare alla fine del mio percorso. Nonostante le mille difficoltà, ogni giorno ha trovato il modo per farmi sorridere, rendendo 'più leggero' il periodo più difficile ma allo stesso tempo emozionante della mia vita.